Report Number: WUCSE-2004-41

2004-08-02

Design of Routers for Optical Burst Switched Networks

Jeyashankher Ramamirtham and Jonathan S. Turner

Optical Burst Switching (OBS) is an experimental network technology that enables the construction of very high capacity routers using optical data paths and electronic control. In this dissertation, we study the design of network components that are needed to build an OBS network. Specifically, we study the design of the switches that form the optical data path through the network. An OBS network that switches data across wavelength channels requires wave-length converting switches to construct an OBS router. We study one particular design of wavelength converting switches that uses tunable lasers and wavelength grating routers. This design is interesting... **Read complete abstract on page 2.**

Design of Routers for Optical Burst Switched Networks

Jeyashankher Ramamirtham and Jonathan S. Turner

Complete Abstract:

Optical Burst Switching (OBS) is an experimental network technology that enables the construction of very high capacity routers using optical data paths and electronic control. In this dissertation, we study the design of network components that are needed to build an OBS network. Specifically, we study the design of the switches that form the optical data path through the network. An OBS network that switches data across wavelength channels requires wave-length converting switches to construct an OBS router. We study one particular design of wavelength converting switches that uses tunable lasers and wavelength grating routers. This design is interesting because wavelength grating routers are passive devices and are much less complex and hence less expensive than optical crossbars. We show how the routing problem for these switches can be formulated as a combinatorial puzzle or game, in which the design of the game board determines key performance characteristics of the switch. In this disertation, we use this formu-lation to facilitate the design of switches and associated routing strategies with good performance. We then introduce time sliced optical burst switching (TSOBS), a variant of OBS that switches data in the time domain rather that the wavelength domain. This eliminates the need for wavelength converters, the largest single cost component of systems that switch in the wavelength domain. We study the performance of TSOBS networks and discuss various design issues. One of the main components that is needed to build a TSOBS router is an optical time slot interchanger (OTSI). We explore various design options for OTSIs. Finally, we discuss the issues involved in the design of network interfaces that transmit the data from hosts that use legacy protocols into a TSOBS network. Ag-gregation and load balancing are the main issues that determine the performance of a TSOBS network and we develop and evaluate methods for both.

Department of Computer Science & Engineering

Washington University in St. Louis
School of Engineering & Applied Science

2004-41

Design of Routers for Optical Burst Switched Networks, Doctoral Dissertation, August 2004

Authors: Ramamirtham, Jeyashankher

August 2, 2004

Abstract: Optical Burst Switching (OBS) is an experimental network technology that enables the construction of very high capacity routers using optical data paths and electronic control. In this dissertation, we study the design of network components that are needed to build an OBS network. Specifically, we study the design of the switches that form the optical data path through the network.

An OBS network that switches data across wavelength channels requires Wavelength Converting Switches to construct an OBS router. We study one particular design of wavelength converting switches that uses tunable lasers and wavelength grating routers. This design is interesting because wavelength grating routers are passive devices and are much less complex and hence less expensive than optical crossbars. We show how the routing problem for these switches can be formulated as a combinatorial puzzle or game, in which the design of the game board determines key performance characteristics of the switch. In this disertation, we use this formulation to facilitate the design of switches and associated routing strategies with good performance.

We then introduce Time Sliced Optical Burst Switching (TSOBS), a variant of OBS that switches data in the

SEVER INSTITUTE OF TECHNOLOGY

DOCTOR OF SCIENCE DEGREE

DISSERTATION ACCEPTANCE

(To be the first page of each copy of the dissertation)

DATE: July 30, 2004

STUDENT'S NAME: Jeyashankher Ramamirtham

This student's dissertation, entitled Design of Routers for Optical Burst Switched Networks has been examined by the undersigned committee of five faculty members and has received full approval for acceptance in partial fulfillment of the requirements for the degree Doctor of Science.

APPROVAL: _____ Chairman

_____

_____

_____

_____

WASHINGTON UNIVERSITY

SEVER INSTITUTE OF TECHNOLOGY

DEPARTMENT OF COMPUTER SCIENCE AND ENGINEERING

DESIGN OF ROUTERS FOR OPTICAL BURST SWITCHED NETWORKS

by

Jeyashankher Ramamirtham

Prepared under the direction of Professor J. Turner

A dissertation presented to the Sever Institute of
Washington University in partial fulfillment
of the requirements for the degree of

Doctor of Science

August, 2004

Saint Louis, Missouri

WASHINGTON UNIVERSITY
SEVER INSTITUTE OF TECHNOLOGY
DEPARTMENT OF COMPUTER SCIENCE AND ENGINEERING

ABSTRACT

DESIGN OF ROUTERS FOR OPTICAL BURST SWITCHED NETWORKS

by Jeyashankher Ramamirtham

ADVISOR: Professor J. Turner

August, 2004
Saint Louis, Missouri

Optical Burst Switching (OBS) is an experimental network technology that enables the construction of very high capacity routers using optical data paths and electronic control. In this dissertation, we study the design of network components that are needed to build an OBS network. Specifically, we study the design of the switches that form the optical data path through the network.

An OBS network that switches data across wavelength channels requires *wavelength converting switches* to construct an OBS router. We study one particular design of wavelength converting switches that uses tunable lasers and wavelength grating routers. This design is interesting because wavelength grating routers are passive devices and are much less complex and hence less expensive than optical

crossbars. We show how the routing problem for these switches can be formulated as a combinatorial puzzle or game, in which the design of the game board determines key performance characteristics of the switch. In this disertation, we use this formulation to facilitate the design of switches and associated routing strategies with good performance.

We then introduce *time sliced optical burst switching* (TSOBS), a variant of OBS that switches data in the time domain rather that the wavelength domain. This eliminates the need for wavelength converters, the largest single cost component of systems that switch in the wavelength domain. We study the performance of TSOBS networks and discuss various design issues. One of the main components that is needed to build a TSOBS router is an *optical time slot interchanger* (OTSI). We explore various design options for OTSIs.

Finally, we discuss the issues involved in the design of network interfaces that transmit the data from hosts that use legacy protocols into a TSOBS network. Aggregation and load balancing are the main issues that determine the performance of a TSOBS network and we develop and evaluate methods for both.

to my family

Contents

List of Tables

List of Figures

Acknowledgments

This dissertation would not have been possible without the guidance and support of my research advisor, Dr. Jon Turner. His dedication to quality research has been an inspiration for me to pursue doctoral study. It has been a privilege working with you Jon. I'd also like to thank my dissertation committee, Dr. R. Chamberlain, Dr. P. Crowley, Dr. R. Indeck, and Dr. J. Lockwood, for providing invaluable support and feedback in preparing this dissertation.

Thanks to all the people who have made life at Washington University enjoyable: Anshul, David, Ed, Prashant, Praveen, Radhesh, Rama, Samphel, Sherlia, Sumi, Tilman, and Yuhua. A special thanks to the CSE office secretaries, Peggy Fuller, Jean Grothe, Myrna Harbison, Sharon Matlock, and Stella Sung for making life as easy as possible for me as a graduate student.

Finally, I'd like to thank my parents for their support and making it possible for me to pursue what I like.

Jeyashankher Ramamirtham

Washington University in Saint Louis
August 2004

Chapter 1

Introduction

The size of the Internet has been growing rapidly in recent years, with the amount of data sent over the network doubling every year [77] and estimates show that it will continue to do so in the future. Initiatives like the 100×100 project [1] aim to wire 100 million households in the United States of America with connections at 100 Mbps or more per household. In countries like Japan and Korea, initiatives to wire households with broadband connections have met with great success.

Wavelength Division Multiplexing (WDM) [12] has made it possible to harness the enormous bandwidth potential of fiber in a cost-effective way and is thus becoming the method of choice for information transmission in data networks. Consequently, transmission capacity in data networks has been able to keep up with the growth of the Internet. Systems with 40 wavelengths per fiber and each wavelength running at OC-48 (2.5 Gbps) have been deployed and systems with 160 wavelengths, each supporting 10 Gbps are becoming available [23]. Laboratory experiments [27] have demonstrated the feasibility of 160 Gbps transmission per wavelength channel, resulting in a capacity of 12.8 Tbps per fiber with 160 wavelengths per fiber. The number of wavelength channels per fiber has also been increasing and laboratory experiments [27] have demonstrated systems with 1022 wavelength channels per fiber.

However, electronic switching speeds have been doubling every eighteen months following Moore's law and this leads to a serious disparity between electronic switching speeds and optical transmission capacity (it can take 5-10 equipment racks to hold the electronic line cards needed to terminate the channels from just a single fiber). Optical switching seeks to eliminate electronic switching and switch the data in its optical form, thus eliminating the opto-electronic components which contribute

a large fraction of the cost of electronic routers. Optical switching has other potential benefits, including bit-rate independence, protocol transparency, and low power consumption.

Optical switching is currently used in networks to provision very high capacity circuit-switched point-to-point "pipes" and the packet switching is done in the electronic domain. In these networks, known as wavelength routed networks, each lightpath or a circuit has the capacity of a wavelength channel and this capacity is much more than what is necessary for most packet switching applications [6, 9, 68, 83, 87, 107]. This leads to under utilization of the bandwidth. Optical burst switching (OBS) is a network technology that uses optics to switch data in a much smaller granularity resulting in more efficient utilization of bandwidth. In this dissertation, we study the architecture and design of network components that can make it cost effective to build optical burst switched networks.

There have been various studies to build packet/burst switched routers using optical components [10, 37, 21, 40, 46, 54, 31, 30, 71, 89, 102, 104]. Unfortunately, the optical components needed are expensive making it difficult for optical burst switching to be an economically effective alternative to electronic networks. Most of the optical packet switching studies have been done in research laboratories and have not been successful in demonstrating a case for implementing optical packet switched networks commercially.

Now we present a brief description of the architecture of an optical burst switched network and present a summary of existing approaches for building optical switches.

1.1 Optical Burst Switching Concept

Optical Burst Switching (OBS) [7, 18, 78, 80, 79, 85, 91, 92, 95, 98, 101] is an experimental network technology that seeks to use optical switching for the data path, while still retaining the flexibility of electronics for control. By exploiting the high channel counts of advanced WDM systems, it achieves excellent statistical multiplexing performance with little or no buffering.

The basic burst switching concept is illustrated in Fig. 1.1. The transmission links carry data on tens or hundreds of wavelength channels and user data bursts can be dynamically assigned to any of these channels by the OBS routers. One (or possibly several) channel on each link is reserved for control information that

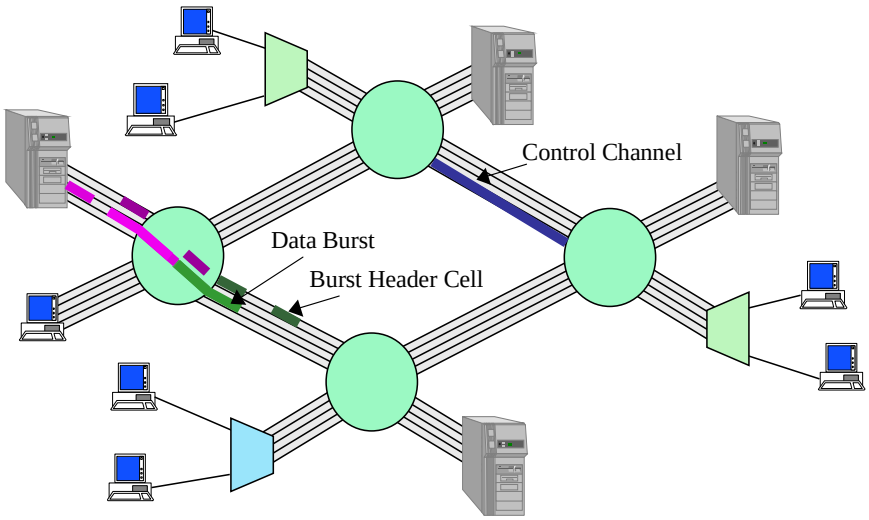

Figure 1.1: Burst Switching Concept

is used to control the dynamic assignment of the remaining channels to user data bursts. Terminals and/or other networks connect to a burst-switched network through concentrators that convert data on lower speed interfaces (e.g. IP-over-Ethernet at 100 Mb/s or 1 Gb/s), to the burst data format. Concentrators may switch packets received on low speed interfaces as single bursts, or may aggregate packets to form larger bursts. Aggregation increases the average burst length on the links, potentially improving efficiency and reducing the amount of control processing required. When a concentrator has a burst of data to send, an idle channel on the access link is selected and the data burst is sent on that channel.

Shortly before the burst transmission begins, a *Burst Header Cell* (BHC) is sent on the control channel, specifying the channel on which the burst is being transmitted and the destination of the burst. The OBS router, on receiving the BHC, assigns the incoming burst to an idle available channel on the outgoing link leading toward the desired destination and establishes a path between the specified channel on the access link and the channel selected to carry the burst. It also forwards the BHC on the control channel of the selected link, after modifying the cell to specify the channel on which the burst is being forwarded. This process is repeated at every router along the path to the destination. The BHC also includes an *Offset* field which contains the time between the transmission of the first bit of the BHC and the first bit of the burst, and a *Length* field specifying the time duration of the burst. The offset and length fields are used to perform time switching operations in the OBS routers, and the offset field is adjusted by the routers to reflect variations in the processing

delays encountered in the routers' control subsystems. If a router does not have idle channels available at the output port, the burst can be stored in a buffer.

Reference [91] describes a scalable OBS router architecture consisting of a set of *Input/Output Modules* (IOM) that interface to external links and a multistage interconnection network of *Burst Switch Elements* (BSE). The interconnection network uses a Benes topology, which provides parallel paths between any input and output port. A three stage configuration comprising d port switch elements can support up to d^2 external links (each carrying many WDM channels). The topology can be extended to 5,7 or more stages. In general, a $2k-1$ stage configuration can support up to d^k ports. For example, a 5 stage network constructed from 8 port BSEs would support 512 ports. If each port carried 256 channels at 10 Gb/s each, the aggregate system capacity would be $1,310$ Tb/s.

Input IOMs process the arriving BHCs, performing routing lookups and inserting the number of the output IOM into BHCs before passing them on. The BSEs use the output port number to switch the burst through to the proper output. Each of the components that does electronic processing on the cell keeps track of the time spent and updates the offset field in the BHC to maintain synchronization with the burst.

The focus of the first part of this dissertation is the design of the optical data path in each BSE. Optical components are used to build the BSEs and they are electronically controlled by the switch controller to switch the data to the destination output port, as determined by the route lookup in the IOM. We now present a brief summary of the available optical technologies that can be employed to build such a switch.

1.2 Enabling technologies

A typical optical switch has to implement three basic functions: demultiplexing and multiplexing, switching, and contention resolution. The generic structure of an optical packet switch is shown in Fig. 1.2. Demultiplexing of the individual wavelengths from input fibers and multiplexing them back onto outgoing fibers is done using passive couplers that are quite inexpensive. Switching is performed using high speed switching components that are discussed later in this section. In a packet switch, contention occurs whenever two or more packets try to leave the switch fabric on the same output port at the same time. In electronic switches, contention resolution is handled

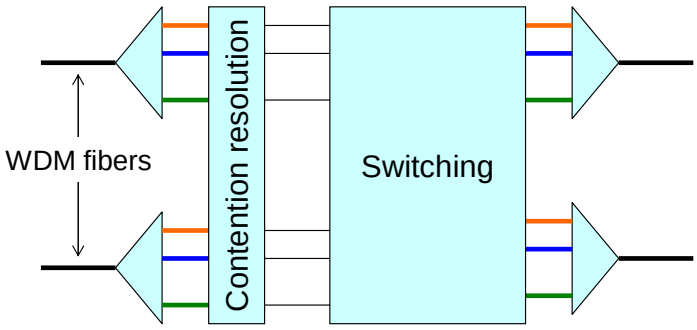

Figure 1.2: Optical switch architecture

by using buffers and storing the packet that loses out on contention and transmitting it at a later time when the outgoing channel becomes available. Typically, electronic routers use buffers that can buffer about one half seconds worth of data or 5 Gigabits for a 10 Gbps channel. The contention resolution can be done either at the input side (before the switching) or at the output side (after the switching) or both.

There are three methods of contention resolution in optical systems, optical buffering, wavelength conversion, and deflection routing. We now present an overview of the technologies that are available to perform each of these functions [74, 84, 90].

1.2.1 Switching

Switching is the process of directing signals from an input port to an output port as determined by the address lookup performed on the burst header cell. Optical switches are available for a range of applications. Wavelength routed networks that provision connections on a per-wavelength basis require switches with switching times of the order of a millisecond. Packet switching or burst switching, on the other hand, requires high speed switches (usually crossbars) to switch packets or bursts onto outgoing links. The switching speed of the crossbar determines the minimum size of the bursts that can be switched and the lower the minimum size of bursts, the better the statistical multiplexing performance of the network. A packet of size 100 bytes is about 80 ns long on an optical fiber that has a bandwidth of 10 Gbps per wavelength. If we were to handle bursts of the order of 100 bytes, we need optical crossbars that have switching times of 1-10 ns.

Apart from the switching time, other important characteristics of switches are extinction ratio, insertion loss, and crosstalk. These characteristics determine the

quality of the signal when it is switched through the devices. Higher loss characteristics imply that the signal needs to be regenerated more often in the network, which amounts to an increase in cost of the system. Extinction ratio is the ratio of the output power of a switch in the "on" state (when the input is connected to some output) to the output power in the "off" state (when the output is not connected to any input). This ratio should be as high as possible. While mechanical switches have extinction ratios of 40-50 dB, high-speed switches have extinction ratios of 10-25 dB. Insertion loss is the fraction of the signal power lost as a result of placing the switch in the data path and must be as small as possible. In a switch, even if an input is connected to some output, it is possible that power from other inputs can be coupled onto the signal at the output. The crosstalk of a switch is the ratio of the power at an output from the desired input to the power from all other inputs.

The two technologies that have switching times of a nanosecond or less are Electro-optic Lithium Niobate based switches and semiconductor optical amplifiers based switches. Other technologies that are commonly found like Micro-Electro-Mechanical Systems (MEMS) switches [76], Liquid Crystal switches, and Bubble-based Waveguide switches have switching times of a millisecond or more and cannot be used for burst switching. Lithium Niobate switches have very fast switching times of less than 1 ns and allow for modest levels of integration. A 16×16 switch with nanosecond switching times has been demonstrated [75]. However, they have a relatively high insertion and polarization dependent loss.

Semiconductor optical amplifiers (SOAs) are promising components that can be used to build fast switches. An SOA is used as an on-off switch and is controlled by a bias voltage. When in the off state, the signal is absorbed by the device and in the on state, the signal is amplified. This results in very large extinction ratios. SOA gate switching has been demonstrated in [33, 34, 53]. Reference [53] discusses the construction of a 4×4 switch matrix using SOA gates and Reference [34] discusses the construction of an 8×8 switch matrix. However, these switches are expensive components and challenges remain in integrating them into large-scale switching fabrics. Also, use of SOAs results in amplified spontaneous emission noise and this leads to degradation of the signal quality.

Reference [69] tabulates properties of the different switching technologies available.

1.2.2 Fiber delay lines

In optical switching systems, the only practical method of buffering is to circulate the optical signal through a fiber delay line for the amount of time required [58]. If we use a single lengthy fiber to store the packets, the amount of fiber required is excessive (half a second corresponds to 150,000 km of fiber) and fiber delay lines are also not random access. The other approach to using fiber delay lines is to use a smaller length fiber and recirculate the signal through the fiber repeatedly until the required amount of delay is achieved. This method results in excessive signal degradation that makes it impractical to use. Also, this method requires the use of WDM to maintain high buffer capacity. Thus, optical packet switching systems typically use very little buffering if any at all and depend on other contention resolution methods for good performance.

For small amounts of buffering, fiber delay lines can be packaged by wrapping the fiber around a cylindrical ring. The cladding diameter of a single mode fiber is usually 125μm and there is a layer of coating on top of the cladding which makes the diameter 250μm. A spool of fiber [2] that has an outer diameter of 27 cm (a little less than 11 inches) and a width of 18 cm (less than 7 inches) holds 50 km of fiber. The fiber delay lines may have to be temperature controlled depending on the conditions because temperature variations can cause the signal quality to degrade.

1.2.3 Deflection routing

Deflection routing [16, 43, 51, 57, 72] is another contention resolution method that has been studied. This is a multiple-path routing technique where packets that lose contention are routed to nodes other than their next-hop nodes and get routed to the destination from there on. Deflection routing is also known as hot-potato routing.

Deflection routing could cause out-of-order delivery of packets at the destination requiring resequencing. Also, the effectiveness of this method depends heavily on the network topology and the offered traffic pattern. Deflection routing works well in highly regular networks like the Manhattan Street network or the shuffle-exchange network since a deflection does not result in a large "detour". Thus, using deflection routing reduces the flexibility in designing the network. Deflection routing also results in an increased delay through the network as compared to a network that uses buffers to resolve contention. Another issue with using deflection routing is that packets/bursts can be routed away from the destination endlessly. This behavior, called

livelock, can be avoided by dropping the packet after a fixed number of hops. We do not study deflection routing as a contention resolution mechanism in this dissertation.

1.2.4 Wavelength conversion

Wavelength conversion offers effective contention resolution without relying on buffers at a switching node. By using wavelength conversion, we can switch bursts onto different output wavelength channels. Reference [91] presents the statistical multiplexing performance of a multiplexor that uses wavelength conversion with and without buffering. Also, wavelength conversion does not rely on the network topology or offered traffic intensities to provide acceptable performance and it is not cumbersome to use as compared to fiber delay lines. This makes it an ideal choice for contention resolution in optical burst switches. Wavelength conversion technologies are discussed in [32, 25, 105]. Very broadly, there are four types of wavelength conversion mechanisms, optoelectronic, optical gating, interferometric, and wave mixing.

The optoelectronic approach converts the optical signal back into electronic form and then retransmits it using a laser tuned to a different wavelength. There are three types of optoelectronic converters depending on the kind of regeneration used. Using 1R regeneration, where the incoming signal is simply amplified, makes the system transparent to the modulation format of the signal and the converter can handle analog data also. A wavelength converter employing 2R regeneration performs reshaping of the signal in addition to amplifying it. This operation can be performed on digital data only and it introduces additional phase jitter into the signal. A wavelength converter employing 3R regeneration performs retiming of the signal in addition to amplifying and reshaping it. This operation completely regenerates the signal. However, retiming is bit-rate specific and hence, the transparency of the system is lost. The rate of operation of optoelectronic wavelength converters is determined primarily by the electronic circuitry and hence, wavelength converters employing this method encounter bandwidth limitations at very high speeds. Also, the power consumption of optoelectronic converters is very high. Optoelectronic wavelength converters operating at 2.5 Gbps have been reported in References [36].

Wavelength converters based on optical gating make use of a device that acts as a gate modulated by the input optical signal and the input information is transferred to a probe signal that is on a different wavelength. The target wavelength is isolated at the output using a filter. The main technique using this principle is

cross-gain modulation (XGM), using a nonlinear effect in a semiconductor optical amplifier (SOA). This device can handle bit rates of 10 Gbps and is expected to be able to handle 100 Gbps. Also, this method of wavelength conversion is polarization independent, can handle a wide range of input wavelengths, and has reasonably high conversion efficiency (ratio of the output power to the input power of the probe). However, this method has several drawbacks too. The achievable extinction ratio is small and the input signal power must be high. Also, the carrier density and the refractive index in the SOA varies resulting in pulse distortion and phase variation.

As the carrier density varies with the input signal in an SOA, the phase of the probe is modulated (This results in pulse distortions in the converters based on the optical gating technique described above). The phase modulation can be converted into intensity modulation using an interferometer such as a Mach-Zehnder Interferometer (MZI). This approach is called cross-phase modulation (XPM). The advantage of this approach is that the input signal power needed is much lesser than in the optical gating approach and can be used with high input probe power. Also, wavelength converters using this method can achieve better extinction ratios. Reference [70] reports an implementation of a monolithically integrated tunable wavelength converter on a single chip using a semiconductor optical amplifier Mach-Zehnder interferometer that operates at 2.5 Gbps. Wavelength converters using Michelson interferometers have been demonstrated at 10 Gbps [28, 39] and 40 Gbps [63] respectively.

Four wave mixing is another nonlinear phenomenon that is used to perform wavelength conversion. This method is transparent to modulation formats and can handle signals at high speeds. The disadvantages are that signals in other wavelengths need to be filtered out and the conversion efficiency decreases significantly as the separation between the input signal wavelength and the probe signal wavelength increases. This method is most likely to be employed in very high speed systems ($\geq$ 40 Gbps). Reference [94] describes a 5-channel wavelength converter using four-wave mixing with each channel operating at 40 Gbps .

Tunable lasers are essential components of all wavelength converters and there have been dramatic advances in tunable lasers recently. For optical burst switches, very fast tuning speeds (of the order of 10 ns) and a wide tuning range are key requirements. Lasers that use mechanical or thermal tuning are unsuitable for packet switching applications that need tuning speeds of 1-10 ns. Electrically tunable semiconductor lasers, such as distributed Bragg Reflector (DBR) lasers [61], satisfy the

	λ_0	λ_1	λ_2	λ_3
I_0	O_0	O_1	O_2	O_3
I_1	O_1	O_2	O_3	O_0
I_2	O_2	O_3	O_0	O_1
I_3	O_3	O_0	O_1	O_2

Figure 1.3: Routing matrix of a 4×4 WGR

necessary requirements. Injecting current into a semiconductor laser causes the refractive index of the medium to change. This changes the wavelength of the laser's output signal. DBR lasers have tuning speeds of a few nanoseconds and can provide wide tuning range.

Wavelength conversion, however, still remains expensive because most wavelength conversion technologies use a laser or an equivalent component making it difficult for switches that use wavelength conversion to achieve lower costs than electronic routers.

1.2.5 Arrayed Wavelength Grating Routers

An $h \times h$ Arrayed Wavelength Grating Router (WGR) is a passive static wavelength-routing device that provides complete connectivity between its inputs and outputs, by passively routing h^2 optical connections on h wavelengths [24]. A WGR has a fixed cyclical-permutation-based routing pattern between its input and output ports. A connection at input i using wavelength k gets routed to the same wavelength on output $(i+k) \bmod h$, $\forall\, i, k \in [0, h-1]$. The routing pattern for a 4×4 WGR is shown in Fig. 1.3. A connection at input I_2 using wavelength λ_3 gets routed to output O_1 and a connection at input I_3 using wavelength λ_0 gets routed to output O_3.

WGRs can be used to switch signals when used in combination with tunable wavelength converters (TWC). This is shown in Fig. 1.4. Consider a TWC connected to the ith input of a WGR, $0 \leq i < h$, where h is the number of inputs of the WGR. If a signal coming in at the TWC is tuned to wavelength k, the signal is routed to output $(i + k) \bmod h$. Thus, a signal arriving at input 0 will be routed to output 3 if tuned to λ_3 (Fig. 1.4(a)) and a signal arriving at input 3 will be routed to output 4 if tuned to λ_1 (Fig. 1.4(b).

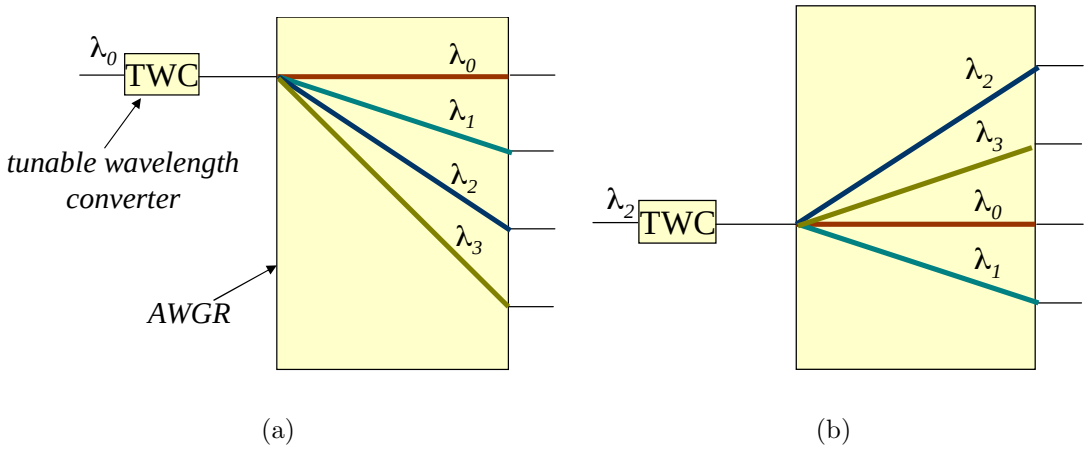

Figure 1.4: Examples showing how TWCs and WGRs can be used to switch signals

The use of a WGR has several advantages including easy fabrication, commercial availability and relatively low cost. Also, these devices typically have very low losses. WGRs are widely used in dense WDM systems currently. Silica-based WGRs are available commercially with 40 channels or more and larger WGRs are becoming available [8].

1.3 Related work

In this section, we present the various approaches to implement optical packet switches.

1.3.1 Architecture using wavelength converters and fast optical space switches

Reference [42] describes an optical packet switch that uses wavelength converters, a space division optical switch and optical buffer (see Fig. 1.5). If d is the number of input fibers, h is the number of wavelength channels, and b is the buffering capacity, the space switch is constructed using $dh^2(b/d+1)$ gates and passive optical splitters and the switch uses dh wavelength converters. The paper studies the performance of the switch under burst traffic and shows that using wavelength converters can help increase the throughput of the switch. The switch uses about h/d optical gates and one TWC for each input port.

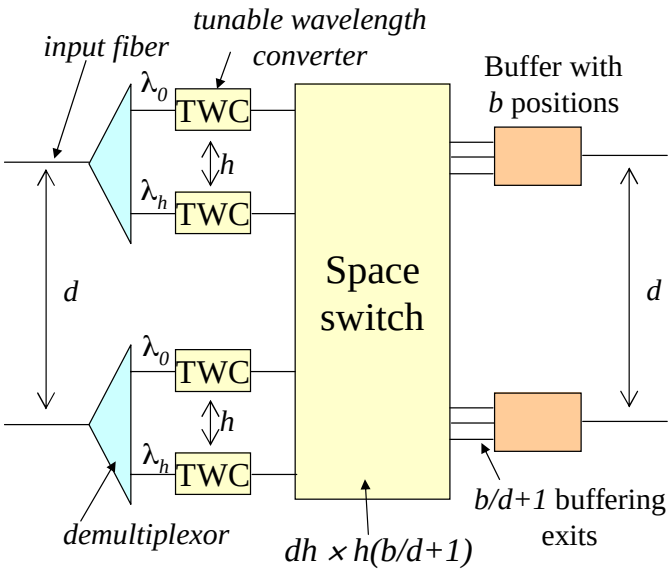

Figure 1.5: Optical packet switch with wavelength converters and buffering using a space switch [42]

1.3.2 Wavelength routing switches

KEOPS (Keys to Optical Packet Switching) [40, 29] was a project that demonstrated many key building blocks that are necessary to build optical packet switches. The project demonstrated systems that used transmission rates of 2.5 Gbps and 10 Gbps per wavelength channel. Two different packet switch architectures were put together and demonstrated. The first switch architecture is called a wavelength routing switch and is shown in Fig. 1.6. Each input carries a single wavelength channel and packets are of a fixed length. In the WDM version with h wavelength channels per fiber, the switch has h planes of the wavelength routing switch. The first stage of the switch distributes packets to the various multiplexors in the middle. The second stage routes the packets to the output ports on wavelengths that are available at the output. The fiber delay lines after the distribution stage serve as input buffers and they prevent head-of-line blocking from occurring. The paper presents algorithms to route packets to the output ports without creating conflicts at the intermediate stages and at the outputs. This switch needs two stages of wavelength conversion, thus needing $2dh$ tunable wavelength converters, where d is the number of input fibers and h is the number of wavelength channels per fiber.

Optical Label Switching (OLS) is another technology to perform optical packet switching. It is very similar to OBS in that the control plane operations are performed

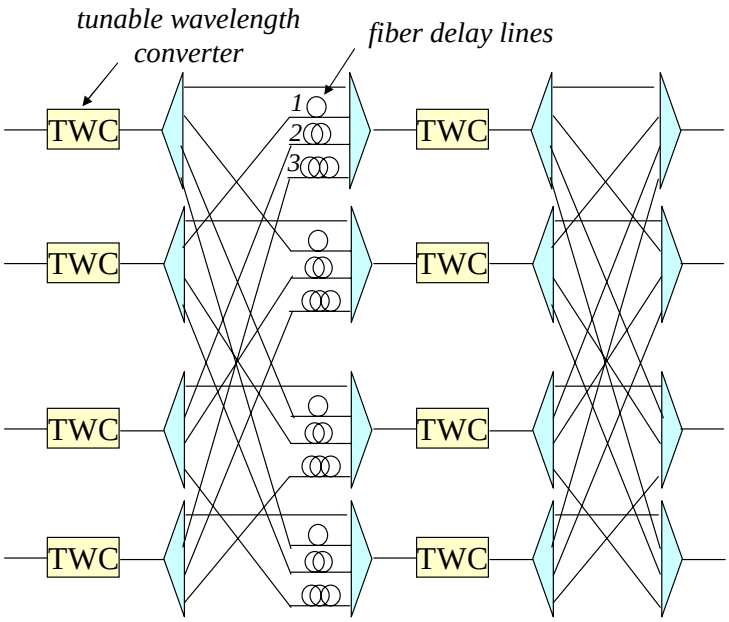

Figure 1.6: The KEOPS wavelength routing switch fabric [40, 29]

electronically and the data forwarding is done optically. However, the control header (label) is sent optically on the same wavelength as the data and the label is extracted from (or added to) the packet using technologies like sub-carrier multiplexing. Also, the data payload has to be delayed while the control operations are determined. References [62, 103, 41] describe the implementation of an OLS router. The switch fabric used is shown in Fig. 1.7. The switch is nonblocking and uses Arrayed Wavelength Grating Routers (WGRs) in combination with two stages of wavelength conversion, one of which uses tunable wavelength converters and the other uses fixed wavelength conversion. The tunable wavelength converter is used to route a packet to the destination port through the WGR. The fixed wavelength converter converts the signal to a wavelength channel that is not in use at the destination port. It needs a very large WGR and uses two stages of wavelength converters ($2dh$ wavelength converters). Reference [41] describes a way to scale the switch while using a small WGR (256×256 WGR for a 40 Pbps switch). However, this leads to some blocking within the switch. In this switch, the cost of wavelength conversion can be a crucial factor in determining its commercial feasibility.

Reference [108] describes a switch that also uses the wavelength domain to route data through the switch and the switch is shown in Fig. 1.8. The switch architecture uses two stages of tunable wavelength converters and three WGRs to switch the data signals. Also, the switch uses one stage of input buffering or output

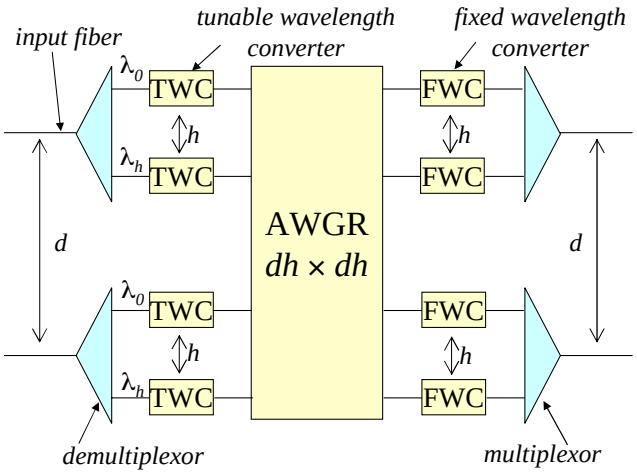

Figure 1.7: Optical packet switch with wavelength converters and AWGR in an Optical Label Switch [103]

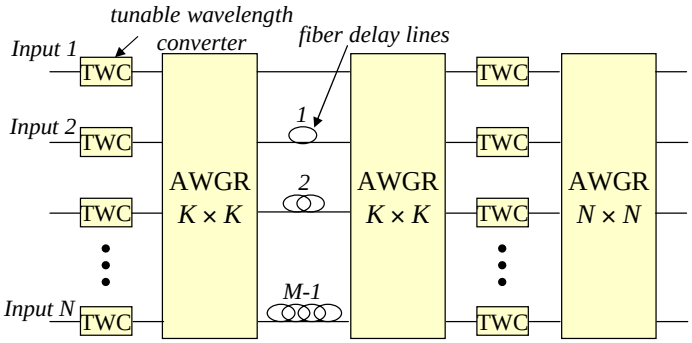

Figure 1.8: Optical packet switch with input buffering capability using wavelength converters and WGR [108]

buffering using fiber delay lines to resolve contention. For a system with d input fibers and h wavelength channels per fiber, the switch uses $2dh$ tunable wavelength converters and needs WGRs of the order of $dh \times dh$. Here again, the size of the WGR needed is not scalable for large systems and the cost of wavelength conversion makes this switch relatively expensive as compared to electronic routers. The WASPNET switch [31] also uses two stages of tunable wavelength converters in combination with a $2dh \times 2dh$ AWGRs. The switch uses a few ports of the WGR to provide buffering using fiber delay lines.

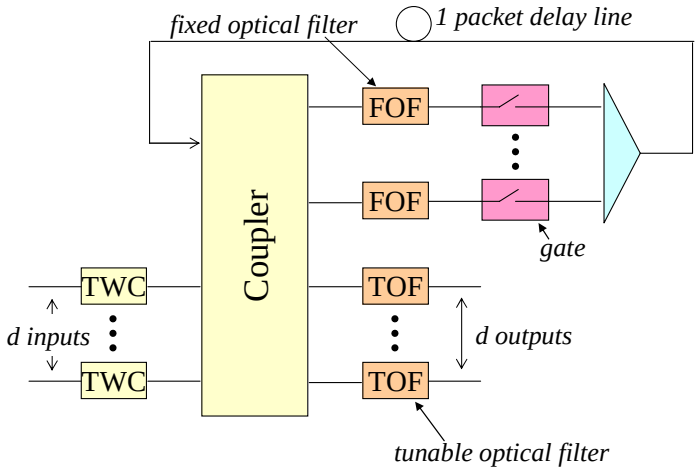

Figure 1.9: Broadcast and Select switch with a recirculating buffer [35]

1.3.3 Broadcast and Select switch architectures

In broadcast and select architectures, packets from input ports are sent to all output ports on different wavelengths and each output port chooses the packet that it has to transmit using a wavelength selective device (like a tunable optical receiver). In general, Broadcast and Select architectures can support only a limited number of input ports (up to the number of wavelength channels) because there would be wavelength conflicts otherwise. Thus, they are suitable for building switches that have a relatively small aggregate bandwidth. Broadcast and Select switches naturally support multicasting making them attractive options to build switches that need to support this capability.

Reference [35] describes a broadcast and select switch with a recirculating buffer. Each input carries data on some wavelength and packets are of some fixed length. The number of wavelengths, h, is greater than the number of inputs, d. Each input signal is tuned to some wavelength using a tunable wavelength converter and the different signals are combined using a passive coupler and the combined signal is transmitted to d tunable optical filters and h fixed optical filters. Also, the signals, that are recirculated, pass through a delay line that can hold one packet in each wavelength and are then fed back into the coupler. Of the signals in the coupler, up to d of them are transmitted to the output ports using the tunable filters and up to h are recirculated back into the coupler. This architecture uses one tunable wavelength converter and one tunable filter for each input channel. Also, the recirculation buffer uses h fixed filters and h gates.

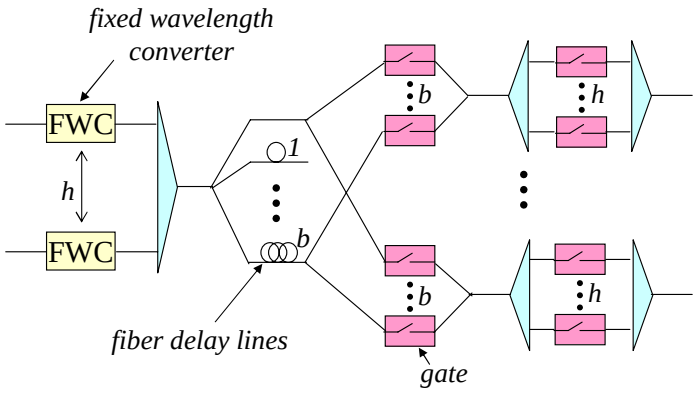

Figure 1.10: The KEOPS Broadcast and Select switch [40, 29]

The KEOPS project demonstrated a broadcast and select switch that is shown in Fig. 1.10. The switch operates on fixed packet lengths. Here again, each packet is transmitted using a different wavelength into the buffers. Using the gates and the multiplexors, it can be shown that this switch emulates an output buffered switch with a buffer capacity of b packets at each output.

1.3.4 Switching in the time domain

Photonic Slot Routing [19, 106] is a time domain switching mechanism where data is transmitted in fixed length timeslots and the switching is performed across timeslots. Each timeslot corresponds to a fixed duration of transmission across all wavelength channels and a timeslot is switched as a whole unit. Hence, all wavelength channels are treated as a single transmission channel as far as switching is concerned. This approach is similar to Time Sliced Optical Burst Switching (TSOBS) that we propose in this dissertation. However, in TSOBS, the timeslots on each wavelength channel are switched independently. This leads to better utilization of the network bandwidth. The switch designs discussed for TSOBS could be applied to Photonic Slot Routing switches.

Terahertz optical asymmetric demultiplexor (TOAD) is a device that can work as an AND gate and is described in Reference [86]. It has been demonstrated at a line speed of 100 Gbps. In a demonstration of a single routing node, packets from slower speed sources were interleaved onto the 100 Gbps link and a bank of TOADs extract individual streams.

1.3.5 Optical switch fabrics in electronic switches

Recently, there has been interest in using optics to build the switch fabric within an electronic switch because of the capacity offered by optical switches. It has been identified that the main deterrent to building high speed internet routers is the power density of the switch fabric racks [65]. By using optics to build the switch fabric, the power requirement can be reduced and thus, this makes it possible to build very high speed switch fabrics. Reference [65] describes a design for a switch, that has an aggregate capacity of 100 Tbps. A key observation, made in the paper, is that a switch fabric can be built by using a static interconnection of links, each link having twice the bandwidth capacity as the input link speed. Since optics gives us abundant bandwidth capacity, the switch uses optics for the interconnection network. The switch uses MEMS switches used in a static configuration to provide the interconnection network that is reconfigurable in the face of linecard failures.

Reference [52] describes a switch fabric that is built using tunable lasers and a WGR to route the signals to the output port. The switch aggregates packets electronically at the line card and switches them to the output using the switch fabric as described in Section 1.2.5 (tunable lasers are used instead of wavelength converters). The paper describes a demonstration that uses four ports each running at 40 Gbps through a switch fabric that can support an aggregate capacity of 1.2 Tbps.

1.4 Dissertation outline

The problem with the optical switches that have been discussed is that they use components that are expensive and hence, make the systems expensive relative to electronic routers. Most designs that use tunable wavelength converters and wavelength grating routers require two tunable wavelength converters per input channel and require a very large Arrayed Grating Router to resolve contention. Other designs require both tunable wavelength conversion and fast optical switches.

The objective of this dissertation is to develop less expensive and more economically viable optical switches that can be used in the data path of burst routers. We propose a design for *wavelength converting switches*, used in OBS routers, that use passive wavelength grating routers in place of optical crossbars. This design makes the switch less expensive because wavelength grating routers are easier to fabricate

and are much less expensive than optical crossbars. Also, the size of the wavelength grating routers needed are determined by the number of wavelength channels used and not the number of input ports. However, the use of wavelength routers introduces some blocking in the switch. We model the blocking in the switch through the help of a combinatorial puzzle or a game and discuss the various research problems involved. The design of wavelength converting switches is presented in Chapter 2.

We then propose a variant of burst switching called *Time Sliced Optical Burst Switching* (TSOBS) that eliminates the need for wavelength conversion by switching data in the time domain in Chapter 3. Optical time slot interchangers are key components that are required to implement time slotted switching. We discuss the design of time slot interchangers and the scheduling algorithms needed to implement the required switching operations. Through a cost analysis, we show that that TSOBS has the potential of being cheaper than electronic routers and is a promising solution to implement optical burst switching commercially.

Time sliced optical burst switching uses fixed length time slots to switch data. This requires that the data packets from hosts are of comparable size to a time slot to maintain good data transmission efficiency. The average size of packets in the Internet is too small for the time slots used in practical TSOBS networks. Thus, we need an aggregation mechanism at the network interfaces, that connect hosts to a TSOBS network. When multiple hosts transmit packets to the same destination network, we can aggregate the packets to form a "super-packet" that utilizes time slots more efficiently. We discuss an aggregation algorithm and study its performance in a TSOBS network in Chapter 4.

In TSOBS networks, since data is switched in the time domain, individual wavelength channels can get loaded with uneven amounts of data causing a degradation in the network performance. This problem can be alleviated by using load balancing techniques at the network interfaces where we have the freedom to choose the wavelength that a burst is sent on. We study four algorithms for addressing this problem and evaluate their performance in Chapter 5.

Chapter 2

Design of Wavelength Converting Switches

A wavelength converting switch is one that switches data signals that are carried on a wavelength channel of an input fiber to any wavelength channel of an output fiber. Wavelength converting switches require wavelength converters to switch the data across wavelength channels and to provide acceptable statistical multiplexing performance, the number of wavelength channels needs to be large (at least tens, preferably hundreds). More details on the statistical multiplexing performance of optical burst switching can be found in [91].

Each Burst Switch Element (BSE) in a burst switch requires a wavelength converting switch, capable of switching an optical signal from any of the BSE's d input fibers to any of its d output fibers (Fig. 2.1). A BSE with $d = 8$ and $h = 256$ wavelengths would have an aggregate throughput of 2 Tb/s, assuming 10 Gb/s per wavelength.

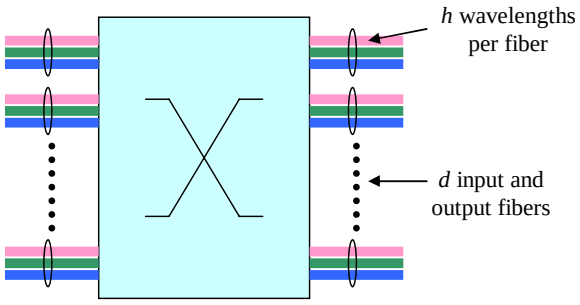

Figure 2.1: Wavelength converting switch with d input/output fibers and h wavelength channels per fiber

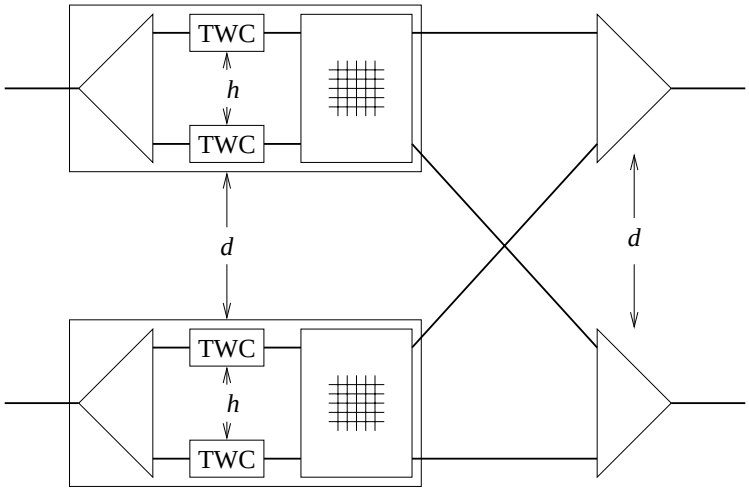

Figure 2.2: Wavelength converting switch using Tunable Wavelength Converters (TWC), Optical Crossbars and Passive Multiplexors and Demultiplexors

We describe two designs for wavelength converting switches. The first uses wavelength conversion in combination with fast optical crossbars to perform the required switching operations. This switch design is strictly non-blocking. However, the fast optical crossbars required are expensive components. The second design replaces the crossbars with Wavelength Grating Routers, which are passive devices, resulting in a lower cost switch design.

2.1 Switch Based on Optical Crossbars

Fig. 2.2 shows the first wavelength converting switch design. Each of the d input sections has an optical demultiplexor that separates the different wavelength channels from each other before propagating through Tunable Wavelength Converters that quickly tune to any of the h output wavelengths. The wavelength converters are followed by $h \times d$ crossbars. Outputs of each crossbar are then connected to distinct passive multiplexors, which constitute the output section of the switch. The crossbars can be decomposed into $d \times d$ sections, followed by additional passive multiplexors, reducing the required size of individual crossbar components. Note that the crossbars implement a combination of switching and multiplexing, since there may be several signals on a given input fiber that are propagated to the same output fiber. If they are converted to distinct wavelengths, these signals may share the same crossbar

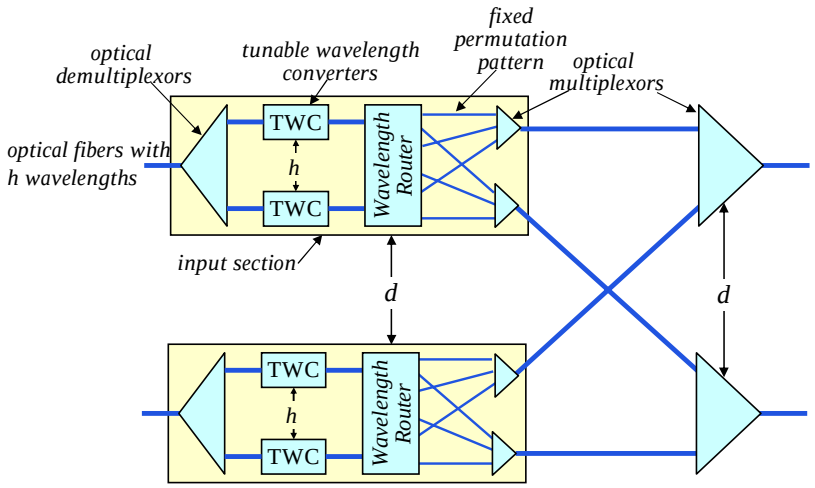

Figure 2.3: Wavelength switch using Tunable Wavelength Converters (TWC) and Passive Wavelength Grating Routers (WGR)

output, so long as the optical crossbar technology is designed to support this. SOA-based crossbar technology is capable of implementing this combined switching and multiplexing function.

To route an incoming burst to an output, the input wavelength is converted to any available wavelength at the required output, and the crossbar is configured to propagate the signal to the required output. The switching and multiplexing capability of the crossbar ensures that there is no blocking, so long as there is an available wavelength on the selected output. Because burst arrival is unpredictable, there will be times in an OBS router when no output wavelength is available for an arriving burst. In routers with no internal buffering, such bursts are discarded. Fortunately, with high channel counts, the probability of burst discards is very low.

As this design requires both tunable wavelength converters and high-speed crossbars, the cost of the system is relatively high and may make it impractical for commercial systems. However, the design is strictly nonblocking making it a good choice for comparison with other switch designs.

2.2 WGR-Based Switch Design

The WGR-based switch design we are interested in is shown in Fig. 2.3. Each of the d input sections consists of four components, an *optical demultiplexor*, a bank of *tunable wavelength converters*, a *wavelength grating router* and a bank of *optical*

multiplexors. The router and the multiplexors are joined through a fixed *permutation pattern*. We will see that the blocking characteristics of the switch depend critically on the choice of this permutation pattern. Each output section consists of a single optical multiplexor. Each input section is connected to each output section by an optical fiber carrying up to h optical signals on different optical wavelengths. Since each wavelength can be used only once on each output fiber, the signals arriving at an output section from different input sections must use distinct wavelengths.

In high performance optical networks, hundreds of different optical signals may be carried on a single fiber, using different wavelengths of light. The optical demultiplexor in each input section separates these signals, so that they can be individually switched to different output fibers. The tunable wavelength converters use a tunable laser and an optical modulator to transfer the information carried on one input wavelength to a different (and dynamically selectable) output wavelength. This wavelength conversion is needed to allow input signals on different input fibers to be switched to the same output fiber, even if the input signals are carried on the same wavelength. The wavelength grating router is a passive optical device that switches optical signals based on their wavelength. Specifically, an optical signal carried on wavelength i at input j is switched to output $(j + i) \bmod h$ where h is the number of wavelengths. Thus, the choice of wavelength used for a given signal determines which output section the signal is forwarded to. A demonstration of a combination of tunable wavelength converters and wavelength routers has been discussed in Reference [96].

In this construction, there are h/d different wavelengths that can be used by a given input signal to reach a particular output, but different inputs may use different sets of wavelengths to reach the same output. The permutation patterns used in each of the input sections determine these wavelength sets. To reach an output fiber, the wavelength converter at the input is tuned to one of these wavelengths and the incoming signal is "steered" to the required output through the wavelength router. In this design, the wavelength converters play the dual role of selecting the free output wavelength as well as providing the required space switching through the switch.

Since a given input channel is not able to use any wavelength to reach a given output fiber, blocking can occur. That is, there may be situations where all of the wavelengths that can be used to get to a desired output are in use at the output, causing blocking to occur even when there are free wavelengths available on the outgoing link. In the next section, we present this blocking problem as a puzzle on

a game board in order to make the nature of this blocking problem more apparent, and to clarify the issues that affect the blocking performance.

2.3 Design of WGR-based switches

In this section we study the routing problem in WGR-based switches and show how the blocking performance of these switches is affected by the permutation pattern used within each of the input sections of the switch.

2.3.1 Routing Multiple Channels Simultaneously

The problem of simultaneously routing a set of channels through a WGR-based switch can be formulated as a combinatorial puzzle. This formulation makes it easier to understand the intrinsic structure of the problem, yielding insights that are useful in design and analysis.

The puzzle is played on a game board made up of dh^2 squares arranged in h columns and dh rows. The board is divided into d square *blocks* of h rows each. Each square has one of d different colors, with each row containing h/d squares of each color and each column containing h squares of each color. To setup the puzzle we place colored *tokens* beside some or all of the rows. A setup can include at most h tokens of any color. An example of a setup game board with $d = 2$ and $h = 8$ is shown in Fig. 2.4(a). To solve the puzzle, we must place each token on a square of the same color, in the row where the token was placed. The token placement must also satisfy the constraint that no two tokens of the same color be placed in the same column. An example solution to the puzzle is shown in Fig. 2.4(b).

Each row in the puzzle corresponds to one of the h input channels on one of the d input fibers. More specifically, row i in block j of the game board corresponds to input channel i of input fiber j. The color of the token that is placed by a row corresponds to the output fiber that the corresponding input channel is to be switched to. More specifically, placing a token of color r on row i of block j corresponds to switching channel i of input fiber j to output fiber r. The columns of the array correspond to different output wavelengths. Placing a token in a particular column corresponds to choosing that output wavelength. The color of each square corresponds to the output that is reached if the wavelength converter for the input channel corresponding to that square's row is tuned to the wavelength corresponding to the column. So,

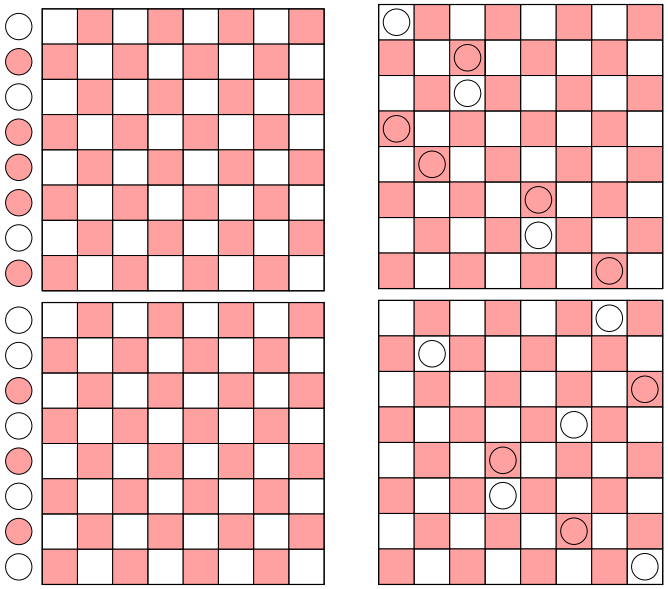

(a) Example puzzle setup (b) Example solution

Figure 2.4: An example puzzle setup and solution

placing a token of color r in column q of row i of block j corresponds to switching channel i of input fiber j to channel q of output fiber r. Note that the puzzle rule requiring that no two tokens of the same color occupy the same column corresponds to the requirement that no two input signals going to the same output fiber use the same wavelength.

In order to complete the correspondence between the puzzle and the routing problem, we note that within each block the rows must have closely related color patterns, in order to model the routing characteristics of the WGRs. Specifically, the pattern of colors within each row can be obtained from the previous row's pattern by a cyclic rotation of one column. This relationship only holds within each block. There is no requirement that different blocks have similar color patterns. The color pattern for each block corresponds to the permutation pattern within the input sections of the switch. This is illustrated in Fig. 2.5 which shows two example configurations of a system with $d = 2$ and $h = 8$ and the corresponding game boards.

Whenever the puzzle has a solution, it means that there is a way to route the input signals to the output channels that are specified by the tokens placed by each row. If the puzzle does not have a solution, then there is no way to route all the channels simultaneously. If, for all possible puzzle setups, there is a solution, the

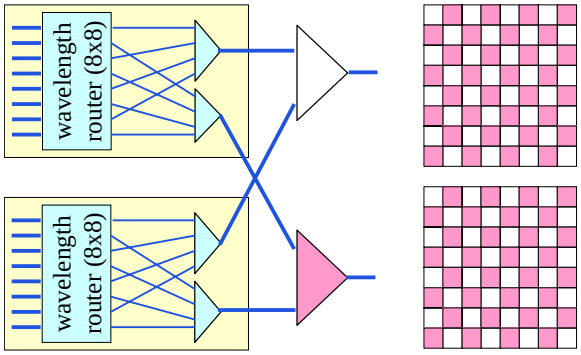

(a)

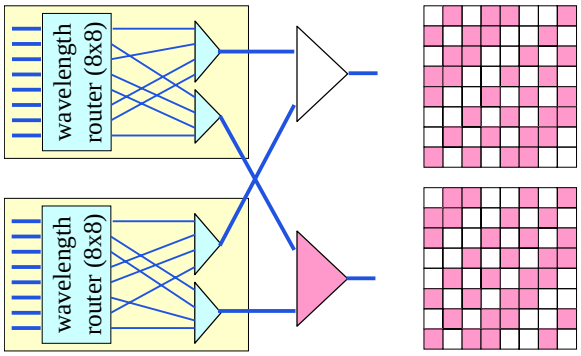

(b)

Figure 2.5: Two configurations and the corresponding game boards of a system with $d = 2$ and $h = 8$

switch is *rearrangeably non-blocking*. It is easy to see that the switch in Fig. 2.5a is not rearrangeably non-blocking, since the puzzle setup in which tokens of one color are placed in even-numbered rows and tokens of the other color are placed in odd-numbered rows has no solution. On the other hand, this setup does have a solution when played on the game board in Fig. 2.5b.

To generalize the problem of routing connections simultaneously, we restrict the number of tokens of a particular color to some value $k \leq h$.

Definition 2.3.1 *A game board is* k-solvable *if every puzzle setup with at most k tokens of each color has a solution.*

We show below that no game board is h-solvable. Fortunately, in practice, it can be sufficient to find game boards that are k-solvable for values of k fairly close to h.

2.3.2 Routing problem as a bipartite matching problem

The problem of solving the puzzle can be reformulated as a matching problem in a bipartite graph. We start by constructing the bipartite graph. The graph consists of two subsets of vertices; let us call them the "left" and "right" subsets. The "left" subset includes vertex $u(i, j)$ that corresponds to row j in block i of the game board (or channel j of input fiber i). The "right" subset includes a node $v(q, r)$ that corresponds to color q and column r (or channel r of output fiber q). We include the edge $\{u(i, j), v(q, r)\}$ in the graph if the color of the token in row j of block i is q and the color of the square in column r of row i and block j is q. In terms of the WGR switch, you include the edge if the signal on input fiber i, channel j is to be switched to output fiber q, and you can reach output fiber q using wavelength r.

In each row of the game board, there are h/d squares of the color corresponding to output q or h/d wavelengths that switch signals to output q. Thus, for each token that is placed at row j of block i, there are h/d edges that are drawn from the "left" subset to the "right" subset. One observation about this graph is that it breaks apart into separate subgraphs corresponding to the different outputs. This just corresponds to the fact that the placement of tokens of one color is independent of the placement of tokens of other colors.

This is illustrated in Fig. 2.6(a) for a system with 2 input fibers and 8 wavelengths per fiber for one output. The token placed in the second row of block 0 has four squares of the same color as the token in columns 1, 4, 5, and 7 respectively. This results in 4 edges in the bipartite graph from vertex $(0, 1)$ to vertices corresponding to λ_1, λ_4, λ_5, and λ_7 at the output. Similarly, 4 edges are drawn from vertex $(1, 3)$ to vertices corresponding to λ_2, λ_3, λ_5, and λ_7 at the output. This is repeated for each token placed beside the game board.

Now find a maximum size matching in this bipartite graph. If there is an edge for every token, you have a solution. In particular, if $\{u(i, j), v(q, r)\}$ is in the matching, then put the token in block i and row j in column r (equivalently, tune the wavelength converter for channel j of input fiber i to output wavelength r). Using a well-known maximum size matching algorithm based on max flows in unit networks, one can solve the puzzle in $O(h^{5/2})$ time, assuming a solution exists.

A maximum size matching for the bipartite graph in the example is shown in Fig. 2.6(a). Note that one of the left vertices, $(1, 7)$, cannot be matched to any output vertex because there does not exist an available vertex at the output that can be matched to this vertex. Given the matching in the graph, we can place the tokens

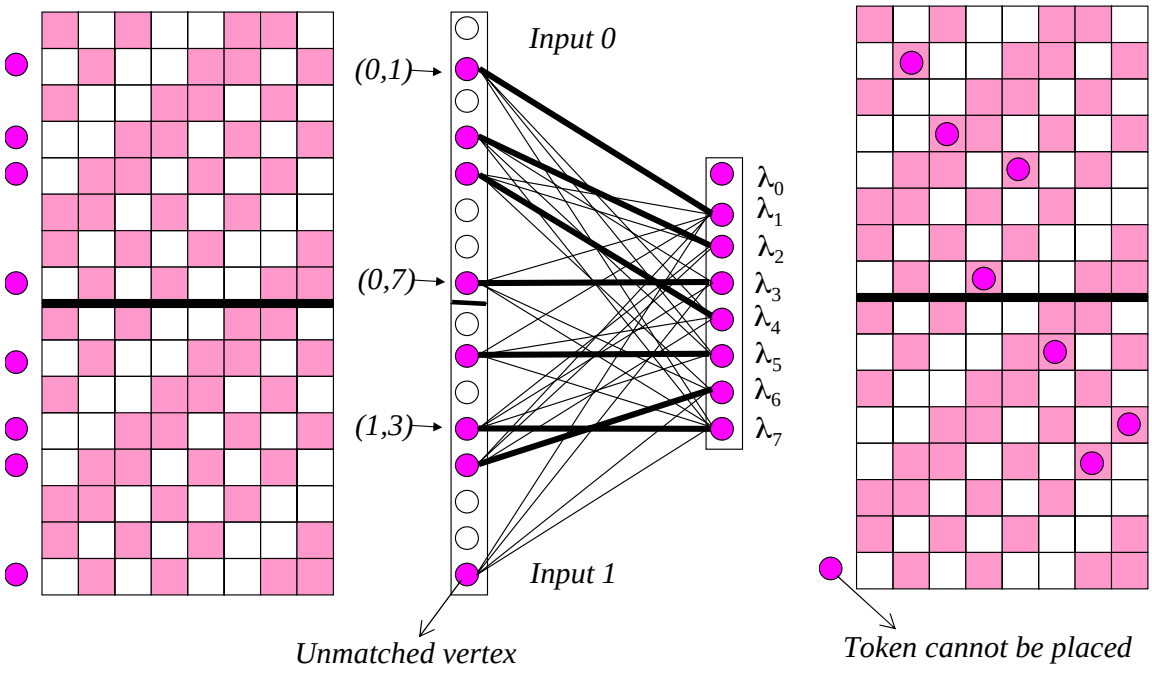

Figure 2.6: (a) Example bipartite graph formulation of a puzzle; (b) Solution to puzzle

on the game board as shown in Fig. 2.6(b). For example, token $(0, 1)$ is placed in the second column of the game board corresponding to λ_1, token $(0, 7)$ is placed in the fourth column, and token $(1, 3)$ is placed in the eighth column respectively.

The connection with matching also yields an algorithm for rearranging existing connections to accommodate new ones, which corresponds directly to the augmenting path algorithm for bipartite graphs. This can be described in terms of the game board as follows. If it is not possible to place a token of color x in row r_1 (satisfying the required constraints), then find an "x-augmenting path" in the game board starting at some square of color x in row r_1. Call this square (r_1, c_1) where c_1 is the column number. An x-augmenting path in the game board is a sequence of squares $(r_1, c_1), (r_2, c_2), (r_3, c_3), ..., (r_m, c_m)$ satisfying the following properties:

- All squares in the sequence have color x.
- Squares $(r_2, c_1), (r_3, c_2), ..., (r_m, c_{m-1})$ all contain a token of color x.
- There is no token of color x in column c_m.

Given such a path, we place a token on (r_1, c_1) and for $1 < i \leq m$ we move the token on square (r_i, c_{i-1}) to (r_i, c_i).

We can find such a path by performing a breadth-first search through the game board. We construct the search tree as follows. The nodes, N_i $(1 < i \leq hd)$, of the tree correspond to the rows of the game board. To place a token of color x in row r_1, let N_{r_1} be the root node of the tree. If column c in row r_1 has a square of color x and row r_k has a token of color x in column c, then we add an edge from N_{r_1} to N_{r_k} in the tree. There are h/d nodes adjacent to node N_{r_1}. We can construct the tree by recursively adding nodes at distance 1 from the newly added nodes. The search stops when we have a row that has a column with no token of color x placed in it; that is, we can move the token in the row to this free column.

Note that once a node N_{r_i} has been added to the tree, another node corresponding to the same row r_i will not be added at a lower level. This is because the subtree at both the nodes will be the same and the augmenting path is the shortest through the first instance of the node (since this is a breadth-first search). The search can stop without finding an augmenting path. This happens when none of the nodes in the tree has a column of color x with no token placed in it and we cannot add more nodes to the tree (other than nodes corresponding to rows that have already been added). In this case, the new token cannot be placed on the board and the puzzle cannot be solved.

Fig. 2.7 illustrates the rearrangement algorithm for a system with $d = 3$ and $h = 9$. Fig. 2.7(a) shows the state of the system before the placement of a token at $(1, 2)$. The game board configuration shows only the first two blocks. We assume that the last block does not have any tokens placed on it. Also, only the squares corresponding to the output we are interested in are represented by the dark squares. The other 6 squares (light colored squares) in each row correspond to the other two output fibers and the row configuration for them does not affect the token placement for the output we are interested in.

To place the token, we start a breadth first search starting with the row we want to place the token in, $(1, 2)$, as the root node. The columns that this row can use to reach the output are 0, 3, and 7. All three columns are occupied by other rows. The algorithm searches for a free column in rows that have tokens in the above columns. Thus, $(0, 0)$, $(0, 6)$, and $(0, 2)$ are added as the first level nodes in the search because they have tokens in columns 0, 3, and 7 respectively. The columns that the two rows share are indicated beside the edge in the graph. All three rows do not

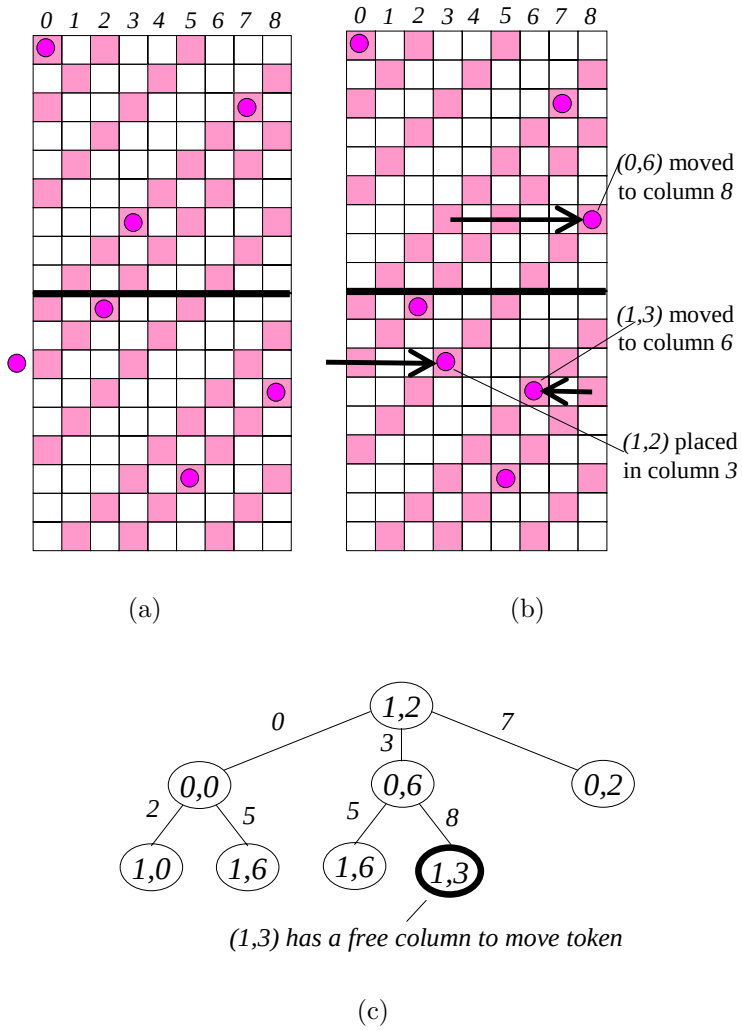

Figure 2.7: (a) Game board before placing token; (b) Rearrangement to place new token; (c) Breadth first tree to rearrange tokens on the game board

have free columns to move their tokens to. The algorithm searches one more level of nodes. Row $(0, 0)$ shares columns 2 and 5 with rows $(1, 0)$ and $(1, 6)$ respectively and neither of these has a free column. So, the algorithm adds nodes $(1, 0)$ and $(1, 6)$ as children of node $(0, 6)$ in the tree. Row $(1, 3)$ shares the column 8 with row $(0, 6)$ and column 6 is available. Thus, the search terminates and we have an augmenting path $((1, 2), 3), ((0, 6), 8), ((1, 3), 6)$. The breadth first tree is shown in Fig. 2.7(c). The token in row $(1, 3)$ is moved to column 6, the token in row $(0, 6)$ is moved to column 8, and the new token is placed in column 3 of row $(1, 2)$. Fig. 2.7(b) shows the game board after the token is placed.

2.4 Finding Good Game Boards

The design of the game board has a big influence on our ability to solve the puzzle. Since the game board design corresponds to the permutation pattern of the input section, this means that the permutation pattern affects the likelihood of blocking. The game board in Fig. 2.5a has many puzzle setups that have no solution, making it a poor design, from the perspective of the puzzle solver. What makes it a poor design is that many rows have exactly the same pattern of colors. This means that if tokens of the same color are placed in these rows, the number of columns they have to choose from is limited, and may be smaller than the number of tokens. This suggests that a good game board design will be one in which different rows have different patterns, and in particular, have as few columns in common as possible with squares of the same color.

Definition 2.4.1 *A* cover *of some row, say i, for some color "blue" is defined as the set of columns that have a blue square in row i in the game board.*

The cover of a set of rows R is defined as the union *of the covers of each of the rows that is contained in the set R.*

A game board is k-solvable if and only if in each of its associated bipartite graphs, there is a matching of size t between any set of $t \leq k$ inputs and all its outputs. By the well-known Marriage Theorem for bipartite matching, such a matching exists if and only if every set of $t \leq k$ nodes in the "left" subset has at least t neighbors in the "right" subset. We can restate this in terms of the puzzle, as follows. A game board is k-solvable if and only if for all colors j and all $r \leq k$, all sets of r rows *cover* at least r columns.

2.4.1 Upper bounds on puzzle solvability

We first show that no game board is h-solvable. Consider an arbitrary game board and color blue. There are exactly h blue squares in any column of the game board, meaning that there are $dh - h$ squares that are not blue. If we select any h rows from among the $dh - h$ rows that do not have blue squares in the given column, then any puzzle setup that has blue tokens in these h rows is unsolvable, since none of the tokens can be placed in the selected column, and we must place each of the h tokens in a distinct column. Similarly, if we consider any $i \leq d - 1$ columns, there must be at least $(d - i)h$ rows that do not contain blue squares in any of these columns. So,

any puzzle setup that has blue tokens in more than $h - i$ of these rows is unsolvable. These results make it clear that we cannot expect to construct a WGR-based switch that will guarantee our ability to place more than $h - d + 1$ tokens of the same color. Fortunately, the value of h is typically much larger than d for configurations of practical interest, which means that the degree of blocking implied by this limitation may be acceptable. This gives us

Theorem 2.4.2 *For any k-solvable game board on d colors and h columns,* $k \leq h - d + 1$

For larger values of d, we can get a stronger bound using the following theorem which is proved in Reference [82].

Theorem 2.4.3 *Let G be a game board on d colors and h columns and let s be any integer that satisfies*

$$dh\big(h - (h/d)\big)^{\underline{s}}/h^{\underline{s}} \geq h - s + 1$$

where $x^{\underline{r}} = x(x-1)\ldots(x-r+1)$. *If G is k-solvable, then* $k \leq h - s - 1$.

Fig. 2.8 shows the upper bound of the number of tokens that can placed as a function of the number of wavelengths, h, for various values of d. For $h = 256$ and $d = 8$, 15 is the largest value of s that satisfies the inequality, giving a limit of 240 on the solvability of game boards with $h = 256$ and $d = 8$. If we increase d to 16, the largest s increases to 41 and the limit becomes 214. If we fix a value of d and let $h \to \infty$, the theorem implies that $k \leq h - \lceil \log_{d/(d-1)} d \rceil$. Since $\log_{d/(d-1)} d$ is roughly $d \ln(d)$ for larger values of d, we can use $h - d \ln d$ as an estimate of the bound, which for larger values of d is significantly smaller than the $h - d + 1$ implied by *Theorem 2.4.2*. However, for $h >> d$, even this stronger bound does not rule out the existence of practically useful game boards.

2.4.2 Contiguous game boards

A *repetitive game board* is a game board whose d blocks are the same. A *contiguous game board* is a repetitive game board in which the first row of each block is divided into d contiguous monochrome blocks of size h/d each. Remarkably, for $d = 2$, contiguous game boards are $h - 1$ solvable. To see this, fix a color and note that any set of i rows in the same block covers at least $(h/d) + i - 1$ columns. Any set of k rows in the game board must have at least $\lceil k/d \rceil$ rows in some block, and so must

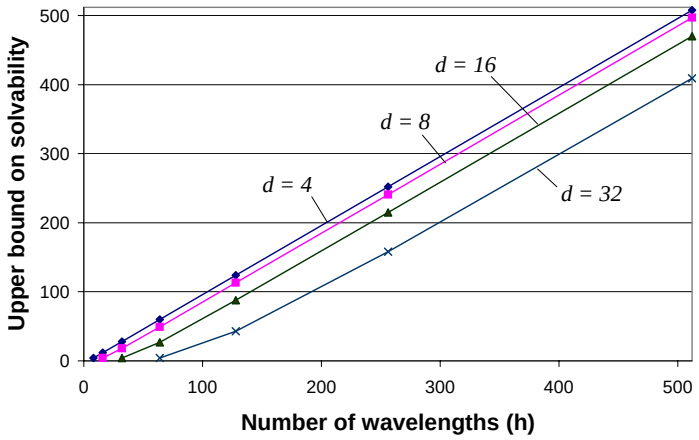

Figure 2.8: Upper bound on the solvability of game boards

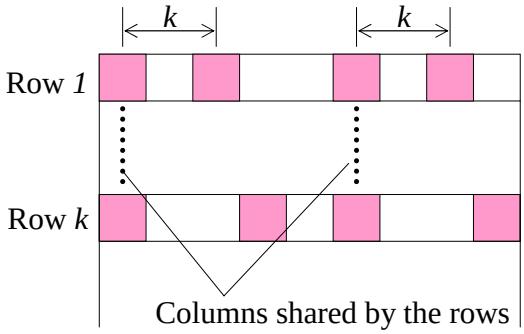

Figure 2.9: Example showing rows sharing columns

cover at least $(h/d) + \lceil k/d \rceil - 1$ columns. For $k = h - 1$, this is $2(h/d) - 1$, which is $h - 1$ when $d = 2$. That is, a contiguous game board with $d = 2$ is $(h-1)$-solvable, matching the upper bound in the previous sub-section. For arbitrary values of d, we have the following theorem from Reference [82].

Theorem 2.4.4 *A contiguous game board on h columns with d colors is k-solvable if and only if $k - \lceil k/d \rceil \leq h/d - 1$. The largest value of k that satisfies this condition is*

$$k^* = \begin{cases} (h/(d-1)) - 1, \textit{ if } d-1 \textit{ divides } h/d, \\ (h/(d-1)) - (h/d \bmod d-1)/(d-1), \textit{ otherwise.} \end{cases}$$

The first part of the theorem follows directly from the discussion above. The second part can be shown by substitution.

2.4.3 Random Game Boards

We now show how random game boards can be good choices for constructing switches with good blocking performance. Any row in a game board has h/d squares of the same color. When two or more rows have a square of the same color in a column, the column is said to be *shared* by the rows. The number of columns covered by any two rows in a game board is $2h/d$ minus the number of columns that are shared by these rows. Consider any two rows in the same block of the game board, row 1 and row k, without loss of generality. By the construction of the game board, row 1 is circularly shifted k squares to the left to obtain row k. Suppose row 1 has a square of some color in column i and a square of the same color in column $i + k$, then row k has a square of the same color in column i because the square in column $i + k$ in row 1 moves to column i in row k when shifted left by k squares. Thus, the two rows share the ith column. In general, the number of columns shared by row 1 and row k is the number of pairs of squares that are at a distance of k from each other in row 1. Fig. 2.9 illustrates this.

To construct good game boards, we need to maximize the number of columns covered by any set of rows. This is equivalent to minimizing the number of columns shared by the set of rows. Thus, we need to minimize the number of pairs of squares that are at a distance k from each other, for all values of k. Regular constructions of game boards can minimize the number of columns shared by rows for some values of k but may do poorly for other values of k. Randomizing the positions of the squares within a row can be expected to spread the distances between pairs of squares across all possible values. This reduces the number of columns shared by all possible row sets.

Our criterion for a good game board is one in which any set of r rows covers at least r columns, for each color. For larger values of h and d, we can expect random game boards to do well, in this respect. Consider an arbitrary set of r rows within a single block of a random game board. The probability that a particular column is not covered for some fixed color is

$$\frac{h-r}{h}\,\frac{h-r-1}{h-1}\,\cdots\,\frac{h-r-h/d+1}{h-h/d+1} = \frac{(h-r)^{\underline{h/d}}}{h^{\underline{h/d}}}$$

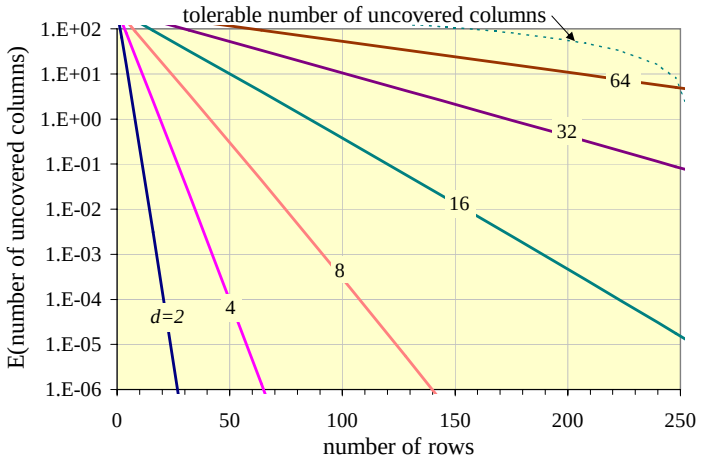

Figure 2.10: Number of columns not covered by row sets of all sizes ($h = 256$)

Thus, within one block, the expected number of columns not covered by r rows is

$$h \frac{(h-r)^{\underline{h/d}}}{h^{\underline{h/d}}}$$

The expected number of columns not covered by r rows selected from d independent random blocks in the game board is

$$\begin{aligned} &= h \frac{(h-r_1)^{\underline{h/d}}}{h^{\underline{h/d}}} \frac{(h-r_2)^{\underline{h/d}}}{h^{\underline{h/d}}} \ldots\ldots \frac{(h-r_d)^{\underline{h/d}}}{h^{\underline{h/d}}} \\ &\leq h \left(\frac{(h-r/d)^{\underline{h/d}}}{h^{\underline{h/d}}} \right)^d \end{aligned}$$

where $r = r_1 + r_2 + \ldots + r_d$, and r_i is the number of rows in the ith block of the game board. The expected number of columns not covered is plotted as a function of the size of the row set, r in Fig. 2.10. The expected number of columns not covered gives us an upper bound on the probability that a given set of rows fails to cover one or more columns. In the figure, the curve labeled "tolerable number of uncovered columns" is h minus the size of the row set.

For the values of d of most practical interest (≤ 16), the number of columns not covered by any random row set is much less than the tolerable number. For $d = 8$, the probability that a set of 140 or more rows fails to cover any column is less than one in a million. Another way to look at this is to note that while a nonblocking switch can implement all mappings of the input channels to output links, the blocking switch can implement all but a minuscule fraction of the set of possible mappings.

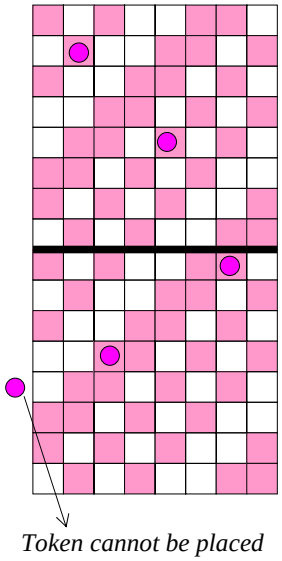

Figure 2.11: Example showing that a blocker with more than h/d tokens of some color can beat a naive setter

2.5 Routing Connections Online

The puzzle introduced above corresponds to the version of the routing problem in which we are asked to simultaneously route a whole set of connections. More often, we are interested in routing individual connections one-at-a-time, without disturbing connections routed previously. This problem can be formulated as a two player game, played on the same game board as the puzzle.

Let's call the first player the *blocker* and the second player, the *setter*. The blocker is given $k \leq h$ tokens of each of the d different colors. The blocker takes a turn by removing zero or more tokens from the board and placing one token beside some unoccupied row of the board. The setter takes its turn by placing the token put down by the blocker, in a square of the same color as the token in the selected row. When placing the token, the setter must not use any column that already contains a token of the same color. The blocker wins if the setter is not able to place the token on the board without violating the conditions. The blocker loses if the setter is able to keep the game going indefinitely.

The switch is *strictly nonblocking* if no matter how badly the setter plays, there is no way for the blocker to force a win. The switch is *wide-sense nonblocking* if there is a winning strategy for the setter (that is a strategy that will keep the game going forever, regardless of how well the blocker plays).

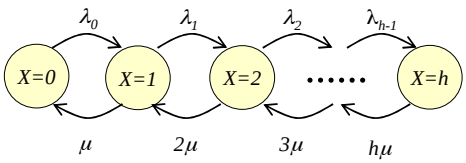

Figure 2.12: Birth-death modeling an output of the switch

Since a winning strategy for the setter would imply that the corresponding puzzle always has a solution, we cannot expect a winning strategy in versions of the game where the blocker has more tokens than allowed by the upper bounds in Section 2.4. It's easy to see that the setter has a trivial winning strategy when the number of tokens of each color is limited to $\leq h/d$. Hence, the switch is strictly nonblocking in these cases. It's also easy to see that the blocker can beat a naive setter if the blocker is allowed more than h/d tokens of each color. This is illustrated in Fig. 2.11. The blocker just needs to get the setter into a state where the h/d columns of some row are already being used by other tokens. In Fig. 2.11 the new token cannot be placed because the columns it can use to place the token are already in use by other tokens. In other words, the switch is strictly nonblocking if and only if the blocker is limited to $\leq h/d$ tokens of each color.

We now present an approximate analytical model for evaluating the performance of wavelength converting switches in OBS routers. The performance metric used is the fraction of arriving bursts that must be discarded. This is called the *burst rejection probability*. We phrase the model in terms of the game board. Since the tokens of different colors are independent, we focus on tokens of a single color. New tokens arrive at rate λ, and if possible are placed on the game board. Tokens stay on the game board for an average time period of $1/\mu$. If the token interarrival time and the token "dwell time" are exponentially distributed, we can model the system by the birth-death process shown in Fig. 2.12, where the state index corresponds to the number of tokens on the game board. The transition rate from state i to state $i-1$ is $i\mu$, where $1/\mu$ is the expected time duration for which a token stays on the game board. The transition rate from state i to $i+1$ varies for different states since the probability that an arriving token is actually placed on the game board decreases as the number of tokens on the board increases. The rate, λ_i, is the rate at which tokens are placed on the board, and is equal to λ times the probability that an arriving token is successfully placed. So, for $i < h/d$, $\lambda_i = \lambda$. For $i \geq h/d$ and a random game

board, we can approximate λ_i by

$$\lambda_i = \lambda \left(1 - \binom{h - h/d}{i - h/d} / \binom{h}{i}\right)$$

Note that $\binom{h}{i}$ is the number of sets of columns that can be used by i tokens and $\binom{h-h/d}{i-h/d}$ is the number of column sets used by i tokens that would prevent placement of a new token.

If we let π_i be the steady state probability that the system is in state i, then it can easily shown that

$$\pi_i = \frac{\lambda_0 \lambda_1 \ldots \lambda_{i-1}}{i!\, \mu^i} \pi_0$$

Using $\pi_0 + \pi_1 + \ldots + \pi_h = 1$ and solving for π_0, we can determine the individual steady state probabilities. The burst rejection probability is then given by

$$P_{rejection}(\rho) = \sum_{i=h/d}^{h} \pi_i \binom{h - h/d}{i - h/d} / \binom{h}{i}$$

where ρ is the offered load to the system given by $\lambda/h\mu$ and $\binom{h-h/d}{i-h/d}/\binom{h}{i}$ is the probability of a burst being rejected in state i.

2.5.1 Simulation results for random game boards

We now study how the blocking characteristics of the WGR-based switch affects the statistical multiplexing performance of an OBS router using simulation and compare the results with the analysis.

Here, we consider only the case of routers in which there are no buffers available to store bursts which can't be routed to the proper output without a wavelength conflict. Burst arrivals on each input channel are independent and each arriving burst is randomly assigned to a different output fiber. Burst lengths and the idle times between successive bursts on the same channel are exponentially distributed. The simulations used random regular permutation patterns at the input sections of the switch. Arriving bursts are assigned to a random wavelength that takes them to the proper output that is not already in use at that output.

The burst rejection probabilities for systems with different values of d and h and varying loads are shown in Fig. 2.13. Also shown are the burst rejection probabilities for systems that use strictly nonblocking switches in place of WGR-based switches.

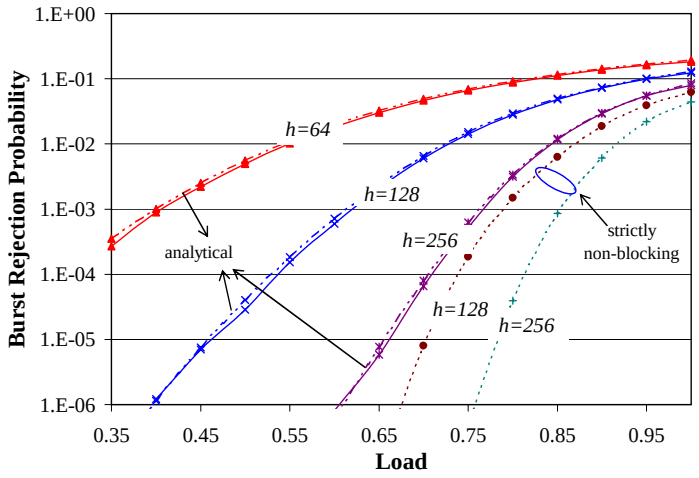

Figure 2.13: Burst rejection probabilities of different system configurations ($d = 8$)

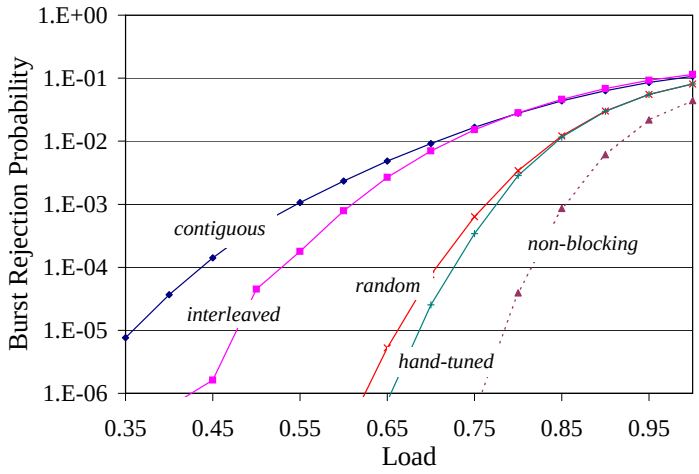

Figure 2.14: Burst rejection probabilities of different game boards ($d = 8$,$h = 256$)

For a system with $d = 8$ and $h = 256$, the rejection probability is 10^{-6} at a load of approximately 0.62 for the WGR-based switch and at a load of 0.75 for the strictly nonblocking switch. For systems designed to operate with a burst rejection ratio of 10^{-6}, the WGR-based switch can provide a throughput which is approximately 82% of what the nonblocking switch can provide. We also show the burst rejection probabilities as determined by the analysis of the burst switch. The analysis is pretty accurate as can be seen in Fig. 2.13.

2.5.2 Effects of game board configurations

The next set of results show how different game board configurations can affect system performance. Fig. 2.14 shows the result of using four different configurations for a system with $d = 8$ and $h = 256$. The first configuration corresponds to a "contiguous" permutation pattern, wherein, each input block's first h/d outputs are connected to the first output, the next h/d outputs are connected to the second output, and so on. The second configuration corresponds to a perfect shuffle between the wavelength router stage and the input side couplers. The third configuration corresponds to a randomly generated game board. The fourth configuration is a hand generated configuration where colors corresponding to any output in a row are distributed such that two rows have very little overlap and hence, the number of wavelengths available to reach a given output between a set of rows is increased. As can be seen from Fig. 2.14, the first two configurations perform poorly. This is because they do not try to maximize the number of wavelengths available to a subset of input rows uniformly. The fourth configuration performs slightly better than the random pattern and has a burst rejection probability of 10^{-6} at a load of 0.65. With this design, the WGR-based switch achieves 87% of the throughput that is achieved with the strictly non-blocking switch.

2.5.3 Effect of reconfiguring connections in the switch

The simulations described above were done with the restriction that once assigned to a wavelength channel, a burst occupies that wavelength for its entire duration. We also simulated a situation in which bursts could be dynamically switched to different wavelengths to accommodate newly arriving bursts. Although this is not a realistic scenario, it allows us to separate the effects due to the intrinsic blocking character of the WGR-switches from those due to the restriction on rearrangements. The simulations were done using the rearrangement algorithm described in Section 2.3.2. The burst rejection probabilities in these simulations matched the strictly non-blocking results almost exactly for the given traffic pattern. This confirms the implications of Fig. 2.10. Even though the WGR-based switch is not rearrangeably nonblocking, it performs nearly as well as a rearrangeably nonblocking switch, when rearrangements are allowed. This suggests that a better wavelength assignment strategy (the strategy used by the *setter* to place tokens on the game board) may help reduce the burst rejection probabilities further, when rearrangement is not allowed.

2.5.4 Effect of the wavelength assignment algorithm

In an OBS router, bursts can arrive at unpredictable times and we need to be able to find an available wavelength at the output to send the burst out on. In a strictly non-blocking switch, it is sufficient to select any available wavelength at the output and as long as there are no more than h bursts that need to be routed to an output at any time, where h is the total number of wavelength channels per fiber, there will be no blocking. However, we have shown that there is blocking in the switch design we are interested in. Thus, we need to try to minimize the blocking in the switch by appropriately routing any burst through the wavelength channel that maximizes the probability of other bursts that arrive in the future having wavelengths available at the outputs. In the game formulation described in 2.5, this translates to defining a strategy for the setter to place tokens on the game board.

Note that the wavelength assignment does not play a role in determining the performance for the interleaved game board configuration. In this configuration, if a set of rows share some column in the game board, they share all h/d columns. So, it does not matter which column we place the token in.

To obtain the results presented in Section 2.5.1, experiments on the game boards were performed by using a random available wavelength assignment algorithm. In this algorithm, the arriving burst is assigned to a random wavelength channel at the output that is unused. We examined three other wavelength assignment algorithms. Two of those algorithms, first available wavelength assignment algorithm and least affecting wavelength assignment algorithm, did not yield better performance than the random available wavelength assignment algorithm. The most available wavelength assignment algorithm resulted in a much improved performance for the contiguous board configuration and marginal improvement in the performance for the random and hand-generated game boards.

First available wavelength assignment algorithm

The first available wavelength assignment algorithm picks the first wavelength at an input that is not already in use at the output. This corresponds to placing the token in the leftmost square in the game board that is available. We performed experiments with a switch with 8 input/output fibers (d), 256 wavelengths per fiber (h) and random traffic with exponentially distributed interarrival times and burst

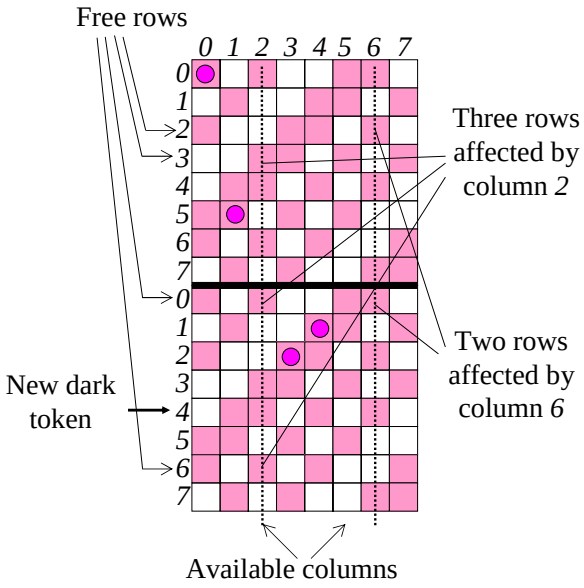

Figure 2.15: Least affecting wavelength assignment example

lengths. The first available wavelength assignment algorithm did not perform any better than the random available wavelength assignment algorithm.

Least affecting wavelength assignment algorithm

When a token of some color is placed by the setter in a column of some row, the column cannot be used to place tokens in the other $h-1$ rows that have squares of the same color. This does not affect rows that are occupied with a token placed in them (each row can have only one token placed in them at a time). However, the unoccupied rows get affected by losing one column that could have been used to place a token when it arrives. Thus, when the token needs to be placed by the setter in some row, we first find the columns that are available. For each available column, we count the number of unoccupied rows that get "affected" by choosing this column for token placement. The least affecting wavelength assignment algorithm places the token in a column such that the least number of unoccupied rows get affected.

To illustrate the algorithm, let us assume that the state of a switch is as represented by the game board with $h = 8$ and $d = 2$ shown in Fig. 2.15. We consider connections to the output that has colored squares (as opposed to white squares) and let us assume that tokens to the output have already been placed as indicated in the figure. Denote rows as (i, j), where i represents the block and j represents the row within the block. If we have to place a dark token in row $(1, 4)$, we have two columns,

column 2 and column 6, that are available. Also let us suppose that inputs $(0, 2)$, $(0, 3)$, $(1, 0)$, and $(1, 6)$ are currently free. By choosing column 2, we are reducing the number of wavelengths available to three rows, $(0, 3)$, $(1, 0)$, and $(1, 6)$, by one. However, choosing 6 reduces the number of wavelengths available to only two rows, $(0, 2)$ and $(1, 0)$, by one. Thus, the least available wavelength assignment algorithm picks column 6.

To evaluate the performance of the algorithm, we performed experiments for a switch with 8 input/output fibers and 256 wavelengths per fiber and random traffic with exponentially distributed interarrival times and burst lengths. It was observed that the performance of the least affecting wavelength assignment algorithm is comparable to the performance of the random available wavelength assignment algorithm. The problem with the algorithm is that it does not ensure that all rows have columns that can be used to place tokens. In the example shown in Fig. 2.15, row $(0, 2)$ has only one column (column 6) available where a dark token can be placed. Placing the token at row $(1, 4)$ in column 6 results in row $(0, 2)$ having no columns available to place a dark token. Thus, if a dark token is placed beside row $(0, 2)$ by the blocker, the setter will not be able to place it on the game board. In other words, a burst arriving at input $(0, 2)$ will have to be dropped because there are no available wavelengths to route the burst through the switch.

Effect of using most available wavelength assignment algorithm

We now present a routing algorithm that attempts to maximize the number of wavelengths available to free inputs to any output and study the effects of using the algorithm on the performance of the switch.

Define *availability*, a_{ij}, of a row i for color j to be the number of columns that have a j-colored square and are available in the row and we define these columns to be *available* columns. Equivalently, a_{ij} is the number of wavelengths at an input i that take us to output j and are not used by any other input.

Let us suppose a token of color m needs to be placed in row n. If $c_1, c_2, \ldots, c_k$ are the available columns in row n that have an m-colored square (That is, $a_{nm} = k$), we need to make a choice among one of the k available columns. Let $i_1, i_2, \ldots, i_s$ be the rows that are free currently in the game board and $a_{i_1 m}, a_{i_2 m}, \ldots, a_{i_s m}$ be their availabilities for color m. If we place the token in column c_l, the availability of rows that have c_l as an available column gets decremented by one. Let the new

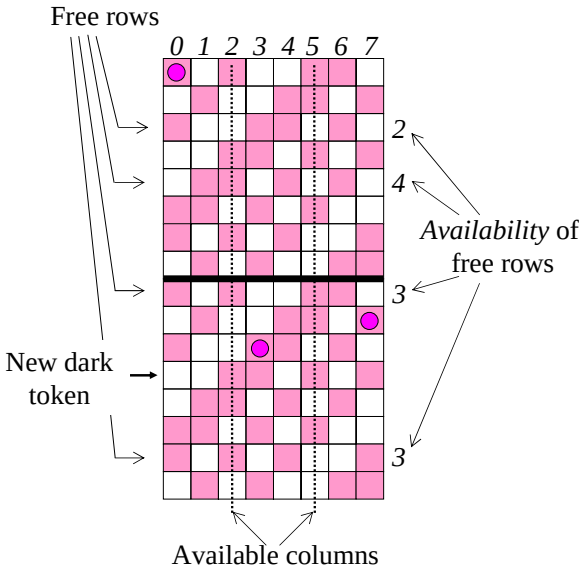

Figure 2.16: Switch state for routing example

availabilities be $a^l_{i_1m}, a^l_{i_2m}, \ldots, a^l_{i_sm}$, where

$$a^l_{i_km} = \begin{cases} a_{i_km} - 1 & \text{if } c_l \text{ is an available at row } i_k \\ a_{i_km} & \text{otherwise} \end{cases}$$

Now we can define the *availability vector*, A_{c_l}, of a column, c_l, as the *ordered* vector of the resultant availabilities of the free rows if c_l is the column that is chosen for a new token in row n. That is

$$A_{c_l} = \text{Sort}(a^l_{i_1m}, a^l_{i_2m}, \ldots, a^l_{i_sm})$$

Among the columns c_l, $1 \leq l \leq k$, we choose the column that has the *maximum availability*, where the maximum availability is the lexicographic maximum of all the availability vectors. Specifically, if $A = \{a_1, a_2, \ldots, a_x\}$ and $B = \{b_1, b_2, \ldots, b_x\}$ are two availability vectors then

$$A > B \qquad \text{if } \exists i \leq x, \text{ such that } a_1 = b_1, \ldots, a_{i-1} = b_{i-1} \text{ and } a_i > b_i$$

By choosing the column with the maximum availability, we maximize the number of options available to the row with the minimum number of options for placing tokens of color m.

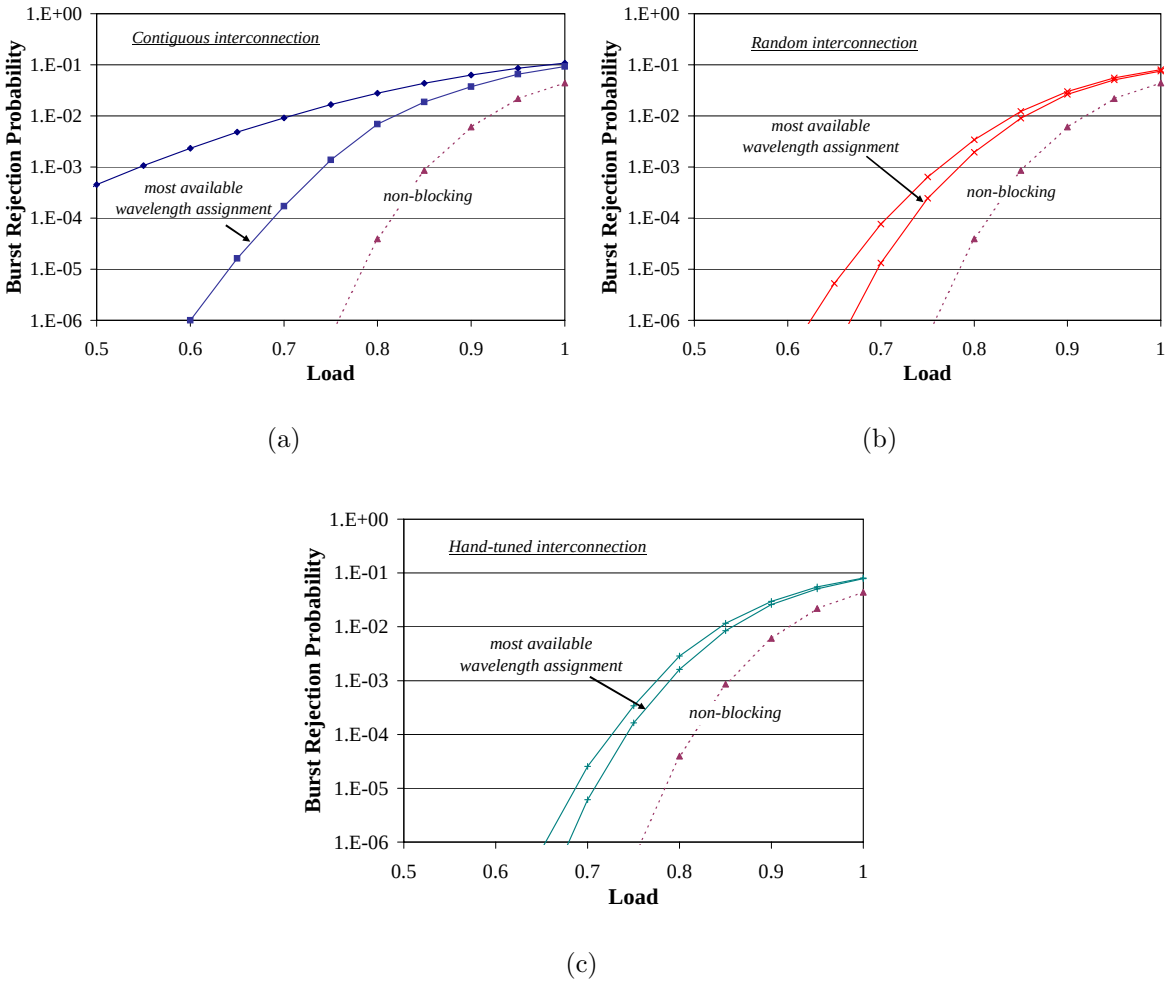

Figure 2.17: Burst rejection probabilities of different game boards with the most available wavelength assignment ($d = 8$,$h = 256$)

To illustrate the routing algorithm, let us assume that the state of a switch is as represented by the game board with $h = 8$ and $d = 2$ shown in Fig. 2.16. We consider connections to the output that has colored squares (as opposed to white squares) and let us assume that tokens to the output have already been placed as indicated in the figure. Here again, denote rows as (i, j), where i represents the block and j represents the row within the block. Suppose we have to place a dark token in row $(1, 3)$, we have two columns, column 2 and column 5, that are available. Also suppose inputs $(0, 2)$, $(0, 4)$, $(1, 0)$, and $(1, 6)$ are currently free, then the availabilities of these inputs are 2, 4, 3, and 3 respectively. The rows that are affected when column 2 is used are $(0, 4)$, and $(1, 0)$ and the row that is affected when column 5 is used is

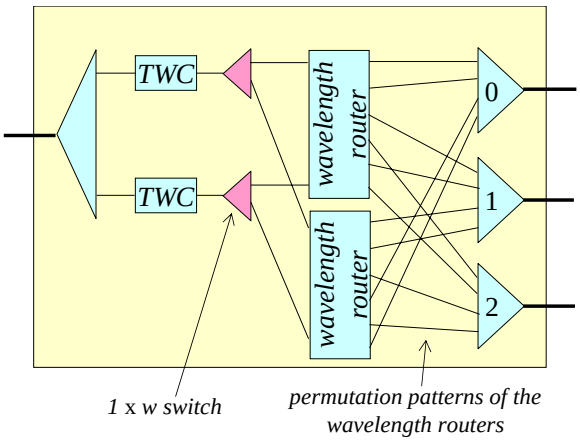

Figure 2.18: Input section of the WGR-based switch with multiple wavelength routers

$(1, 0)$. Thus the availability vectors for the two columns are given by

$$A_2 = \{2, 2, 2, 3\}, \text{ and } A_5 = \{2, 2, 3, 4\}$$

and we can see that $A_5 > A_2$. Thus, we choose column 5 to place the token in.

The simulation results of using the most available wavelength assignment algorithm for different permutation patterns are shown in Fig. 2.17. The algorithm gives tremendous improvement in throughput for the contiguous permutation pattern. It gives reasonable improvement for the random and the hand-tuned permutation patterns. For the hand-tuned permutation, it improves the throughput to about 89% of the non-blocking case at a blocking probability of 10^{-6} with a utilization of 68%.

2.6 WGR-based switch using multiple wavelength routers

An extension to the basic switch design is to use multiple wavelength routers in place of one and expand the routing capability of the switch. Fig. 2.18 shows an input section of this design. The wavelength router in each of the input sections is replaced with w wavelength routers and the signal from the TWC is switched through one of the wavelength routers using a $1 \times w$ optical switch. Each wavelength router connects to the output section using a different permutation pattern. Thus, a single wavelength channel can be used to route bursts to one of up to w output fibers by switching the

0,1	0,1	1,2	2,0	1,2	2,0
0,1	1,2	2,0	1,2	2,0	0,1
1,2	2,0	1,2	2,0	0,1	0,1
2,0	1,2	2,0	0,1	0,1	1,2
1,2	2,0	0,1	0,1	1,2	2,0
2,0	0,1	0,1	1,2	2,0	1,2

Figure 2.19: A block of the game board corresponding to the input section in Fig. 2.18

signal through the appropriate wavelength router. For instance, tuning the signal to some wavelength i and switching the signal through the first wavelength router can route the signal to output 1. However, switching the same signal through the second wavelength router can route the signal to a different output 2. This increases the number of wavelengths available to each input to route the signal to an output.

The game formulation can be modified to model this design as follows. The game board still has d blocks, each with $h \times h$ squares corresponding to the input fibers. Each square in the game board is now colored using w colors instead of one, corresponding to the wavelength routers. A token can be placed in a square of the game board if the color of token is one of the colors used to color the square. A square in column i of some row r of the game board is colored using colors $c_1, c_2, \ldots, c_w$ if by tuning the TWC of input r to wavelength i, the signal is routed to output c_j if we switch the signal through the jth wavelength router, where $1 \leq j \leq w$. Thus, if a token of color c_j is placed on the square by the setter, we tune the TWC to wavelength i and switch the signal through the jth wavelength router to reach output c_j. Here again, the game board is constructed such that a row can be obtained by circularly shifting the previous row within the block to the left by one square because of the routing property of the wavelength router. The game board can be viewed as a multilayer game board, where each layer corresponds to the game board of the corresponding wavelength router had it been used independently in a switch and not in conjunction with the other wavelength routers. An example block of a game board for a system with $d = 3$, $h = 6$, and $w = 2$ is shown in Fig. 2.19. Each square is represented by w numbers and the numbers correspond to the colors of the square.

Each wavelength router has h/d wavelengths to reach an output. Ideally, we would like to have wh/d wavelengths available to an input to reach an output in a switch with w wavelength routers. However, wavelength channels used to reach

an output can overlap between the different wavelength routers. To maximize the number of wavelengths available to any input to reach an output, we must ensure that the game board blocks corresponding to each wavelength router are sufficiently complementary to each other. An easy method to construct the game boards is to take a row's configuration and exchange the positions of the colored squares in a cyclic fashion. Specifically, if the colors are represented by $1, 2, \ldots, d$, and we have a configuration of a game board block of the first wavelength router, then assign the color $(c + 1) \bmod d$ to the corresponding square in the block for the next wavelength router, where c is the color of the square in the block corresponding to the first wavelength router. This ensures that the column set covered by a row is disjoint for the different wavelength router sections. Equivalently, given that a square is colored c_1 in a game board of a wavelength router, we color the square with colors $c_1, c_2, \ldots, c_w$ such that $c_2 = (c_1 + 1) \bmod d, c_3 = (c_1 + 2) \bmod d, \ldots, c_w = (c_1 + w - 1) \bmod d$ in a configuration with w wavelength routers. In this construction, the number of columns with a square that has a particular color is given by wh/d. We use this procedure to derive game boards for the multiple wavelength router constructions from a game board for a single wavelength router. Observe that the case of $w = d$ leads to a trivial construction where the number of wavelengths available to an input to reach an output is h and the switch is strictly non-blocking.

2.6.1 Upper bound

Theorem 2.6.1 *For any k-solvable game board on d colors, h columns, and w layers, $k \leq h - \frac{d}{w} + 1$*

The proof of this theorem is very similar to the proof of Theorem 2.4.2. Consider a game board constructed as described above with each row having wh/d squares containing some color blue. Each column has exactly wh squares that contain the color blue. If we consider any $i \leq \frac{d}{w} - 1$ columns, there can be at most iwh rows that have a square with color blue in any of these columns. Thus, there must be at least $(d - iw)h$ rows that do not contain squares with color blue in any of these columns. So, any puzzle setup that has blue tokens in more than $h - i$ of these rows is unsolvable. Thus, we cannot expect to construct a switch that will guarantee our ability to place more than $h - \frac{d}{w} + 1$ tokens of the same color.

2.6.2 Random game boards

Random boards resulted in good performance in the construction using a single wavelength router and we can expect them to give good performance in constructions using multiple wavelength router too. We construct a random game board by constructing a random game board for a single wavelength router and deriving the game board for the multiple wavelength router construction. Consider an arbitrary set of r rows within a single single block of a random game board. The probability that a particular column is not covered for some fixed color is

$$\frac{h-r}{h}\,\frac{h-r-1}{h-1}\,\cdots\,\frac{h-r-wh/d+1}{h-wh/d+1}=\frac{(h-r)^{\underline{wh/d}}}{h^{\underline{wh/d}}}$$

Thus, within one block, the expected number of columns not covered by r rows is

$$h\,\frac{(h-r)^{\underline{wh/d}}}{h^{\underline{wh/d}}}$$

The expected number of columns not covered by r rows selected from d independent random blocks in the game board is

$$\begin{aligned}
&= h\,\frac{(h-r_1)^{\underline{wh/d}}}{h^{\underline{wh/d}}}\,\frac{(h-r_2)^{\underline{wh/d}}}{h^{\underline{wh/d}}}\,.....\,\frac{(h-r_d)^{\underline{wh/d}}}{h^{\underline{wh/d}}}\\
&\leq h\left(\frac{(h-r/d)^{\underline{wh/d}}}{h^{\underline{wh/d}}}\right)^{d}
\end{aligned}$$

where $r=r_1+r_2+\ldots+r_d$, and r_i is the number of rows in the ith block of the game board. The expected number of columns not covered is plotted as a function of the size of the row set, r for $w=2$ in Fig. 2.20(a) and for $w=3$ in Fig. 2.20(a). Also, Fig. 2.20(c) shows the expected number of columns not covered as a function of the size of the row set for different values of w. For $d=8$ and $h=256$, the probability of a set of 70 rows or more not covering one column is less than one in a million for $w=2$ and the probability of a set of 45 rows or more not covering one column is less than one in a million for $w=3$. Thus, a switch with multiple wavelength routers will reduce the performance difference between the WGR-based switch and the strictly nonblocking switch.

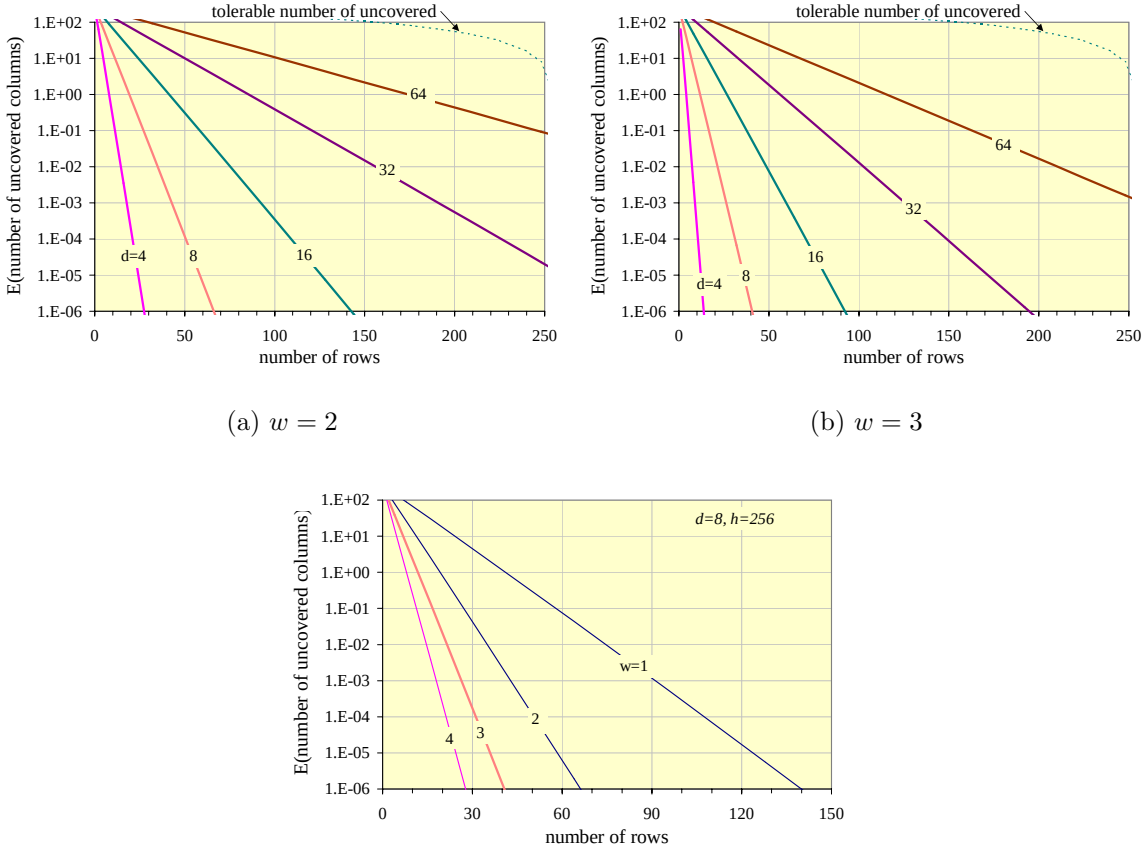

(a) $w = 2$

(b) $w = 3$

(c) $d = 8$

Figure 2.20: Number of columns covered by row sets of all sizes ($h = 256$)

2.6.3 Statistical multiplexing performance

The game version for this design is very similar to the game in the single wavelength router design. The only difference is that the setter places the token in a square on the game board such that the token's color is any of the colors used to color the square. We modify the approximate model presented in Section 2.5 for the single wavelength router design to model this design with multiple wavelength routers. Here too, we focus on tokens of a single color since the tokens of different colors are independent. We model the system by a birth-death process shown in Fig. 2.12, where the state index is the number of tokens placed on the game board. In this design with multiple wavelength routers, the transition rate from a state i to state $i + 1$ is different from the rate in the single wavelength router case because the probability of a token being placed is higher when there are more wavelength routers. The rate, λ_i, can be

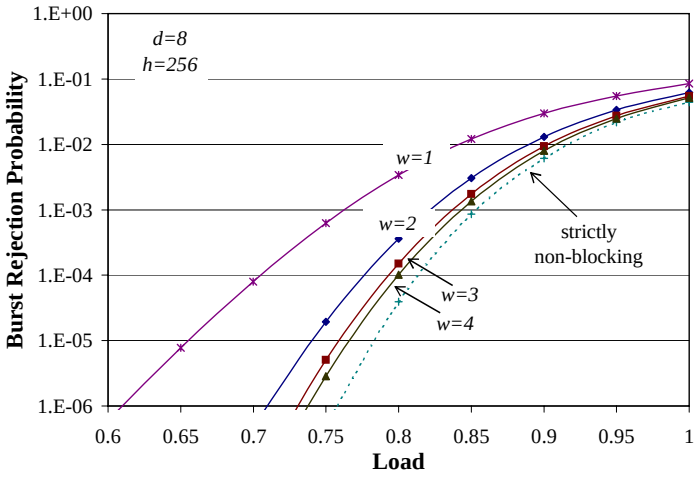

Figure 2.21: Burst rejection probabilities for different values of w ($d = 8$, $h = 256$)

approximated by

$$\lambda_i = \lambda \left(1 - \binom{h - wh/d}{i - wh/d} / \binom{h}{i}\right)$$

where w is the number of wavelength routers in each input section. Note that $\binom{h}{i}$ is the number of sets of columns that can be used by i tokens and $\binom{h-wh/d}{i-wh/d}$ is the number of column sets used by i tokens that would prevent placement of a new token.

If we let π_i be the steady state probability that the system is in state i, then it can easily shown that

$$\pi_i = \frac{\lambda_0 \lambda_1 \ldots \lambda_{i-1}}{i!\, \mu^i} \pi_0$$

Using $\pi_0 + \pi_1 + \ldots + \pi_h = 1$ and solving for π_0, we can determine the individual steady state probabilities. The burst rejection probability is then given by

$$P_{rejection}(\rho) = \sum_{i=h/d}^{h} \pi_i \binom{h - wh/d}{i - wh/d} / \binom{h}{i}$$

where ρ is the offered load to the system given by $\lambda/h\mu$ and $\binom{h-wh/d}{i-wh/d}/\binom{h}{i}$ is the probability of a burst being rejected in state i.

The burst rejection probabilities for varying numbers of wavelength routers for a system with $d = 8$ and $h = 256$ are shown in Fig. 2.21. For a system that uses two wavelength routers ($w = 2$), the throughput provided is 93.4% of the throughput of a strictly nonblocking switch and a system with three wavelength routers and four wavelength routers, the throughput provided is 96% and 97.3% respectively.

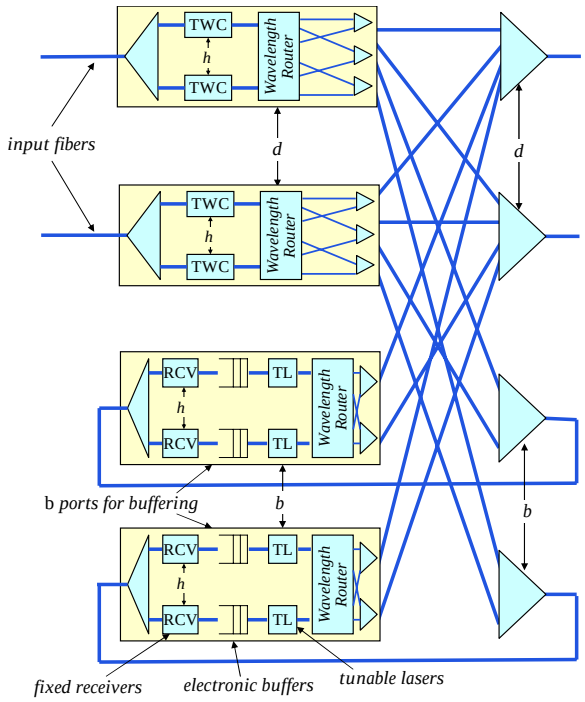

Figure 2.22: WGR-based switch with buffering ports

2.7 WGR-based switches with buffering

Buffering can be expected to improve the performance of the switch and this can bring down the performance gap between the WGR-based switch design and the strictly nonblocking switch further. Another extension to the basic switch design (Fig. 2.22) is to have a few ports that convert the optical signal back to electronic form and store them in buffers and transmit them using tunable lasers when the output ports become available. The input section of each input fiber now transmits signals to $d+b$ ports instead of d ports in the original design, where d is the number of input/output fibers and b is the number of buffering ports. The number of wavelengths each input can use to reach an output (or a buffering port) is $\lfloor h/(d+b) \rfloor$ and the few additional wavelengths are assigned to random outputs. At the input section of each buffering port, the signals are demultiplexed into the individual wavelength channels and then converted into electronic form using fixed optical receivers. The signals are then stored in electronic buffers, each of which can hold up to s bursts. Each buffering port has h buffers, one corresponding to each wavelength channel. Once a wavelength becomes available at the output, the signals are transmitted to the output ports using a tunable

laser through a wavelength router. Each electronic buffer has h/d wavelength channels to reach an output.

This form of buffering, commonly referred to as recirculation buffering, is attractive because the buffers can be shared by all the inputs and hence, the cost of adding additional ports is shared among all inputs (as opposed to adding buffers to each input). The addition of one buffering port requires h optical receivers, h electronic buffering units, h tunable lasers, a wavelength router, and the optical multiplexors and demultiplexors for the interconnection between the input and the output sections. The performance gains due to the addition of the buffering ports must justify this cost. Assuming that a channel in the buffering port is as expensive as a channel in the input section of the switch, the increase in cost can be estimated as b/d times as much as the cost of the switch without buffering. For a system with $d = 8$, the addition of one buffering port increases the cost of the system by 12.5% and the addition of two buffering ports increases the cost by 25% approximately.

The game formulation does not capture the dynamics of the routing process effectively and so, we do not describe the routing problem using the game formulation. However, the game board structure can still help us understand the routing issues involved in the switch.

In this case, the game board of the switch is constructed as follows. The routing matrix has $d+b$ blocks, each having $h \times h$ squares. The first d blocks correspond to the d input/output fibers and the last b blocks correspond to the buffering ports. Each row in the first d blocks represents an input of the switch, each column corresponds to a wavelength channel. The squares in the rows of the first d blocks are colored using one of $d + b$ colors, where the first d colors correspond to the output ports and the next b colors correspond to the buffering ports. There are $\lfloor h/(d + b) \rfloor$ squares of each color in each row. The remaining $h \bmod (d+b)$ squares are assigned to randomly chosen colors. The routing matrix, also, has the constraint that each row within a block is derived by circularly shifting the previous row to the left by one square. The squares in the rows of the last b blocks, corresponding to the buffering ports, are colored in the same manner as squares in a game board with no buffers. The squares of each row in a block corresponding to a buffering port are colored using one of the d colors corresponding to the outputs. An example game board for a switch with $d = 2$, $h = 8$, and $b = 1$ is shown in Fig. 2.23.

Each input has at least $\lfloor h/(d+b) \rfloor$ wavelengths to reach an output and another $b\lfloor h/(d + b) \rfloor$ wavelengths to reach buffering ports if the burst cannot be routed to

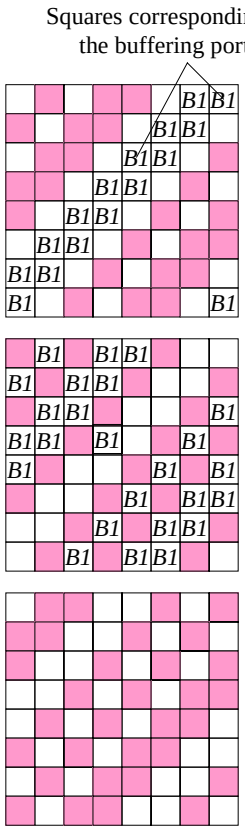

Figure 2.23: Game board of a switch with $d = 2$ and $h = 8$ and one buffering port, $b = 1$

the output directly. Each row in the last b blocks represents a buffer in the buffering ports and each buffer in the buffering port has h/d wavelengths to reach an output.

In terms of the burst switch, this implies that whenever an incoming burst does not have a wavelength that is available, the burst is routed to a buffering port. If the burst cannot be routed to a buffering port, the burst is dropped. The burst is stored electronically in buffers in the buffering port. It is then transmitted from the buffer to the output port when a wavelength channel that routes the burst to the output becomes available. Note that we can buffer up to s bursts in each buffer. When there is more than one burst in a buffer, head of line blocking can reduce the performance of the switch. If the first burst in a buffer is destined to some output and no wavelength is available to send the burst to the output, the second (and the subsequent) burst in the buffer cannot be sent even though it could have been sent had it been in the front of the queue. This problem can be solved using virtual output queues to store the bursts, where each burst is stored in a separate logical queue corresponding to the outputs in the buffer. Thus, even if a burst destined to some output cannot be sent,

bursts to other outputs can still be sent. The use of virtual output queues has been studied extensively in the context of crossbar scheduling. Using virtual output queues increases the information needed to route and forward bursts through the switch and increases the average processing time needed per burst. In this study, we do not use virtual output queues. Instead, we forward the bursts in the buffers in a first in first out order.

By adding buffering ports, the number of wavelengths available to an input goes up to $\lfloor h/(d+b) \rfloor + b\lfloor h/(d+b) \rfloor$, including the wavelengths used to route bursts to buffering ports. However, we reduce the number of wavelengths an input can use to route bursts to an output directly from h/d to $\lfloor h/(d+b) \rfloor$. Also, while routing bursts from the buffering ports to an output, the wavelength used cannot be used by other inputs. The performance gain due to buffering needs to be greater than the performance reduction due to the increased blocking in the switch to justify the addition of buffering ports.

2.7.1 Extra ports for routing as a special case of buffering

A special case of using extra ports is one that has no electronic buffers in the buffering ports ($s = 0$, where s is the number of bursts that can be stored in a buffer). Instead, the extra ports are used to provide additional routing paths to outputs. We refer to these extra ports as *rerouting ports*. Each rerouting port has h *rerouting channels*, one for each wavelength channel and each rerouting channel has a tunable wavelength converter instead of the fixed receiver, the electronic buffer, and the tunable laser. The tunable wavelength converter is used to retune the signal to another wavelength and transmit the signal through a wavelength router. The rerouting ports provide us with another stage of routing within the switch. If an input needs to transmit a burst to some output and no wavelength is available to transmit the burst directly, we determine a rerouting channel, that is not already in use, in some rerouting port such that a wavelength is available to send the burst from the input to the rerouting channel and a wavelength is available to send the burst from the rerouting channel to the output. If such a rerouting channel exists, we route the burst to the output through this rerouting channel. Otherwise, we drop the burst.

Each input has $\lfloor h/(d+b) \rfloor$ wavelengths to reach an output directly. In addition, it has $b\lfloor h/(d+b) \rfloor$ wavelengths to reach rerouting channels in the rerouting ports and each rerouting channel has h/d wavelength channels to reach the output. The game

board is constructed exactly as in the case with buffers. A rerouting channel is a row in the block corresponding to the rerouting ports. If the square in column j of some input row i is colored k, where k corresponds to a rerouting port, a burst transmitted on wavelength channel j from input i is routed through the jth rerouting channel in rerouting port k.

Definition 2.7.1 *A rerouting channel j in rerouting port k is said to be* accessible *to a row i in the game board if it has a square in column j of row i that is colored k.*

A column w is said to be accessible *to some row i for a color o in the game board if there exists a square in column w of row j in some block k that is colored o such that row j in block k is accessible to row i.*

For a switch, whose game board is shown in Fig. 2.23, the row $(6, 2)$ in block 2 corresponding to a rerouting channel in the rerouting port is *accessible* to row $(0, 0)$ because column 6 of the row $(0, 0)$ in the game board is colored with the rerouting port's color. Also, column 7 is *accessible* to row $(0, 0)$ through the rerouting channel $(6, 2)$ to reach the output corresponding to the dark colored squares. Note that column 7 is not directly available to row $(0, 0)$ to reach the output.

Definition 2.7.2 *A row i is said to* directly cover *a set of columns for color o if the set of columns have a square of color o in row i.*

The cover *of a row i for some output o is defined as the set of columns in the game board that have an o-colored square in row i or have an o-colored square in row r, where r is an accessible rerouting channel of input i.*

The cover of a set of rows, R, is defined as the union *of the covers of each of the rows contained in R.*

In other words, the *cover* of an input is the union of the set of wavelength channels that it covers directly and the set of wavelength channels that are accessible to it through rerouting channels. A good switch construction is one that maximizes the cover of the input channels to all outputs.

Random game boards

As in the game board constructions without buffering ports, a random routing matrix is a natural choice for switches with rerouting ports (or buffering ports). Assuming a random routing matrix construction, we now derive the average number of columns

covered by a set of rows. Consider $r = r_1 + r_2 + \ldots + r_d$ rows, where r_i is the number of rows in the ith block of the game board. In any row, the number of squares that belong to an output is given by $\lfloor h/(d+b) \rfloor$. We ignore the $h \bmod (d+b)$ squares that are assigned to random inputs. These squares increase the routing capability within the switch and hence, the average number of columns covered is more than estimated by this analysis. Denote the number of accessible rerouting channels of a set of r rows that belong to a rerouting port by c_b. The columns covered by these rerouting channels for some color give us the accessible columns of the set of rows.

The number of rerouting channels that are accessible to any row is given by $\lfloor h/(d+b) \rfloor$. We can show that the expected number of accessible rerouting channels of a set of r rows for one rerouting port is

$$c_b \leq h - h \left(\frac{(h - r/d)^{\underline{x}}}{h^{\underline{x}}} \right)^d$$

where $x = \lfloor h/(d+b) \rfloor$. This result can be obtained by using the equations derived in Section 2.4.3 and using $\lfloor h/(d+b) \rfloor$ instead of h/d as the number of columns available to an input.

The probability that rows in a rerouting port, that are accessible to the set of input rows, miss a column is given by

$$\frac{(h - c_b)^{\underline{h/d}}}{h^{\underline{h/d}}}$$

Equivalently, this is the probability that a column is not accessible to the set of input rows through rerouting channels.

The probability that the input rows miss a column is given by

$$\leq \left(\frac{(h - r/d)^{\underline{x}}}{h^{\underline{x}}} \right)^d$$

Thus, the expected number of columns that are neither covered by the r rows directly nor are accessible through rerouting channels is given by

$$\leq h \left(\frac{(h - r/d)^{\underline{x}}}{h^{\underline{x}}} \right)^d \left(\frac{(h - c_b)^{\underline{h/d}}}{h^{\underline{h/d}}} \right)^b$$

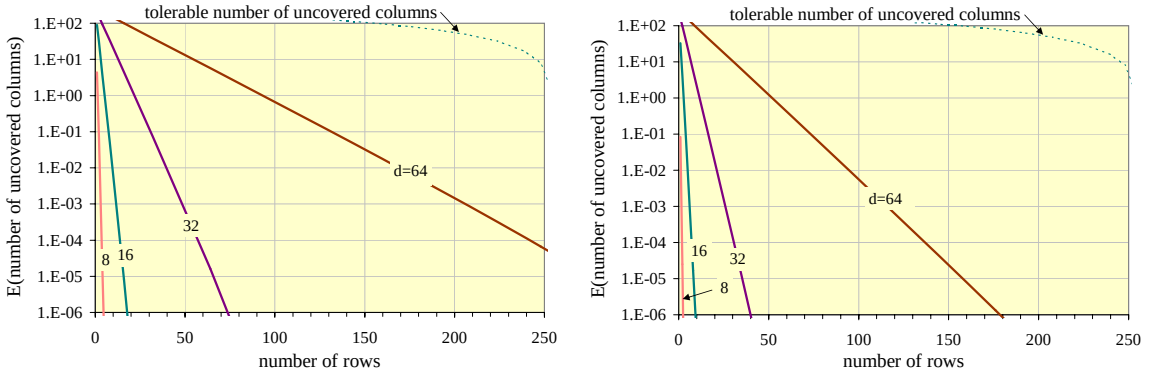

Figure 2.24: Number of columns not covered by row sets of all sizes for (a) $b = 1$ and (b) $b = 2$ ($h = 256$)

The expected number of columns that are not covered is plotted as a function of the size of the row set r in Fig. 2.24 for one and two extra ports respectively. The number of columns not covered is dramatically decreased because of the rerouting ports. For $d = 8$, the probability that about 5 rows miss one column is one in a million with one rerouting port and the probability that about 3 rows miss one column is one in a million with two rerouting ports. Thus, the addition of rerouting ports dramatically increases the available routing options for large values of h/d. Also, the number of columns not covered for small values of h/d ($d = 32$ or 64) is reduced drastically. Thus, adding rerouting ports is an effective method of increasing the performance of the switch without increasing the cost by much.

2.7.2 Performance of random game board constructions with buffering

Next we study the performance of the switch with buffering ports or rerouting ports in a burst switching scenario. To study the performance, we use random routing matrices for values of $d = 8$, $h = 256$, and one and two buffering (or rerouting) ports. We simulate the system for independent burst arrivals with exponentially distributed interarrival times and exponentially distributed burst lengths with each burst assigned to a random output fiber. We simulated the system for different burst store sizes, s.

In the case with buffering, we select the first available wavelength to transmit the burst to an output. If no wavelength is available to send the burst, we select the

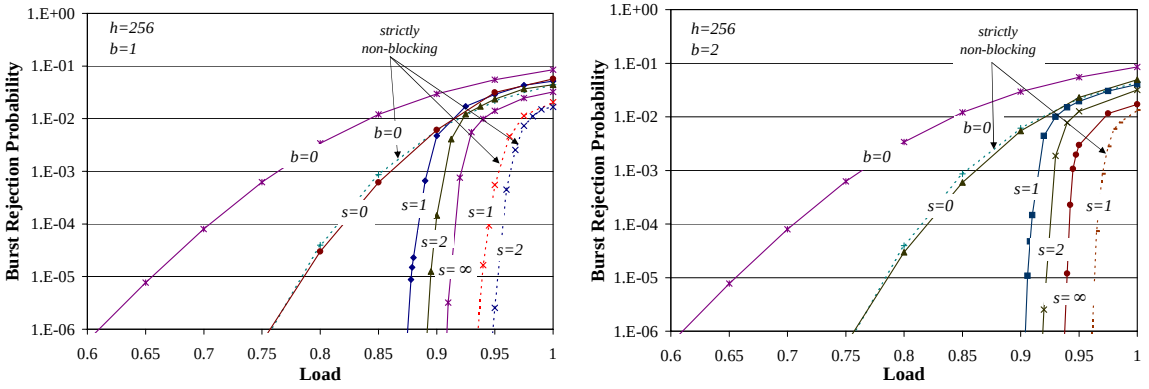

(a) (b)

Figure 2.25: Burst rejection probabilities of random game boards for (a) $b = 1$ and (b) $b = 2$ ($d = 8$, $h = 256$)

first wavelength that selects a buffer that has not exceeded its storage capacity to send the burst to. At the buffer, we select the first available wavelength to send the burst to the output. In the case of rerouting, we select the first available wavelength to transmit the burst to an output. If a wavelength is not available to send the burst, we select the first wavelength that selects a rerouting channel that has a wavelength channel available to send the burst to the output.

The burst rejection probabilities for a system with one buffering port are shown in Fig. 2.25(a) and for a system with two buffering ports in Fig. 2.25(b). The case $s = 0$ represents the switch when the extra ports are used as rerouting ports. Also, shown are the results for a system with no buffering or rerouting port ($b = 0$). The burst rejection probabilities for a strictly non-blocking switch with and without buffering are indicated by the dashed curves.

Note that with just one rerouting port with no electronic buffers, the performance of the switch matches the performance of a strictly nonblocking switch with no buffering. This is in accord with the earlier result that even a set of 5 rows covers the entire set of 256 columns with a very high probability. For a burst rejection probability of 10^{-6}, the throughput of a system with one buffering port and burst store sizes of $s = 1, 2$, and ∞ are 115%, 117%, and 119% of the throughput of a strictly non-blocking switch with no buffering respectively. A strictly nonblocking switch with one port of buffering and burst stores of $s = 1$ and 2 has a throughput of 122% and 125% of the throughput of a strictly nonblocking switch with no buffering respectively. For

a WGR-based switch with two ports of buffering and burst stores of $s = 1, 2$, and ∞, the throughput of the switch is 118%, 121%, and 123% of the throughput of a strictly nonblocking switch with no buffering. A strictly nonblocking switch with one buffering port and $s = 1$ has a throughput of 160% of a strictly nonblocking switch with no buffering. Since the increase in cost of the switch with the addition of one buffering port and two buffering ports is 12.5% and 25%, the addition of one buffering port for this system results in a performance gain that best outweighs the cost increase.

2.8 Conclusion

Wavelength converting switches are essential components needed to build optical burst switches. We have studied two wavelength converting switch designs in this chapter. The first uses tunable wavelength converters in combination with optical crossbars to switch the bursts to the output fibers. The use of wavelength converters and optical crossbars make this design relatively expensive. The second design replaces the optical crossbars with wavelength grating routers. This design is attractive because wavelength grating routers are passive components and are hence, relatively inexpensive.

The use of wavelength grating routers, however, results in some blocking in the switch. Although the blocking nature of these switches results in higher burst rejection probabilities, the performance penalty is small enough to make them a viable alternative. By formulating the routing problem as a combinatorial puzzle or game, we have been able to develop insights that facilitate the analysis and design of WGR-based switches. We have shown that the problem of solving the puzzle can be reformulated as a matching problem in a bipartite graph. Also, an average case analysis shows us that we can almost always solve the puzzle. Further, we have shown some basic limits to the nonblocking potential of WGR-based switches and have also shown that by selecting the permutation patterns appropriately, one can greatly improve their performance. Simulation results show that in practical switch system configurations, routers using WGR-based switches can achieve more than 87% of the throughput of routers using strictly non-blocking switches.

Our simulations also showed that if we allow bursts to be reassigned to different wavelength channels during transmission, the performance of the WGR-based switch matches the strictly non-blocking one almost exactly. We then presented the *most available* wavelength assignment algorithm and studied its performance in the

switch. We noticed that this algorithm improved the throughput of the switch using the contiguous permutation pattern. However, it did not yield significantly better performance for the randomized permutations. Using this algorithm, WGR-based switches can achieve 89% of the throughput of routers using strictly non-blocking switches.

A design option to make the performance of the switch better is to use multiple wavelength routers in place of one in the input sections of the switch. We showed that a system with two wavelength routers can achieve more than 93% of the throughput of a strictly nonblocking switch and a system with three wavelength routers can achieve 96%.

Another design option is to use buffering to store bursts when they are blocked. We do this by adding a few buffering ports to the switch and routing the bursts to these ports when a burst cannot be routed to the desired output fiber. The burst is then transmitted from the buffering port to the output when a wavelength channel becomes available. We showed that with one buffering port, the switch achieves 115 to 119% of the throughput of a strictly nonblocking switch depending on the amount of burst storage available. The extra ports can also be used as an extra stage of routing and having no buffers. This greatly increases the available routing options and performs comparably to a strictly nonblocking switch even with one extra port when the total number of ports is 8 and the number of wavelength channels is 256.

2.9 Future Work

There are several ways in which we can augment the switch to provide additional functionality.

A simple method to augment the switch with multicasting capability is to use the electronic buffers in buffering ports to perform the multicasting. The electronic buffers can make copies of the burst and send the bursts sequentially to the output ports. The performance of the switch needs to be studied, since the extra load added by the multicast traffic will increase the number of buffering ports needed to achieve the required performance.

The wavelength assignment algorithms that we studied in this chapter were for a system that forwards bursts in a first come first serve order. For a switch that needs to support Quality of Service guarantees for flows, the scheduling algorithm must be modified to support it.

Limited range TWCs are a cheaper alternative to full range ones. The use of limited range TWCs potentially increases the blocking within the switch further. The game board configuration also changes because of the use of limited TWCs. An analysis of the performance of this switch would help us evaluate its effectiveness for burst switching.

Reference [52] describes a switch fabric for electronic routers that uses an optical switch based on tunable wavelength lasers and wavelength grating routers. The size of the WGR used places a limit on its scalability. The WGR-based switch design described in this dissertation with tunable lasers instead of tunable wavelength converters could be used to scale the capacity of that switch fabric. If this were done, the scheduling algorithm used in the router would need to be changed to accommodate this switch because of its blocking nature.

Chapter 3

Time Sliced Optical Burst Switching

Time Sliced Optical Burst Switching is a proposed variant of optical burst switching, in which switching is done in the time domain, rather than the wavelength domain. Fig. 3.1 illustrates the concept of a time-sliced optical burst switched network. Switches are connected with WDM links with multiple wavelength channels carrying data. The information sent on each wavelength is organized into a series of *frames*, each of which is sub-divided into fixed length *timeslots*. Terminals and/or other networks connect to a TSOBS network through concentrators that convert data on lower speed interfaces (e.g. IP-over-Ethernet at 100 Mb/s or 1 Gb/s), to the TSOBS data format. Concentrators transmit user data bursts in time-division channels. The control information needed to switch the data bursts is sent in *Burst Header Cells* (BHC), which are carried on separate control wavelengths. A given fiber optic link may contain multiple control wavelengths. If the ratio of the expected burst length to the BHC length is L, each link will require about one control wavelength for every $L - 1$ data wavelengths. Concentrators may switch packets received on low speed interfaces as single bursts in the TSOBS network, or may aggregate packets to form larger bursts. The issue of aggregation is addressed in detail in the following chapter.

The switching of data bursts through a TSOBS network is done entirely in the optical domain. Space-division optical switches are dynamically configured to switch the data from incoming timeslots to timeslots on the appropriate outgoing links. This is done using carefully-timed switching operations to transfer user data bits from input links to output links. Switching a timeslot may involve delaying the data, to shift it from one timeslot position to another. Frames transmitted on different wavelengths

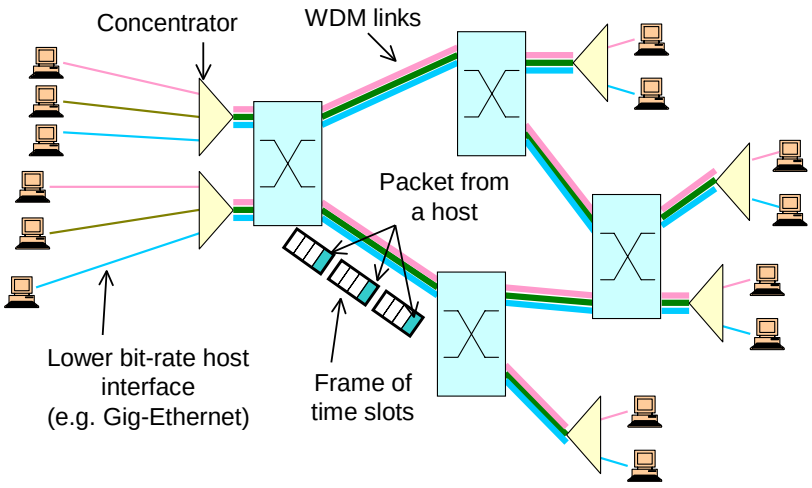

Figure 3.1: Time sliced optical burst switched network architecture

are synchronized with one another, allowing the timing of switching operations on the data wavelengths to be determined from the frame timing on the control wavelengths.

Solid-state optical switches can perform switching operations with a precision of 10 ns or less. To allow for timing uncertainties, timeslots must be separated by a *guard time* of at least 10 ns and possibly as large as 100 ns. To achieve reasonable data transmission efficiencies, timeslot durations should be at least ten times the guard time, or 100 ns to 1 μs. A 1 μs time slot would allow roughly 1100 bytes of user data to be sent in a single time slot, assuming a transmission rate of 10 Gb/s per wavelength, or 4400 bytes of user data, assuming a transmission rate of 40 Gb/s. With a 1 μs timeslot duration and 40 Gb/s transmission speeds, a system with 350 timeslots per frame would support an individual channel rate of about 100 Mb/s. This would correspond to a frame duration of 350 μs. This is the maximum period that a timeslot would have to be delayed when passing through a TSOBS router. By contrast, a conventional router may have to delay data by hundreds of milliseconds in order to provide acceptable performance, requiring very large amounts of data storage. Of course, a shorter timeslot duration or a smaller number of timeslots per frame would allow this maximum delay for a TSOBS router to be reduced proportionally.

In a large TSOBS network, bursts may pass through many hops before reaching their destination, leading to excessive degradation of the optical signal [84]. To avoid the need for strict limits on the number of hops and/or the distance traveled by bursts, we provide for periodic regeneration of bursts. This is done by including fields in the BHC, which record the distance traveled by a burst since its last regeneration

and the number of optical switching operations that the burst has been subjected to since its last regeneration. This information can be used to regenerate bursts *as necessary*, as they pass through a large network. Each switch includes some small number of either all optical or opto-electronic regeneration circuits that bursts can be passed through when regeneration is needed. If bursts can travel through an average of ten or more routers before requiring regeneration, TSOBS could achieve a decisive cost advantage over electronic routers. Since each switch operation that a burst is subjected to attenuates the signal and adds noise, it is important to minimize the number of switching operations required by each router. The number of switching operations is hence a key metric for TSOBS router designs.

3.1 Statistical multiplexing performance

The statistical multiplexing performance of a TSOBS network is determined primarily by the number of timeslots per frame. A simple case of a TSOBS switch is a multiplexor that corresponds to a $S \times 1$ switch receiving bursts from S input channels that can be accommodated by a single timeslot. If the multiplexor assigns each arriving burst to the first available outgoing timeslot, the multiplexor operates like an M/D/1 queueing system with a buffer capacity of N, where N is the number of timeslots per frame.

Fig. 3.3(a) shows the burst discard probabilities for a multiplexor with various values of N. Notice that the discard probability drops very quickly with N, but increases beyond a certain point yielding diminishing returns. 32 timeslots is sufficient to maintain a discard probability of 10^{-6} at an offered load of about 83%. Doubling N increases the load at which this target discard probability is reached to about 92%. While increasing the number of timeslots per frame improves the statistical multiplexing performance, this improvement comes at the cost of longer frame

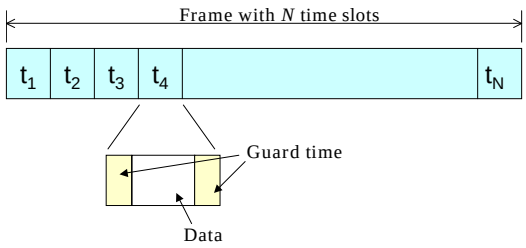

Figure 3.2: Format of a frame and a time slot within it

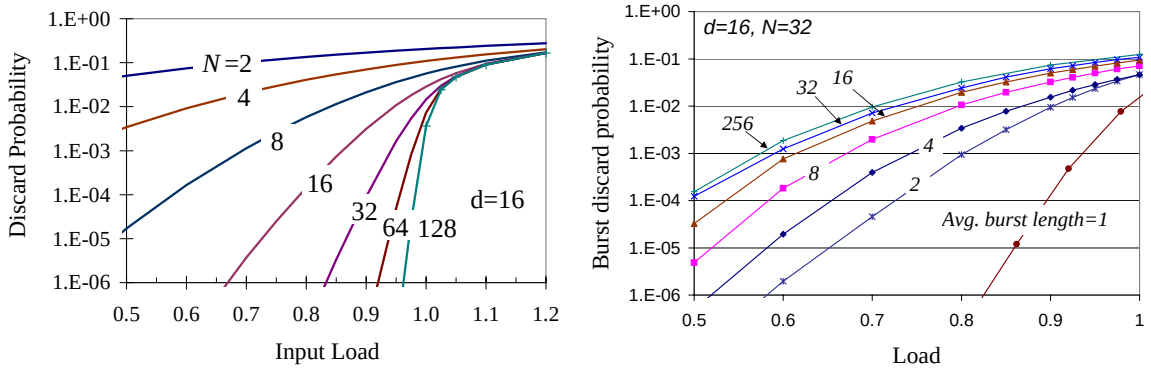

(a) (b)

Figure 3.3: (a) Burst discard probability for a system with 16 sources and different frame times (N)s; (b) Burst discard probability for varying average burst lengths for a system with frame size of $N = 32$

durations, which translates to larger optical buffering requirements. This illustrates the central trade-off for TSOBS networks. In Section 3.4 we look in more detail at the performance of a TSOBS router, using simulation. Variable length bursts lead to higher discard probabilities, but the number of timeslots per frame remains the key determinant of performance. Fig. 3.3(b) shows the burst discard probabilities with varying average burst length in time slots. We can see that the performance of the system rapidly degrades with increasing burst lengths. Thus, we need to keep the average burst lengths small to achieve good performance. However, if we try to reduce the average burst length, the number of bursts that are transmitted increases. This leads to an increase in the amount of control information sent (in the form of burst header cells). So, there is a tradeoff between reducing the average burst length and the amount of control information that the network can handle.

TSOBS has been designed to make wavelength conversion unnecessary. At the same time, the overall architecture does not preclude the switching of bursts to different wavelengths, should wavelength conversion become inexpensive enough to make this practical.

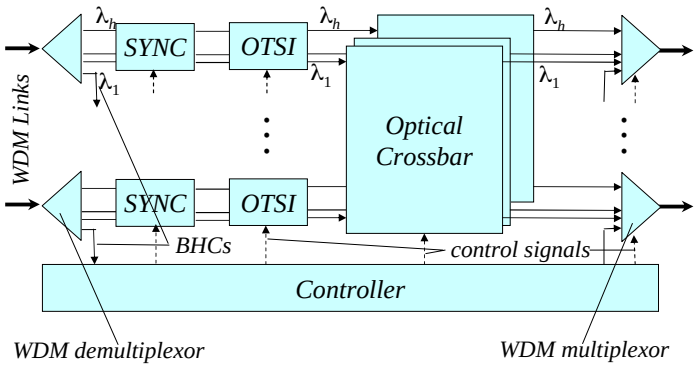

Figure 3.4: The overall Time-Sliced Optical Burst Switch design

3.2 Switch architecture

3.2.1 Overview

Fig. 3.4 shows the overall design for a TSOBS router. Each incoming WDM link terminates on a *Synchronizer* (SYNC) which synchronizes the incoming frame boundaries to the local timing reference. This is done using variable delay lines, with feedback control of the delays being provided through the system controller. The synchronizers are followed by Optical Time Slot Interchangers (OTSI), which provide the required time domain switching for all wavelengths. The OTSIs also separate the control wavelengths carrying the BHCs and forward those to the system controller. In addition the input OTSIs separate the data wavelengths and forward these on separate fibers to each of a set of Optical Crossbars at the center of the diagram. The crossbars perform the required space division switching operation. These are followed by a set of passive optical multiplexors, which combine the data wavelengths with the control wavelengths (carrying the outgoing BHCs) on the output fibers. The controller uses the information in the BHCs to make switching decisions and generates electronic control signals which are used to control the operation of the OTSIs and the crossbars.

Fig. 3.5 shows a high level design for one of the OTSIs. Each OTSI contains a set of optical crossbars for switching timeslots among the inputs, outputs and a set of delay lines. The signals are demultiplexed to perform the switching operations and re-multiplexed onto the delay lines, allowing the cost of the delay lines to be shared by the different wavelengths. The number of delay lines and the choice of delay line values are key design parameters, significantly affecting both the cost and performance of the OTSI.

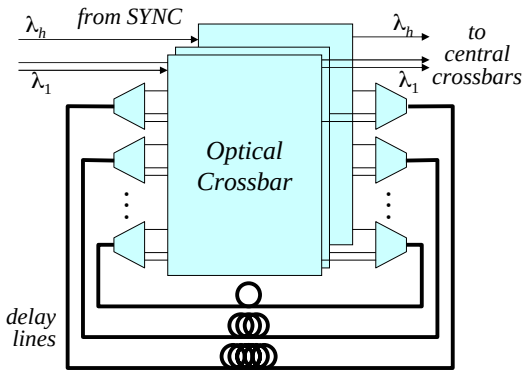

Figure 3.5: Optical Timeslot Interchanger

Another factor that determines a good OTSI design is the average number of times a burst gets switched within the OTSI. Each time a burst gets switched through the crossbar, the optical signal quality degrades. Thus, the most suitable OTSI design is one that also minimizes the average number of switching operations performed on each burst.

The complexity of the scheduling operation to switch a burst onto an outgoing timeslot plays an important part in the design of OTSIs. Longer burst sizes lessen the burden on the control subsystem because the number of burst header cells that require processing is smaller. However, longer bursts lead to a reduction in the statistical multiplexing performance of the switch. Thus, the control subsystem should be able to handle smaller bursts. Consider a switch with 16 input and output fibers, 128 wavelengths per fiber, 10 Gbps capacity per wavelength channel, a timeslot duration of 1μs, and an average burst length of 10 timeslots (or 100 kilobit average burst size, assuming 100% data efficiency of the time slots). When the incoming channels are fully loaded, we need to process up to 16 burst header cells every 10μs (one BHC for each port) for each wavelength. Since the scheduling of different wavelength channels are independent, we can use parallelism to obtain the necessary performance.

3.2.2 Nonblocking OTSIs

We can classify OTSI designs as either blocking or nonblocking. While nonblocking designs provide the best performance, they are significantly more expensive than blocking designs. We start with the conceptually simplest nonblocking design, which has N delay lines with a delay value equal to the duration of one time slot. With this design, each incoming timeslot i can be delayed by d timeslot intervals by recirculating

it through the ith delay line d times. Since each timeslot is assigned to a separate delay line, there are no conflicts, hence the design is nonblocking. It also uses the smallest possible total delay line length (N, where the unit is the distance light propagates in one timeslot interval). Unfortunately, it requires a large number of separate delay lines (N) and large optical crossbars ($(N+1) \times (N+1)$). The optical crossbars are a particular concern since their cost grows as the product of the number of inputs and outputs. Finally, the design can subject a signal to up to N optical switching operations, causing excessive degradation to the optical signal quality, when N is large. This last fault can be corrected by replacing the delay lines of length 1, with delay lines of length $1, 2, \ldots, N$. This allows each timeslot to be switched through just a single delay line, reducing the number of switching operations to 2. Of course, it comes at the cost of increasing the total delay line length from N to approximately $N^2/2$.

A more practical nonblocking switch design uses delay lines of length 1, 2, 3,...,$(A-1)$, where A is an integer parameter, plus additional delay lines of length A, $2A$, $3A$,...,$(B-1)A$ time slots, where B is a second integer parameter. We call these two sets of delay lines the *short delay lines* and the *long delay lines*. Let us suppose a time slot has to be delayed by a value of T time slots. T can be expressed as a sum, $k_2A + k_1$, where $k_1 \in [0, A)$ and $k_2 \in [0, B)$. To delay the time slot by T, we pass the data through the long delay line of length k_2A and then pass it through the short delay line of length k_1. The maximum we can delay a signal using this configuration is $(B-1)A + (A-1)$ and since the maximum delay needed is $N-1$, this gives us the relation $AB \geq N$. The number of delay lines in this design is $A + B - 2$ and hence, choosing $A = B = \lceil \sqrt{N} \rceil$ gives us the minimum number of delay lines. It can be easily seen that these values of A and B generate all values between 0 and N because k_1 and k_2 are the digits of T when expressed in base $\lceil \sqrt{N} \rceil$ notation.

We next show that this design is nonblocking. Consider any two input timeslots i and j that are to be delayed by amounts d_i and d_j, where $i + d_i \neq j + d_j$. Suppose first that $\lceil d_i/A \rceil = \lceil d_j/A \rceil$. Then both time slots will pass through the same long delay line, but since they arrive at different times, they will emerge from the delay line at different times. Hence, they cannot conflict with each other when entering a short delay line. Since $i+d_i \neq j+d_j$, they must emerge from the short delay lines at different times, ensuring no conflict at the output. Now suppose that $\lceil d_i/A \rceil \neq \lceil d_j/A \rceil$. In this case, the time slots may emerge from their respective long delay lines at the same time, creating a potential conflict if they must be switched to the same short delay

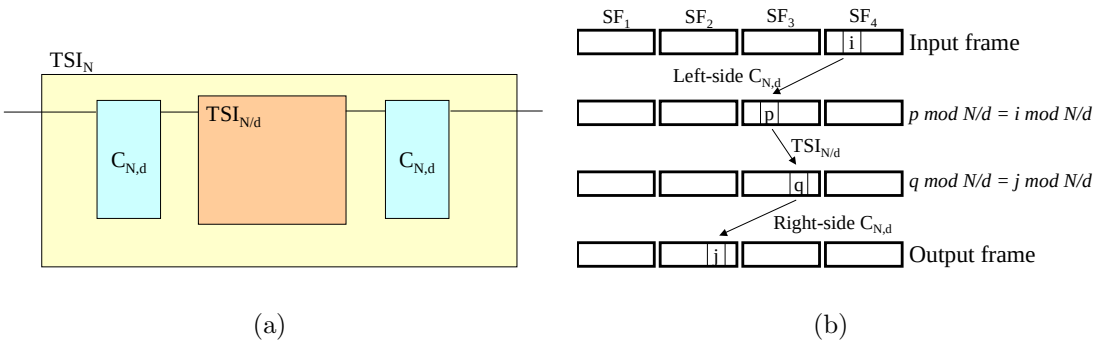

(a) (b)

Figure 3.6: (a) Recursive TSI design; (b) Recursive switching of time slots

line. However, such a conflict can only occur if $i + d_i = j + d_j$, contradicting the condition on the overall delays. Hence, the design is nonblocking, assuming timeslots are always switched first through a long delay line, then through a short delay line.

The size of the crossbar required for this design is $(2\lceil\sqrt{N}\rceil - 1) \times (2\lceil\sqrt{N}\rceil - 1)$ (31×31 for $N = 256$) and the length of the fiber required is $N\lceil\sqrt{N}\rceil/2$ (2,048 when $N = 256$). Thus, we have reduced the size of the crossbar at the expense of increased fiber length, relative to the first design. This design also limits the number of switching operations that a timeslot is subjected to, to at most three. Also note that it is very easy to determine the switching operations needed to switch a timeslot.

Rearrangeably nonblocking TSI design

References [59] and [64] describe a timeslot interchanger design that is *rearrangeably nonblocking* meaning that it can be configured to permute a set of N timeslots in an arbitrary way, assuming that the required permutation is given in advance. For different permutation patterns, the switch is configured in different ways. In a TSOBS network, packets arrive at a switch at arbitrary times. In a rearrangeably non-blocking switch, we may need to reroute existing connections within the switch to accommodate a new connection. This is not possible in a TSOBS network. Thus, the packet has to be dropped even though an output timeslot is available. The design described in Reference [64] is suitable for systems that use 2×2 size crossbars. We present an extension of this design for larger sized crossbars.

The TSI is constructed in a recursive fashion as shown in Fig. 3.6(a). A TSI for a system in which each frame carries N time slots, TSI_N, is constructed by combining a pair of "coarse-grained" switching operations with a "fine-grained" switching

operation using an N/d timeslot TSI, $TSI_{N/d}$. The coarse switching operations are done using a pair of *time slot classifiers*, $C_{N,d}$. The incoming frame is split into d sub-frames of N/d time slots each and the classifiers switch any time slot from one sub-frame to another such that the position of the time slot in the input sub-frame is same as the position in the output sub-frame. The N/d timeslot TSI switches on the basis of these sub-frames.

To switch a signal from input time slot i to output time slot j, we select a sub-frame f and configure the left classifier to switch input time slot i to time slot $i \bmod N/d$ of sub-frame f. Similarly, we configure the right classifier to switch to output time slot j from time slot $j \bmod N/d$ of sub-frame f. To complete the operation, the $TSI_{N/d}$ is configured to switch from input time slot $i \bmod N/d$ to output time slot $j \bmod N/d$ in sub-frame f. This is illustrated in Fig. 3.6(b). Suppose we want to switch time slot i in sub-frame SF_4 to time slot j in sub-frame SF_2, we select an intermediate sub-frame, SF_3, to switch this slot to. Time slot i is switched to time slot p by the left classifier such that $i \bmod N/d = p \bmod N/d$ and p is in SF_3 . Time slot p is switched to time slot q within that sub-frame by the smaller TSI, such that $q \bmod N/d = j \bmod N/d$. Finally, time slot q is switched to time slot j by the right classifier.

Notice that two input time slots i_1 and i_2 can be switched into the same sub-frame by a classifier only if $i_1 \bmod N/d \neq i_2 \bmod N/d$. Similarly, at the output of the TSI, two time slots j_1 and j_2 can be switched from the same sub-frame only if $j_1 \bmod N/d \neq j_2 \bmod N/d$. So, to perform a set of time slot switching operations, we must select mutually compatible sub-frames in order to allow the switching operations to take place. Consider the example shown in Fig. 3.7(a). The input frame's time slots 1, 5, 9, and 13 are at the same relative positions within a sub frame and thus, need to be switched into different outgoing frames at the left classifier. Similarly, the output time slots 1, 15, 16, and 3 are at the same relative positions within a sub-frame and thus, need to arrive from different sub-frames.

The *sub-frame assignment problem* can be stated as follows. Given a set of switching operations (x_1-y_1), (x_2-y_2),...,(x_N-y_N), where x_i corresponds to input time slots and y_i corresponds to output time slots, and integer d, assign a sub-frame SF_i to (x_i-y_i) such that:

$$SF_i = SF_j \quad \text{only if} \quad x_i \bmod N/d \neq x_j \bmod N/d, \text{ and} \tag{3.1}$$

$$y_i \bmod N/d \neq y_j \bmod N/d \tag{3.2}$$

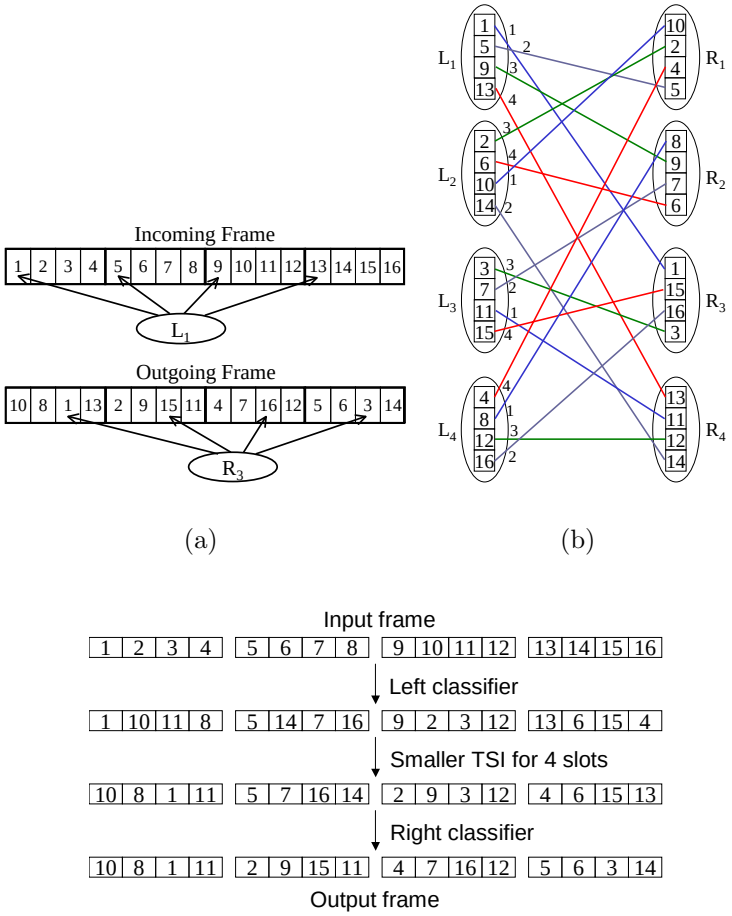

Figure 3.7: (a) Example permutation of the incoming frame (for $N = 16$ and $d = 4$); (b) Bipartite coloring problem to determine how to switch time slots; (c) The output time slots after each stage in the TSI

The problem of finding a compatible set of sub-frame assignments can be formulated as a bipartite graph edge coloring problem. To solve this, define a bipartite graph with two sets of vertices, $\{L_1, L_2, ...L_{N/d}\}$ (the "left" vertices) and $\{R_1, R_2, ...R_{N/d}\}$ (the "right" vertices). The graph has an edge from $L_{x_i \bmod N/d}$ to $R_{y_i \bmod N/d}$ for each connection (x_i,y_i). Note that each vertex has at most d edges incident to it. So, we can use standard edge coloring methods to assign 1 of d colors to each edge in such a way that no two edges incident to the same vertex are assigned the same color. If some color k is assigned to an edge that corresponds to a connection (x_i,y_i), then we select SF_k as the intermediate sub-frame to switch x_i into. If

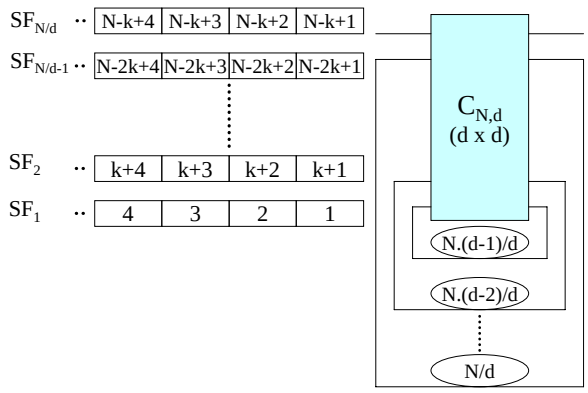

Figure 3.8: Implementation of the Classifier (here $k = N/d$)

$x_i \bmod N/d = x_j \bmod N/d$, then the two edges corresponding to (x_i-y_i) and (x_j-y_j) are adjacent to the same vertex, $L_{x_i \bmod N/d}$, and thus, have different colors assigned to them. Since the colors correspond to the sub-frames, $SF_i \neq SF_j$. This satisfies the first condition in the sub-frame assignment problem. Satisfaction of the second condition can be argued in a similar manner.

Fig. 3.7(b) shows the bipartite graph and the corresponding edge coloring for the example presented in Fig. 3.7(a). The colors have been indicated beside the edges of the graph. Thus, we can see that input time slots 3, 7, 11, and 15 have to be colored differently to use different sub-frames and thus, time slot 3 is switched into sub-frame SF_3, time slot 7 is switched into sub-frame SF_2, and so on. Fig. 3.7(c) shows the time slots at the output of the switching stages of the TSI.

The time slot classifier is implemented using a switch of size $d \times d$ and a set of delay lines of lengths corresponding to N/d, $2N/d$,...,$(d-1)N/d$ time slots as shown in Fig. 3.8. Consider an incoming frame of size N. We first switch the first N/d incoming time slots corresponding to the sub-frame SF_1 onto the delay line of length $N(d-1)/d$, then switch the time slots of sub-frame SF_2 onto the delay line of length $N(d-2)/d$ and so on. After a time of $N(d-1)/d$ time slots, we end up in a configuration that is shown in Fig. 3.8.

The time slots at the head at the ports of the crossbar are the first time slots in each sub-frame and correspond to the vertex L_1 of the bipartite graph. Thus, the first slot sent out through the output port corresponds to the first slot of the outgoing sub-frame SF_1 and this is determined by the edge coloring. The first slot of the second sub-frame SF_2 of the outgoing frame is switched onto the delay line of length N/d and is thus, sent out of the classifier after a delay of N/d. Similarly, the

first time slot of the third sub-frame is switched onto the delay line of length $2N/d$ and so on. After completing this switching operation, the next set of time slots that correspond to the vertex L_2 can be permuted and the switching is determined by the edge coloring at vertex L_2. The operations at the right classifier are similar and are determined by the coloring at the "right" vertices.

Even though, we have used multiple $d \times d$ switches for each of the classifiers and the smaller TSI, we can implement the entire switching operation using a single large switching matrix, assuming we have one of that size. The size of the switch needed is one more than the number of delay lines used and that is given by $x \times x$, where $x = 2(d-1)(log_d N - 1) + d$. This is plotted for various values of d as a function of the number of time slots, N, in Fig. 3.9(a). The length of delay lines needed is given by $(N-1)d + d(d-1)/2$ and is plotted as a function of N for various values of d in Fig. 3.9(b). The number of switching operations required is given by $2\log_d - 1$ and is plotted in Fig. 3.9(c). The size of the crossbar required and the amount of fiber required to implement the delay lines are the least for $d = 2$. However, the number of switching operations needed is higher for $d = 2$. Thus, there is a tradeoff between the number of switching operations we can afford to use for switching timeslots and the cost of the switch.

For $d = 2$, this approach can be implemented using two sets of delay lines of length $1, 2, \ldots, N/4$ and a single delay line of length $N/2$, where N is assumed to be a power of 2. This gives $2(\log_2 N) - 1$ delay lines and a total delay line length of $(3N/2) - 2$. On the other hand, it requires $2(\log_2 N) - 1$ switching operations (15 for $N = 256$) and it requires that the full permutation be known in advance, or that the entire switch configuration be changed as new timeslots are received, making it difficult to apply in the TSOBS context.

Table 3.1 summarizes the four nonblocking TSI designs discussed above and shows their complexity characteristics. Only the third design is a real candidate for practical use, and even it is somewhat expensive, both in terms of total fiber length and crossbar complexity. Also shown is the cost of implementing a blocking design, which is discussed in the next section. We can clearly see that the blocking design has much lower cost.

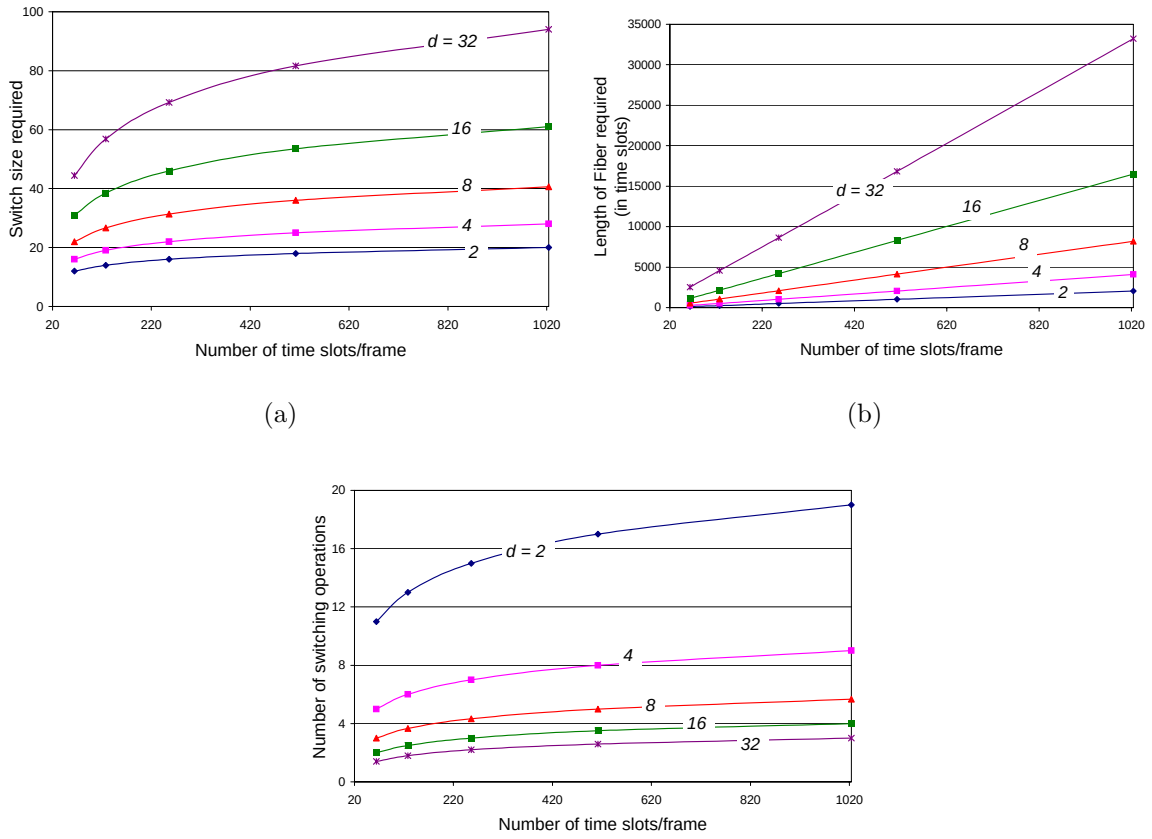

Figure 3.9: (a) Size of the switch required; (b) Length of fiber required for the delay lines; (c) Number of switching operations needed

3.2.3 Blocking OTSIs

Blocking OTSIs are an alternative to nonblocking OTSIs, offering lower complexity, at the cost of some small non-zero blocking probability. In the TSOBS context, the impact of a blocking TSI will be to reduce the statistical multiplexing performance slightly.

Perhaps the most natural choice of delays for a blocking TSI is the set {1, 2, 4,..., $N/2$}. This allows any time-slot to be switched to any of the output timeslots, provides small total delay (255 for $N = 256$) and small crossbar size (8×8 for N=256). We show below that an OTSI with these delays can be operated so as to achieve a small average number of switching operations (≤ 3 under most conditions), and that the impact of blocking on the statistical multiplexing performance is very small.

Table 3.1: Table showing the complexity of the TSI designs

Delay line lengths	Crossbar Size		Fiber Length (in timeslots)		Switching Operations	
		$N = 256$		$N = 256$		$N = 256$
$N \times 1$	$N+1$	257	N	256	N	256
$1, 2, \ldots, N-1$	N	256	$N^2/2$	32896	2	2
$1, \ldots, A, 2A, \ldots, (B-1)A$	$2\lceil\sqrt{N}\rceil - 1$	31	$N\lceil\sqrt{N}\rceil/2$	2048	3	3
$2 \times (1, 2, 4, \ldots, N/4), N/2$	$2\log_2 N$	16	$(3N/2) - 2$	382	$2(\log_2 N) - 1$	15
Blocking TSI: $1, 2, \ldots, N/2$	$\log_2 N$	8	$N-1$	255	variable	2 to 3

For a blocking TSI, we need to define a search procedure to find a sequence of delay lines through which we can switch an arriving timeslot, to deliver it to a free output timeslot. This needs to be done without creating any conflicts at any of the delay lines. The key to implementing the search procedure is a *schedule* that allows us to keep track of which delay lines are available for use at each point in time. The schedule is represented by an array of bits, $sched[i, t]$ with $k+1$ rows and N columns, where k is the number of delay lines and N is the number of timeslots per frame. For $i \in [1, k]$, we let $sched[i, t] = 1$ if the ith delay line is "busy" at time t. We say a delay line is busy at a given time, if there is some timeslot scheduled to exit the delay line at that time. For simplicity, we define $t = 0$ to be the current time. We let $sched[0, t] = 1$ if the output link of the OTSI is busy at time t.

Fig. 3.10(a) shows an example of the schedule array for $k = 3$ and $N = 8$. The delay values for each of the delay lines is shown next to its row. The schedule array implicitly defines a directed graph $G = (V, E)$ that can be used to find a sequence of delay lines leading to a free output timeslot, that can be used for an arriving burst. The vertex set V, is $\{u_0, \ldots, u_{N-1}\}$. Each vertex corresponds to a potential delay that a timeslot may be subjected to. The set of edges E consists of all pairs (u_i, u_j) for which there is some delay line h with delay $j - i$, and $sched[h, j] = 0$. Fig. 3.10(b) gives an example of the graph defined by the schedule in Fig. 3.10(a).

To find the best sequence of delay lines, we essentially perform a breadth-first search on this graph, starting from node u_0. Such a search constructs a *shortest path tree* in the graph, as illustrated in Fig. 3.10(c). The unshaded nodes have delay values that correspond to free timeslots on the output link. The path in the tree to such an output defines a sequence of delay lines that can be used to reach that output. The delay line corresponding to an edge (u_i, u_j) on such a path, is the delay line with delay value $j - i$. The number of switching operations is minimized by selecting a path of minimum length from u_0 to an unshaded vertex. When there are two or more unshaded vertices on minimum length paths from u_0, we select the vertex u_i with the smallest value of i, in order to minimize the delay that a timeslot is subjected to. In

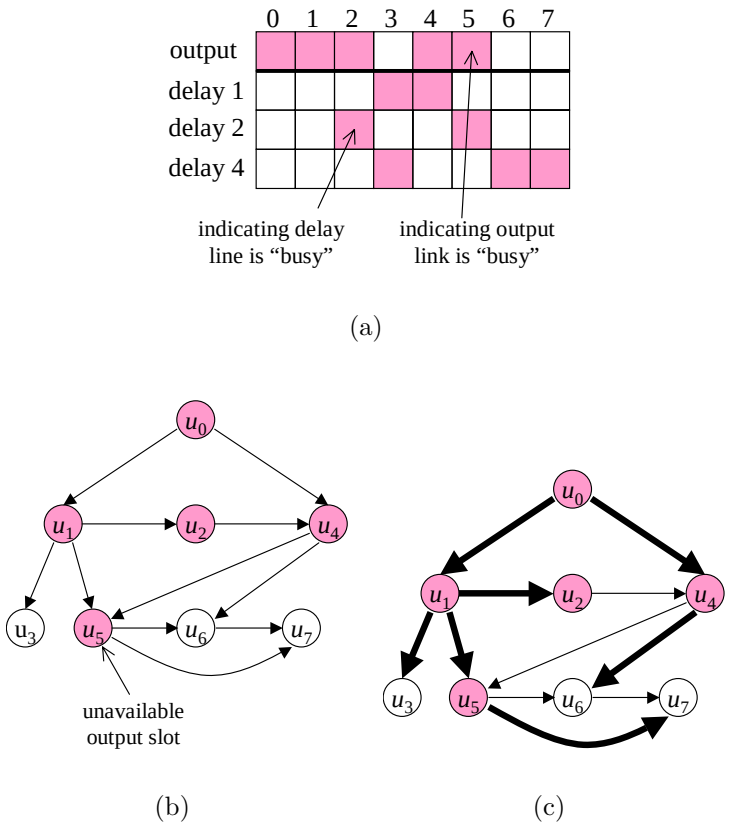

Figure 3.10: (a) Example of the schedule array for $k = 3$ and $N = 8$; (b) Directed graph corresponding to example schedule; (c) Search constructing the shortest path tree (shown in bold)

Fig. 3.10(c), u_3 is selected at the conclusion of the search, and the timeslot is then switched through the delay lines of length 1 and 2.

The example selects a sequence of delay lines for a burst that has one timeslot. For a burst that has multiple timeslots, we determine the sequence of delay lines for the first timeslot. Since the timeslots of any burst occupy the same relative position within a frame, the rest of the timeslots can be scheduled by using the same sequence of delay lines in the subsequent frames.

The search can be done using the schedule array. The procedure does construct the shortest path tree, but does not explicitly construct the graph. A code fragment implementing the required search procedure is shown below. In this procedure, q is a list of nodes from which the breadth-first search needs to be extended next, $p(u_i)$ is the parent of u_i in the shortest path tree constructed by the search procedure and $n(u_i)$ is the number of edges on the path from u_0 to u_i in the tree. The variables

$\delta_1 < \delta_2 < \cdots < \delta_k$ are the k different delay values and s is the number of timeslots that the burst being scheduled requires.

```
q := [u_0];
p(u_i) := Ø for all i;
n(u_i) := ∞ for all i;
b := −1;
while q ≠ [ ] do
    u_i := q[1]; q := q[2..]; // remove u_i from q
    if sched[0, d(u_i)] = 0 then
        if b = −1 or
            n(u_i) < n(u_b) or
            n(u_i) = n(u_b) and i < b then
            b := i;
        end;
    end;
    for h = 1 to k loop
        Let u_j be the vertex with j = i + δ_h;
        if sched[h, j] = 0
            and n(u_i) + 1 < n(u_j) then
            p(u_j) := u_i; n(u_j) := n(u_i) + 1;
            if u_j ∉ q then
                q := q & [u_j]; // add u_j to q
            end;
        end;
    end;
end;
```

When a search terminates successfully, b is the delay value associated with the selected output timeslot. If the path from u_0 to u_b (defined by the parent pointers) goes through nodes $u_0 = u_{i_1}, u_{i_2}, \ldots, u_{i_r} = u_b$ the timeslot is switched through the delay lines with delay values $i_2 - i_1, i_3 - i_2, \ldots, i_r - i_{r-1}$. The schedule must be updated to indicate the busy status of the selected delay lines. This is done by setting $sched[j_q][i_q] = 1$, for $1 < q \leq r$, where j_q is the index of the delay line with delay value $i_q - i_{q-1}$.

The search procedure can be terminated early under certain conditions. In particular, if the node u_i, removed from the front of q, has $n(u_i) > n(u_b)$, then there is no point in continuing the search, since no shorter paths to "exit nodes" will be found. We can also terminate the search early if $n(u_i)$ exceeds some pre-specified limit on the path length. In this case, the search fails without finding a solution, forcing us to drop the burst being scheduled.

The above search procedure determines a set of delay lines for the first timeslots in a frame. For the rest of the timeslots of a burst, the same sequence of delay lines can be used in the subsequent frames.

Table 3.1 gives the complexity of using a blocking TSI and shows the size of the crossbar required, the length of the delay lines, and the number of switching operations. We can see that the blocking design gives us a decisive cost advantage over the nonblocking ones.

3.2.4 Design Issues for the Synchronizers

As a result of the varying length of fibers that terminate at input ports, chromatic dispersion within the fiber, temperature variation leading to phase drift of the optical signals and other fiber transmission non-linearities, the frames arrive at the input ports at random times and completely misaligned with each other. In order to enable the required synchronous switching operations, they must first be realigned. This is the function of the Synchronizers in Fig. 3.4. To synchronize the incoming data, we first need to determine where the frame boundaries are. Assuming that the frames carried on different wavelengths of a given fiber were synchronized when they were transmitted by the upstream router (or network terminal), we can determine the location of the frame boundaries by extracting the requisite timing information from the control wavelengths. Since propagation delay is wavelength-dependent, frames on different wavelengths will not be precisely aligned with the frames on the control wavelengths, but because the differences are systematic, it is straightforward to compensate.

Once we know the start times of the frames on different wavelengths, we need to delay the received data to bring the start times into alignment. This can be done using the same kind of structure that is used for the OTSI. There are two key parameters that affect the cost of the synchronizers, the *precision* and the *range*. The precision of a synchronizer is the difference between successive delay values that the

synchronizer can provide. The range is the maximum delay that it provides. The ratio of the range to the precision defines the number of distinct delay values that the synchronizer must provide. This affects the number of fibers and the size of the optical switch needed to route the signal through one or more fibers to produce the required delay. To minimize the cost of the synchronizer, we'd like to minimize the ratio of range to precision, by reducing the range and/or increasing the precision.

The precision determines where the data in a timeslot can be placed, relative to the nominal start time of the frame. The guard times that separate data blocks in adjacent frames provide some flexibility in where exactly the data must be placed. For example, consider a system with a timeslot duration of 1 μs in which data is transmitted for 900 ns. If we require a *minimum guard time* of 20 ns at the start and end of each timeslot interval, it's sufficient to place the start of the data block within a time interval of 60 ns. This defines the precision required of the synchronizer, assuming that we know where in the timeslot interval, the data block starts. This information can be carried in the BHCs of transmitted bursts and updated in successive routers as the bursts pass through synchronizers that shift the data blocks of a burst within the timeslot interval. Notice that if the total guard time is too large, we sacrifice transmission efficiency, so we prefer to keep the total guard time a reasonably small fraction of the timeslot interval. The minimum guard time is determined by how accurately switching operations can be timed. With current technology, values as low as 5-10 ns are certainly feasible.

To synchronize the start of all incoming frames to a common time value, we need a range equal to the time duration of a frame. However, it's possible to reduce the required range to the timeslot duration, using a *time shifting switch controller*. The electronic controller that schedules the switching operations can operate with input links that are only synchronized to a common timeslot boundary rather than a frame boundary, so long as it knows where the frame boundary is, relative to a common frame reference time. Using this information, it can compensate for different time shifts within the frame period, when it switches the data through the OTSIs.

Using both of these techniques, the precision-to-range ratio can be as low as 10:1. This makes it feasible to implement the synchronizer using a separate delay line for each delay value. This has the advantage that it limits the number of switching operations that the data is subjected to by the synchronizer to two (one to switch the data into the selected delay line and one to switch it back out of the delay line to the output). This can be cut to a single switching operation by using a slightly

different implementation, in which the delay lines are fed forward through a passive coupler rather than back through the switch.

In systems with a larger number of distinct delay values, we can keep the cost of the synchronizer low by adapting the nonblocking OTSI design described in Section 3.2.2. The size of the crossbar required for this design is $(2\lceil\sqrt{S}\rceil - 1) \times (2\lceil\sqrt{S}\rceil - 1)$ (15×15 for $S = 16$) and the length of the fiber required is $S\lceil\sqrt{S}\rceil/2$ times the precision (32 when $S = 16$). The number of switching operations required is three, but this can be reduced to two using a feed forward configuration, in which we arrange the long and short delay lines in two stages with an intermediate switch. This also reduces the switch cost by almost a factor of four.

3.3 Cost Analysis

For the architecture in Figure 3.4, let d be the number of external fibers, N be the number of timeslots per fiber, h be the number of wavelengths per fiber, m be the number of delay lines in each OTSI, S be the alignment accuracy accuracy, l be the total number of delay lines in each SYNC, D be the total delay line length in each OTSI, and D_s be the total delay line length in each SYNC. Also, let C_f be the cost per unit length of the fiber, C_x be the cost per crosspoint of an optical crossbar and let C_m be the cost per input of an optical multiplexor (also, the cost per output of a demultiplexor). If the data transmission rate for each wavelength channel is R Gbps and there is a 10% overhead for guard times and assuming that we use the second design for the SYNC with the feed forward arrangement, the cost per Gbps of transmission capacity is given by

$$\left[\left((m+1)^2 + \frac{l}{2} + \left(\frac{l}{2}\right)^2 + d\right) C_x + 2\left(m + l + \frac{l}{4} + 1\right) C_m + (D + D_s)\frac{C_f}{h}\right] /.9R$$

For a switch with $d = 16$, $h = 128$, $N = 128$, $m = 7$, $l = 6$, $D = 40$ km, $D_s = 6$ km, and $R = 10$, then the cost per Gbps of capacity is

$$10.2C_x + 3.5C_m + 0.04C_f$$

The above cost does not include the cost of the electronic control subsystem. If we estimate the cost per km of fiber at \$100, the last term in the above expression contributes an insignificant value and hence, can be ignored. If we assume that the

data path of a TSOBS router should cost no more than \$200 per Gbps of capacity and also assume that $C_x = C_m$, then we need both to be about \$15. This means that an 8×8 crossbar should cost no more than \$960, while a 128 port multiplexor should cost no more than \$1920. While current prices are above these values, there seems to be no fundamental obstacle in achieving these price levels. Also, usually $C_m < C_x$ because multiplexors are passive components, and thus the above assumption is pessimistic.

Note that the cost of the system scales linearly with the number of wavelengths. Also, it should be noted that the cost of the optical components is largely independent of the bit rate used on the individual wavelength channels, so if we have $R = 40$ instead of $R = 10$, the cost per Gbps of capacity drops by a factor of 4. This means that we could tolerate a cost of \$3840 for an 8×8 crossbar and \$7680 for a 128 port multiplexor. If devices can be engineered to bring the costs down to the above values, TSOBS can become a cost effective alternative to electronic networks.

3.4 Performance of a TSOBS Router

In this section, we study the performance of a TSOBS router using the blocking OTSI design discussed in the previous section. When a BHC is received by the controller announcing the imminent arrival of a burst at one of the input links, the controller does an address lookup to determine the appropriate outgoing link. It must then determine the set of timeslots that are available on the wavelength being used by the burst, both on the outgoing link and at the output of the OTSI for the input link where the burst is to arrive. It then performs the search discussed in the last section to find a set of delay lines through which it can switch the burst, in order to shift it into an available outgoing timeslot.

To evaluate the performance of the OTBS router using a blocking OTSI, we performed simulations using different OTSI configurations. Our primary performance metric is the burst discard probability, which is the fraction of bursts that need to be discarded, due to blocking at either the outgoing link or due to the OTSI. We also measured the number of switching operations that were used to switch the bursts through the OTSIs. The simulations were done for uniform random traffic with binomially distributed arrivals and deterministic burst lengths of one timeslot. The number of input and output links was 16.

Fig. 3.11(a) shows the packet discard probabilities for a range of different frame sizes. The OTSIs used delay values of $1, 2, 4, \ldots$ with the largest delay value

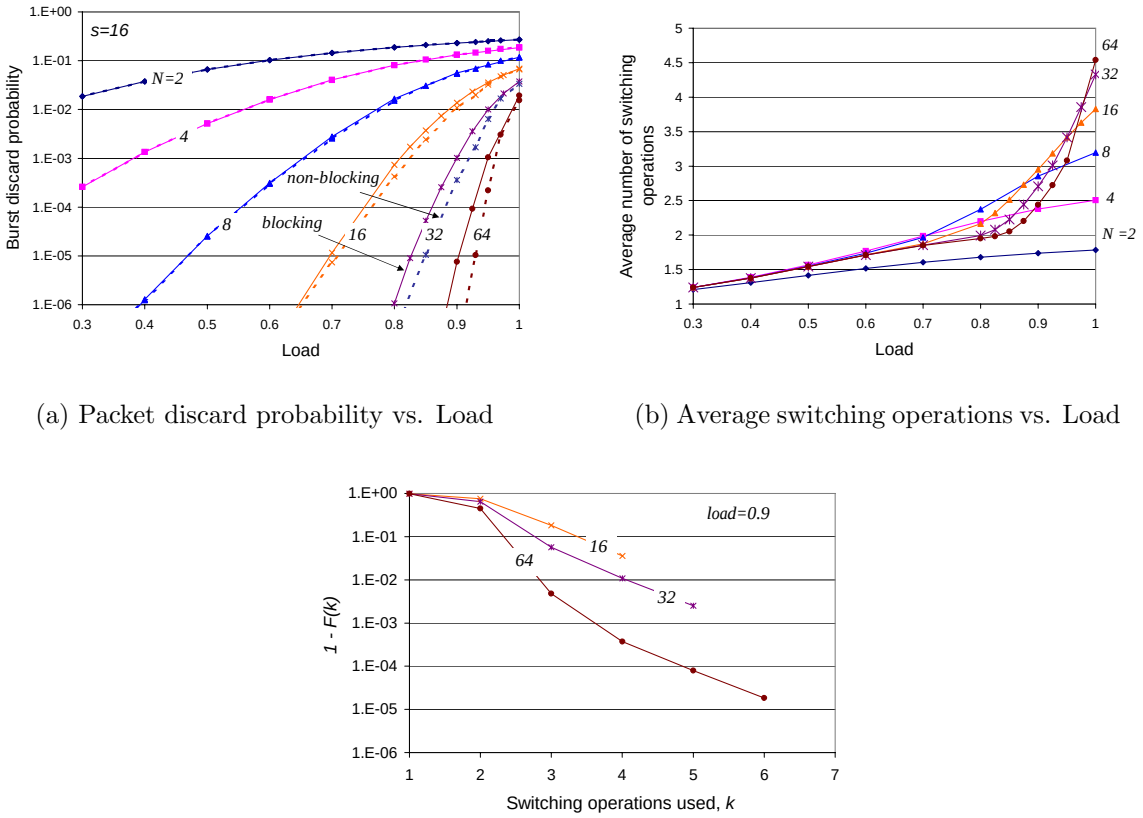

(a) Packet discard probability vs. Load

(b) Average switching operations vs. Load

(c) $1 - F(k)$ vs. k, k = number of switching operations

Figure 3.11: Charts for different number of time slots per frame, N

being equal to half of the frame size. Also shown are the discard probabilities with nonblocking OTSIs. We can see that we do not lose much in the way of performance by using the blocking OTSIs instead of the nonblocking ones, considering that the cost of using nonblocking OTSIs is significantly higher. Figure 3.11(b) shows the average number of switching operations that each burst is subjected to. For loads up to about 70% the average number remains below 2, meaning that the average burst passes through just one delay line and for loads up to about 90% the average number remains below 3, meaning that the average burst passes through two delay lines only. Fig 3.11(c) shows the tail of the distribution of the number of switching operations. Specifically, we define $F(k)$ to be the fraction of bursts that require at most k switching operations. So, $1 - F(k)$ is the fraction of bursts that require more than k switching operations. Note that the chart uses a logarithmic scale for the values of $1 - F(k)$. Fig 3.11(c) shows $1 - F(k)$ when the offered load on the output

links is 90%. For $N = 64$, less than 45% of the bursts require more than two switching operations, so almost 55% use at most two, meaning they only use a single delay line and less than 0.5% of the bursts require more than three switching operations, so almost 99.5% use at most three, meaning they only use two delay lines.

The set of results in Fig. 3.12 shows the effect of placing an upper bound on the number of switching operations that are allowed for each burst. These results are for a system with a frame size of 64. Fig. 3.12(a) shows that if we restrict the number of switching operations too much, we cause a large increase in the burst discard probability, but with a limit of 3, the burst discard probability is almost the same as when there is no limit. The utilization at a blocking probability of 10^{-6} is approximately 0.83 when the number of switching operations is restricted to 3 and is 0.88 when it is 7, giving about 6% reduction. This is consistent with what we observed in Fig 3.11(c). Fig. 3.12(b) shows the average number of switching operations when the number of switching operations is limited. For loads up to 85% the limit has a negligible effect on the number of switching operations, but for loads greater than 90% it produces a significant reduction. Fig. 3.12(c) shows the fraction of bursts using k or more switching operations, when the number is limited.

The final set of simulations were performed to quantify the effect of reducing the number of delay lines available. For this set of simulations, the frame size was fixed at 64. The number of delay lines was varied from 1 to 6, with the longer delay lines being omitted, when the number is restricted. So, for example, when 3 delay lines are used, the delay values are 1, 2 and 4. Fig. 3.13(a) shows the packet discard probabilities. We see that four delay lines gives a comparable blocking performance to six. This is significant, since with four delay lines, the total delay line length is reduced by a factor 4. Fig 3.13(b) shows the effect on the number of switching operations when the number of delay lines is limited. We can see that decreasing the number of delay lines from six to four increases the number of switching operations at high loads. At loads of 90% the average number of switching operations with four delay lines is about 3.3 and is 2.5 for six delay lines, whereas it is 1.87 and 1.85 at loads of 70% for four and six delay lines respectively. Thus, given the benefits we do not lose much by way of the number of switching operations by reducing the number of delay lines to four. Fig 3.13(c) shows the tail of the distribution of the number of switching operations. Here, the differences are more evident, but the absolute magnitudes remain small.

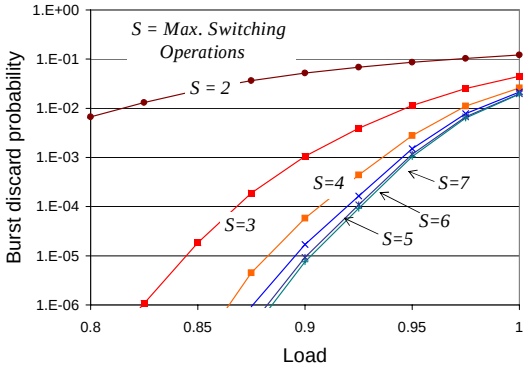

(a) Packet discard probability vs. Load

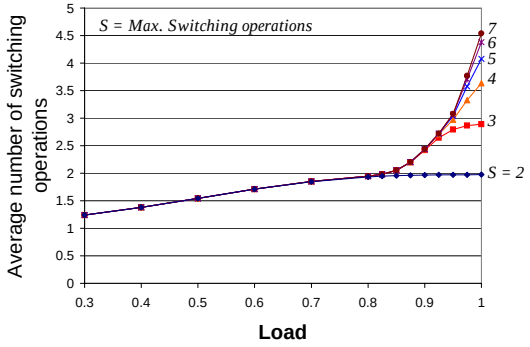

(b) Average switching operations vs. Load

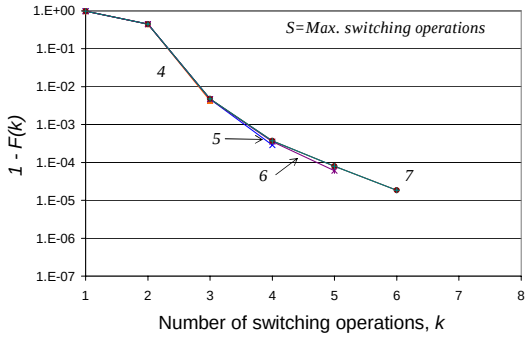

(c) $1 - F(k)$ vs. k, k = number of switching operations

Figure 3.12: Charts for different values of maximum number of switching operations allowed, S

3.5 Conclusion

In this chapter, we have introduced a promising variant of optical burst switching, in which switching is done in the time domain rather than the wavelength domain. This eliminates the need for wavelength converters, the largest single cost component of systems, which switch in the wavelength domain. This may allow optical burst switching to become cost-competitive with electronic packet switching, potentially a very significant development, since no previous optical packet switching architecture has shown any real promise of becoming cost-competitive with electronic alternatives.

Our performance results show that a system with as few as 64 timeslots can provide excellent statistical multiplexing performance, even with blocking OTSIs with just four delay lines. With a timeslot duration of 1 μs, each OTSI would require a

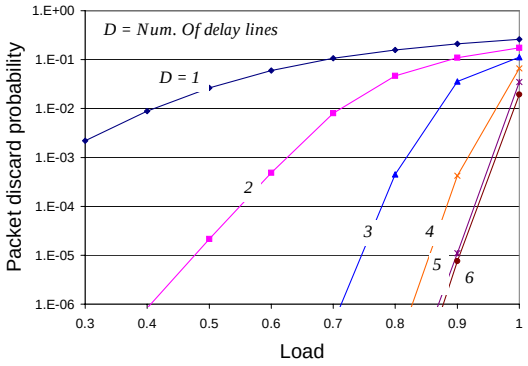

(a) Packet discard probability vs. Load

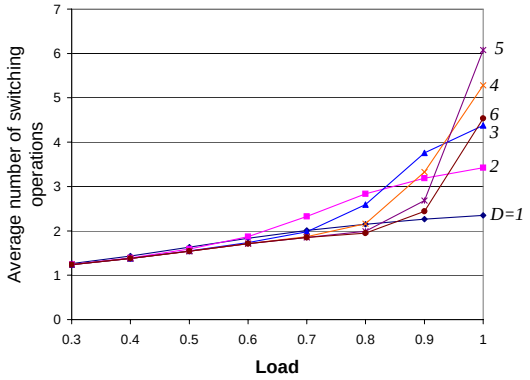

(b) Average switching operations vs. Load

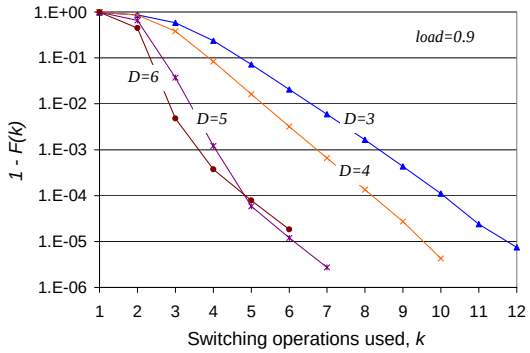

(c) $1 - F(k)$ vs. k, k = number of switching operations

Figure 3.13: Charts for different number of delay lines, D

total delay line length equal to the distance that light travels in fiber in 15 μs (under 4 km). For routers terminating wide area optical links spanning hundreds or thousands of kilometers, this is a very modest overhead. The average number of switching operations that bursts are subjected to is also quite modest, less than four switching operations per hop, for loads up to 90%. This makes it likely that most bursts could be switched from end-to-end with no intermediate conversion to electronic form.

3.6 Future Work

We have shown in this chapter that TSOBS is a promising technology that can used to build optical routers that are cost competitive with electronic routers. There are several other issues and design choices that need to be addressed to implement TSOBS

networks. Two issues, data aggregation and load balancing on wavelengths, shall be addressed in the next chapters.

In a TSOBS network, we could decide to adopt existing protocols like the Internet Protocol for addressing and routing. However, since TSOBS can serve as a subnetwork technology, it is possible to use protocols that are more suited for its requirements. One particular functionality we need in order to perform aggregation of data (discussed in Chapter 4) is the ability to classify packets from hosts in terms of their destination network interfaces, where they exit the TSOBS network. The network interfaces can act as gateways between the legacy networks and the TSOBS network. Additional work, that examines possible addressing and routing mechanisms, is necessary to determine one that fits TSOBS networks the best.

In any network, we can expect to have congestion when the load on the network is beyond what it can handle. Congestion is problem that can acutely affect the performance of TSOBS networks because we do not have buffering in the switches. Congestion can, in general, be handled in two ways. Congestion control is a reactive mechanism that lowers the sending rates of the sources to reduce the load on the network. Congestion avoidance ensures that the sources transmit data at a rate that can be handled by the network. In a TSOBS network, data can be stored electronically at the network interfaces, where we can expect to have a lot of buffering capacity and the congestion avoidance/control can be handled by the network interfaces. Another design choice we have is whether or not the messages indicating congestion are handled end-to-end, like in TCP (Transmission Control Protocol). We can augment a TSOBS network by adding functionality to send messages that indicate congestion to the network interfaces.

Each TSOBS router is equipped with a few ports of regenerators that are used to regenerate bursts when necessary. There can be contention among bursts to get to the regenerator ports within the switch as there is to reach the outputs. It is necessary to quantify the number of regenerator ports needed in order to achieve good performance. We can define a threshold on the number of hops a burst travels and beyond this threshold, the burst is regenerated, even if it can travel a few more hops without needing regeneration. So, even if a burst cannot be regenerated because of contention, the signal quality of the burst is still good and it can be regenerated at a downstream router. This can help reduce the number of regenerator ports needed.

The regenerator ports can also be used to provide multicasting capability in the switch by making copies of the bursts and forwarding them to the desired outputs. The multicast traffic can interfere with the traffic within the switch and cause degradation of the switch throughput. We need to analyze the amount of multicast traffic a switch can handle without a degradation of its performance.

The scheduling mechanism that we have studied in this chapter does not take into account Quality of Service requirements. To provide Quality of Service in the network, we need to augment the scheduling algorithm with methods in which we can prioritize the bursts we transmit when there is contention. The provision of QoS guarantees requires further study.

Chapter 4

Data Aggregation for Time Sliced Optical Burst Switching

The network interface or concentrator shown in Fig. 3.1 is responsible for assembling the data from hosts, that connect to the network using lower speed interfaces, into bursts and transmitting the bursts in the TSOBS format. Transmission of a burst involves determining a wavelength channel and a route through the network to transmit the burst. The concentrator collects packets from hosts to a particular destination or destination network to form "superpackets" or bursts that are larger in size than typical packets. Once the bursts are received by the concentrator at the destination network, the bursts are unpacked and the packets are routed individually to the destination host.

In this chapter, we examine the problem of aggregating packets to form bursts. We present an algorithm to aggregate packets and present an analysis to determine the parameter values that give the best performance.

4.1 Related Work

In Reference [48], a simple algorithm for performing aggregation in burst switched networks was proposed. A time counter T_i is started any time a packet arrives that is destined to some network interface i and the queue for destination i is empty. The algorithm waits for a time period W_i, called the burst aggregation period and during that period, collects all arriving packets for destination interface i in the queue. At the end of the time period, a burst is created with the collected data and queued for

transmission through the network. Finally, the time counter is reset to 0 and remains so until the next packet arrival for destination i.

Reference [100] describes a temporal burstification algorithm or aggregation algorithm where burst generation is triggered either when the burst size reaches a threshold or when a timer expires.

Reference [22] evaluates the impact of aggregation on TCP Reno flows from a source's point of view. It is shown that aggregation tends to have two opposite effects. Sources experience delay penalties due to the delay experienced by the packets at the interface which cause a source to reduce its "send rate". However, since multiple packets from a source have a tendency to get aggregated onto the same burst, a burst delivery or a burst loss results in delivery or loss of consecutive TCP packets respectively. Simulations show that this results in a "correlation benefit" and the send rate of sources with aggregation tends to be higher than the send rate without aggregation. For low access bandwidth sources, the delay penalty tends to be the dominant effect and this results in a lower TCP send rate than without aggregation. For high bandwidth sources, the correlation benefit tends to be stronger and results in a higher send rate. This is because the higher the access bandwidth of the source, the higher the likelihood of multiple packets from the source getting aggregated into the same burst. It is suggested that a reasonable burstification period is around 10-20% of the round trip time.

Reference [15] studies the performance of three aggregation algorithms for TCP/IP traffic, namely Fixed-Assembly-Period (FAP), MinBurstLengthMaxAssemblyPeriod (MBMAP), and Adaptive-Assembly-Period (AAP) algorithms. It is shown that the AAP algorithm performs better than the other algorithms because it adapts the aggregation period based on the sending TCP window sizes.

Reference [50] studies the performance of TCP in Optical Burst Switched Networks when the network uses the latest available unused channel - with void filling (LAUC-vf) scheduling algorithm, described in Reference [101], to determine the data channel to transmit a burst on. The paper studies the impact of burst drop probability, burst-assembly delay, and buffering on the performance of TCP.

In OBS networks, small burst sizes affects the volume of control traffic generated. However, it does not have an effect on the utilization of the network. In Time Sliced Optical Burst Switched networks, a timeslot is the minimum unit of data and if bursts are smaller than a timeslot worth of data, the timeslot is not utilized fully.

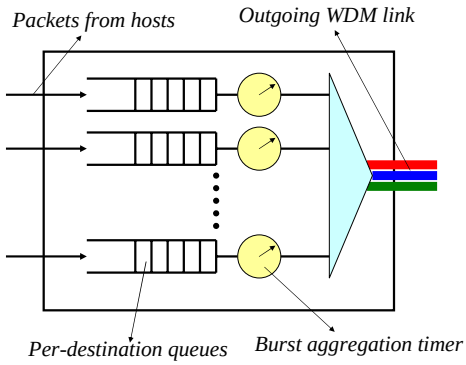

Figure 4.1: The aggregation mechanism in a concentrator

Aggregation helps in creating large bursts that utilize the timeslots more efficiently as well as reduce the volume of the control traffic.

4.2 Burst aggregation mechanism

Hosts are connected to a TSOBS network through concentrators and they send packets on low speed interfaces. The concentrator aggregates the packets from the hosts, that are addressed to the same destination network, into a burst and transmits the burst in the TSOBS format. Each concentrator is equipped with a tunable transmitter or a transmitter array to transmit the burst on the outgoing WDM channels.

The aggregation mechanism at a concentrator is shown in Fig. 4.1. When a packet arrives from a host at the concentrator, the destination network that the packet is addressed to is determined. The packet is then stored in a queue corresponding to the destination network the packet is addressed to. The concentrator starts a timer and waits for a given period of time during which packets accumulate in the queues. When a sufficient number of packets are collected, a burst is formed and transmitted through the network. When a burst is received at the concentrator of the destination network, the individual packets are extracted from the burst and sent to the destination hosts.

Aggregation of packets to form larger bursts is necessary in TSOBS for two reasons. First, the number of bursts transmitted is reduced by a factor proportional to the ratio of the average burst size to the average packet size. This reduces the number of control cells that need to be processed by any TSOBS router. Consider a single fiber link with 64 wavelength channels and 10 Gbps bandwidth per wavelength. If we have minimum size IP packets of 48 bytes and link utilization of 60%, we have

to be able to forward 1 billion packets per seconds for each fiber link that terminates at a router. This does not scale well while using electronic processing for control information. Also, the duration of each packet can be as low as 40 ns and switching data optically at this granularity seems to be out of reach of current technology.

Secondly, as the average burst size increases, the timeslots are utilized more efficiently. In TSOBS networks, a timeslot is the minimum unit of data and a timeslot worth of data is much larger than typical data packets. IP packets can be as small as 48 bytes and each timeslot can store 1100 bytes in TSOBS networks with timeslot durations of 1 μs and 10 Gbps bandwidth per wavelength channel. By aggregating packets into a single burst, the concentrator is able to utilize a timeslot more efficiently by packing the data into the timeslots. To illustrate this, consider a TSOBS network with bursts that are i timeslots long on average and let us assume that the size of each timeslot is l bytes. Also, define *burst aggregation efficiency* as the ratio of the actual size of the burst carried to the bandwidth used to carry the burst. This is a measure of the effective utilization of the bandwidth used to transmit the bursts. Usually in each burst, the last timeslot is not going to be utilized completely. Assume that on average, the utilization of the last timeslot of every burst is 50%. The actual amount of data carried is given by $(i - 0.5)l$ and the average burst aggregation efficiency is given by $1 - 0.5/i$. Thus, if the average burst is 1 timeslot long, the average burst aggregation efficiency is 50%. With burst lengths of 4 and 16 timeslots long, the average burst aggregation efficiencies are 88% and 97% respectively.

A good aggregation algorithm is one that forms large bursts without waiting for a long period of time. The aggregation algorithm we examine in this paper is similar to the MinBurstLength-MaxAssemblyPeriod algorithm described in [15]. For each queue in the concentrator, we define two parameters, the burst aggregation period (denoted by T) and the target burst length (denoted by B timeslots). Denote the size of a queue by S and the timer that is used to keep track of the burst aggregation period by t. The aggregation algorithm is described by the following procedure:

```
for each queue
    if S = 0 and packet received then
        start timer(t);
    end;
    if packet received then
        S := S + size of(packet);
```

```
    end;
    if t = T or S ≥ B then
        transmit burst;
        reset timer(t);
        S := 0;
    end;
end;
```

The burst aggregation period is the maximum time period we wait from the moment we receive the first packet to the time a burst is formed and transmitted on the network. However, if we receive enough packets such that size of the burst is at least as large as the target burst length, we pack the burst and transmit it, even if the burst aggregation period has not expired. Note that bursts can be longer than the target burst length.

The burst aggregation period and the target burst length are key parameters that determine the performance of the aggregation algorithm. In the Internet, the round trip time can be up to a few hundreds of milliseconds. Thus, we can afford to have a burst aggregation period of around 1-10 ms and still not affect the round trip time by much. A larger value of burst aggregation period results in larger bursts because it gives enough time for the concentrator to build up the queue. However, a packet has to be delayed until the burst is formed and transmitted. Thus, a larger burst aggregation period increases the delay experienced by a packet through the network. By imposing the target burst length constraint, a burst is transmitted as soon as the size of the burst exceeds the target burst length. Hence, the concentrator need not wait for the burst aggregation period to expire and this reduces the average delay experienced by a packet due to the aggregation process. The value of the target burst length needs to be chosen such that the burst aggregation efficiency is acceptable. The key to the performance of the aggregation process is that the bursts generated should be sufficiently large even when the load on the wavelength channels is low and the delay incurred due to the aggregation process should be as small as possible.

Consider a TSOBS network with 100 destination interfaces and let us assume that 100,000 hosts connect to the network through some interface and each host sends data at a rate of 100 Mbps each. If 1% of the hosts transmit to some destination interface, the net traffic that is sent is 100 Gbps. This can be carried using about 10 wavelength channels each operating at 10 Gbps. On the other hand, if 0.02% of the

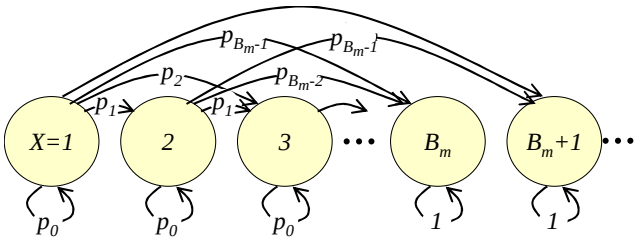

Figure 4.2: Model for fixed packet length analysis

hosts are sending to some destination interface, the amount of data sent goes down to 2 Gbps. This can be carried on a single wavelength channel operating at a load of 20%. The aggregation process should result in good performance for both of these cases. We use the burst aggregation efficiency as the metric to measure performance of the aggregation process. In this chapter, we analyze the aggregation algorithm and suggest values for the aggregation period and target burst length that result in good performance. We measure the performance of the algorithm for load values as low as 20% for different values of the burst aggregation period and target burst lengths. When the amount of traffic sent to some destination interface is much lower, the aggregation efficiency does not affect the utilization of the network significantly.

4.2.1 Analysis of the algorithm

We now present an analysis of the aggregation algorithm when the data packets transmitted by the hosts are of a fixed length and extend the analysis to study the algorithm when the packet length is variable. We analyze the algorithm by determining the length distribution of the bursts that are formed by the aggregation algorithm. Given the burst length distribution, we can determine the efficiency of the aggregation process.

Fixed packet length analysis

An approximate model for a queue in the concentrator with the assumption that hosts transmit packets of a fixed length is shown in Fig. 4.2. Define the state of the system, X, to be the number of packets received by the queue from hosts and let $\pi_i(t)$ be the probability of the system being in state i at time t. The model is a discrete time model and we initialize the system at time 0 and iteratively compute the state probabilities after each time step. The state probabilities at time T (T = burst aggregation period) gives us the burst length distribution of the aggregation

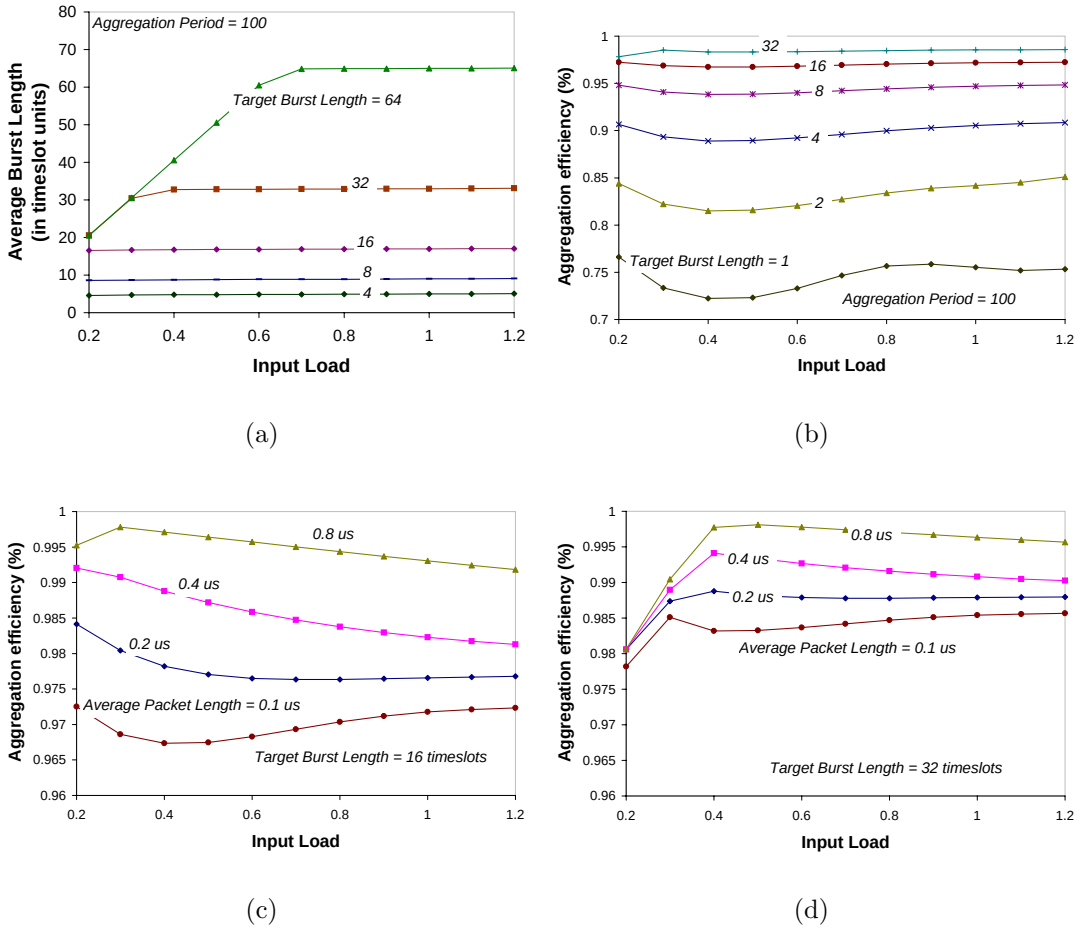

Figure 4.3: Results of fixed packet length analysis for aggregation period of 0.1 ms and timeslot duration of 1 μs (Average packet length = 0.1 μs for (a) and (b))

process. Let B be the target burst length in bytes. If the packet length is x bytes, then $B_m = B/x$ is the minimum number of packets needed to form a burst that is as long as the target burst length.

If p_i denotes the probability of receiving i packets in a time unit, the transition probability from state j at time t to state $j + i$ at time $t + 1$ is given by p_i. The aggregation timer does not start until we receive the first packet. Thus, the aggregation process starts from state 1. Also, once the amount of data in the queue reaches the target burst length or more, the burst is transmitted. Thus, once we reach one of the states $B_m, B_m + 1, \ldots$, the state of the system does not change because the size of the burst is given by that state.

In this model, we assume that the packet arrivals follow a Poisson process and hence, p_i is given by the probability of i arrivals in a Poisson process. That is, $p_i = \lambda^i e^{-\lambda}/i!$, where λ is the mean number of arrivals in a time unit. Given these transition probabilities, we can determine the probabilities of the system being in any state at the end of the aggregation process (at time T) by iterating through the transitions. We initialize the system by letting $\pi_1(0) = 1$ and we determine the state probabilities of the system at time T using the following set of equations:

$$\pi_i(t+1) = \begin{cases} \sum_{j=1}^{i} \pi_j(t) p_{i-j}, \text{if } 1 \leq i \leq B_m - 1, \\ \sum_{j=1}^{B_m - 1} \pi_j(t) p_{i-j} + \pi_i(t), \text{if } i \geq B_m. \end{cases}$$

If l denotes the size of a timeslot and x is the fixed packet length, the average burst length (in timeslots) and the average burst aggregation efficiency are given by

$$B_{avg} = \sum_{i=1}^{\infty} \lceil \frac{i\pi_i(T)x}{l} \rceil$$
$$B_{eff} = \sum_{i=1}^{\infty} \frac{i\pi_i(T)}{\lceil \frac{i\pi_i(T)}{l} \rceil l}$$

To estimate the performance of the aggregation process using this model, we assume a timeslot duration of 1 μs, an aggregation period of 100 μs and a time-step of 0.1 μs. The number of iterations needed to compute the final state probabilities is 1000. Although, the model described above has an infinite number of states, we can approximate it by assuming that the probability of getting very large bursts is zero. For the purpose of this analysis, we assume that the maximum burst we can get for an aggregation period of 100 timeslots is 128 timeslots. If N is the number of states in the model, the number of state transitions is approximately $Nm - m^2/2$. If we assume that the packet length of 0.1 μs, a timeslot duration of 1 μs, and a target burst length of 16 timeslots, the number of state transitions is about 200,000. Thus, the total number of transitions we need to compute is about 200 million.

We can expect this model to accurately estimate the performance of the aggregation process when the packet size is much smaller than a timeslot. Fig. 4.3(a) shows the average burst length estimated by the model for a system with timeslot duration of 1 μs, burst aggregation period of 100 μs and packet length of 0.1 μs (at 10 Gbps = 125 bytes) for different target burst lengths. The burst length reaches the target burst length even for relatively small loads for an aggregation period of 100 μs except

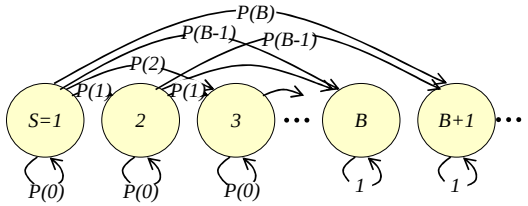

Figure 4.4: Model for variable packet length analysis

for the larger target burst lengths of 32 and 64. Fig. 4.3(b) shows the average burst aggregation efficiency for different target burst lengths. We achieve an efficiency of 90% even for small target burst lengths of 4 timeslots. There is not a significant gain in efficiency by using 32 timeslot target burst lengths as compared to 16 timeslots. Fig. 4.3(c) and 4.3(d) show the aggregations efficiencies for different values of packet lengths for a target burst length of 16 and 32 timeslots respectively. We can see that there is not much of a difference between the different packet lengths. For a target burst length of 16, the aggregation efficiencies are within 3% of each other and 2% of each other for a target burst length of 32. Thus, the packet lengths do not have a significant impact on the performance of the aggregation algorithm.

Variable packet length analysis

We now extend the fixed packet length analysis model to include variable packet lengths as shown in Fig. 4.4. The state of the system is the size of the queue, S, in bytes and $\pi_i(t)$ is the probability of the system being in state i at time t. $P(j)$ represents the probability that we get packets from hosts in a time unit whose total size is j bytes. In this model, the aggregation process stops as soon as the queue size grows to B bytes or more. The aggregation process starts as soon as we get the first packet and the probability that we start in state i is the probability that we get a packet of size i bytes. Assuming that the packet sizes are geometrically distributed, we get $\pi_i(0) = p(1-p)^{i-1}$, where $1/p$ is the mean packet size.

To calculate the probability of receiving packets in u seconds whose net size is j bytes, we assume that the packet arrivals follow a Poisson process. Thus,

$$P(j) = \sum_{h=0}^{\infty} P(j|h \text{ arrivals}) P(h \text{ arrivals})$$

For a Poisson process, the probability of h arrivals is given by $\lambda^h e^{-\lambda}/h!$, where λ is the mean number of arrivals in a time unit. The probability that the sum of h

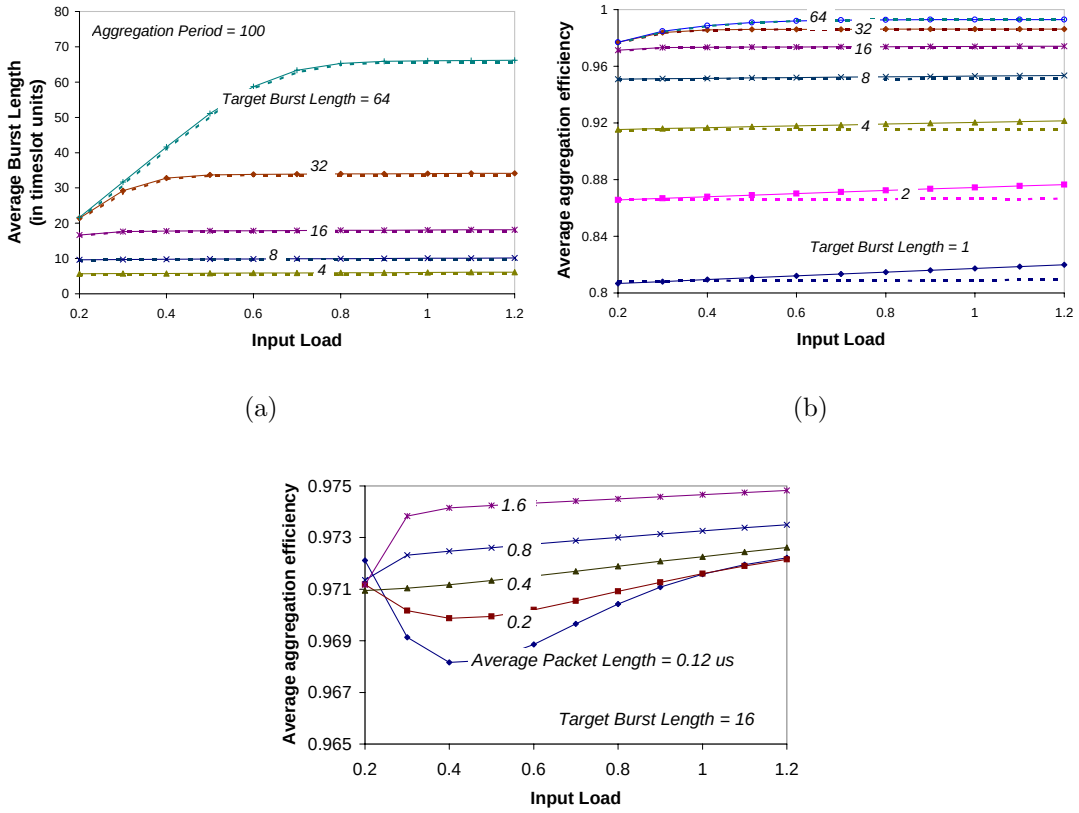

Figure 4.5: Results of the variable packet length analysis for aggregation period of 0.1 ms and timeslot duration of 1 μs (Average packet length = 0.1 μs for (a) and (b))

packets is j bytes assuming that the packet sizes have a geometric distribution with a mean of $1/p$ bytes and are identically and independently distributed is derived in Appendix A and is given by:

$$P(j|h \text{ arrivals}) = \binom{j-1}{h-1} p^h (1-p)^{j-h}$$

We calculate the state probabilities using the equations below:

$$\pi_i(t+u) = \begin{cases} \sum_{j=1}^{i} \pi_j(t) P(i-j), \text{if } 1 \leq i \leq B-1, \\ \sum_{j=1}^{B-1} \pi_j(t) P(i-j) + \pi_i(t), \text{if } i \geq B. \end{cases}$$

If l denotes the size of a timeslot, the average burst length and the average burst aggregation efficiency can be calculated as:

$$B_{avg} = \sum_{i=1}^{\infty} \lceil \frac{i\pi_i(T)}{l} \rceil$$
$$B_{eff} = \sum_{i=1}^{\infty} \frac{\pi_i(T)}{\lceil \frac{\pi_i(T)}{l} \rceil l}$$

In this model too, the number of states and the number of state transitions are dependent on the value of the time-step and the packet length we choose. To keep the computation manageable, we choose a time-step of 0.1 μs, a timeslot duration of 1 μs, and we assume that packet sizes are in increments of 0.1 μs. We compute the results, shown in Fig. 4.5(a) and 4.5(b), for an average packet size of 1.2 timeslots. We also show the results obtained through a simulation of the aggregation process with geometrically distributed burst lengths using dashed curves. Fig. 4.5 shows the performance estimates of the model for an aggregation period of 100 μs. The average burst lengths for various values of target burst lengths are shown in Fig. 4.5(a). The burst lengths are close to the target burst lengths for target burst length values of up to 16 even for small loads. Fig. 4.5(b) shows the average aggregation efficiencies for different target burst lengths. The difference between the aggregation efficiencies when using a target burst length of 16 timeslots and 64 timeslots is about 2%. Fig. 4.5(c) shows the aggregation efficiencies for a system with a target burst length of 16 timeslots and different average packet lengths and the efficiencies are within 1% of each other. Thus, the packet lengths does not affect the performance of the aggregation algorithm significantly for target burst lengths of 16 timeslots or more.

4.3 Simulation results

The analysis presented above is an approximate one because the packet length from hosts is geometrically distributed. This is not true with respect to traffic on the Internet. It has been shown that the traffic on the Internet is more bursty and has a heavy-tailed distribution [67, 20]. This property works in favor of the aggregation process because we can expect the aggregation queues to get filled in a shorter period of time.

To study the effects of heavy-tailed traffic on the aggregation process, we performed simulation experiments using sources that transmit packets whose interarrival

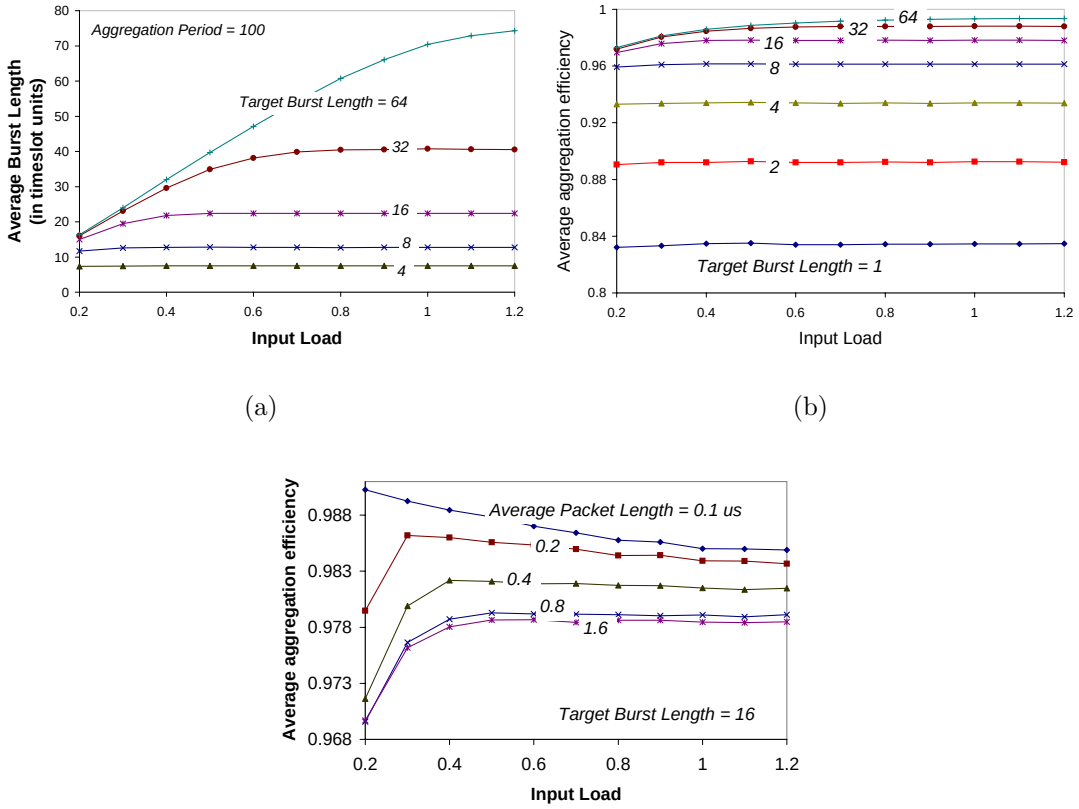

Figure 4.6: Results for different values of target burst length (Burst Aggregation Period = 100 timeslots, average packet length = 1.2 timeslots)

times are exponentially distributed and packet sizes are Pareto distributed with a shape parameter of 1.2. We performed the experiments with $2,000$ sources transmitting at a rate of 10 Mbps each, all transmitting to the same destination network. The bursts are transmitted on a link operating at 10 Gbps and we assume that each timeslot is 1 μs long. We measure the average burst lengths and the average burst aggregation efficiency of the aggregation process for different values of burst aggregation periods and target burst lengths.

4.3.1 Varying the Target Burst Length

Fig. 4.6 shows the results with different target burst lengths for an aggregation period of 100 μs. Fig. 4.6(a) shows the average burst lengths and Fig. 4.6(b) shows the aggregation efficiencies for different values of the target burst length. The difference

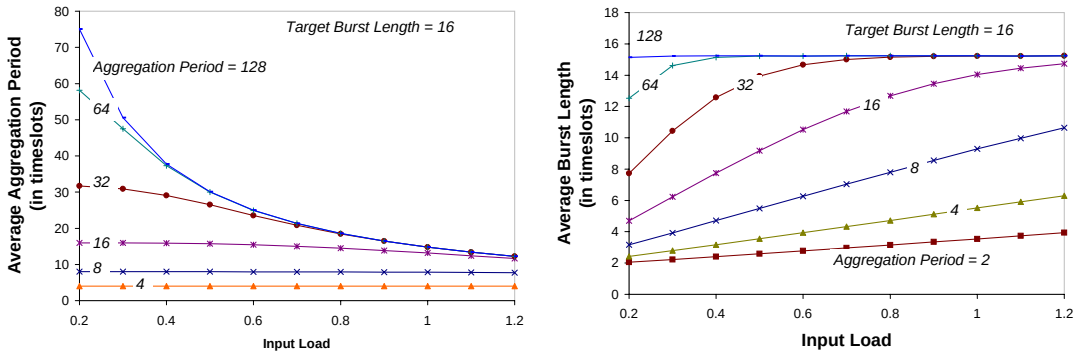

(a) (b)

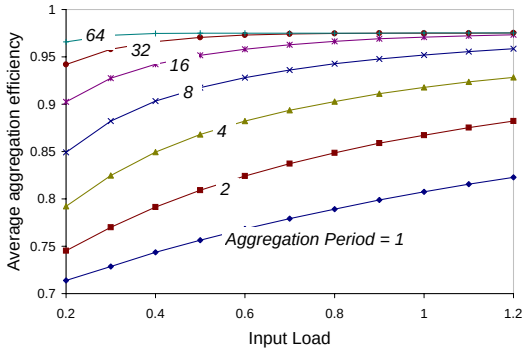

(c)

Figure 4.7: Results for different values of burst aggregation period (Target burst length = 16 timeslots, average packet length = 1.2 timeslots)

in the aggregation efficiency is about 2% between a target burst length of 8 timeslots and a target burst length of 16 timeslots and the difference in efficiency between 16 timeslots and 32 timeslots is 1%. Fig. 4.6(c) shows the aggregation efficiencies for varying average packets lengths for a system with a target burst length of 16 timeslots and they are within 2% of each other. However, the efficiencies are higher for smaller packet lengths.

4.3.2 Varying the Burst Aggregation Period

Until now we have seen how the length of the bursts are affected by the burst aggregation process. Fig. 4.7 shows the results with different values of burst aggregation period for a target burst length of 16 timeslots and packets from sources having an

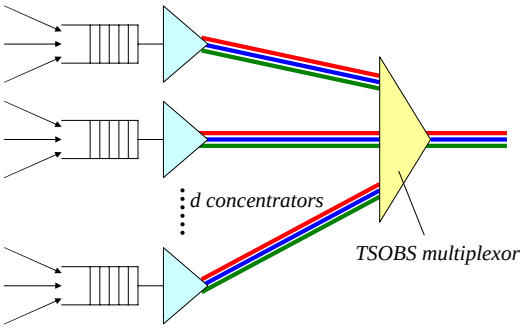

Figure 4.8: System configuration to measure the effect of burst drops on the performance of the aggregation process

average size of 1500 bytes or 1.2 timeslots approximately (here again, the packet length does not affect the performance significantly). With an aggregation period of $64 - 128$ timeslots, the aggregation process forms bursts that are close to the target burst lengths even for small loads. Fig. 4.7(a) shows the average time taken to aggregate the bursts. Fig. 4.7(c) shows the average aggregation efficiencies of the bursts for different aggregation periods. With an aggregation period of 64 timeslots, we achieve an efficiency of 97 % even for small loads. This suggests that an aggregation period of around 100 timeslots or 100 μs should be sufficient for the burst aggregation process.

4.4 Effect of Burst Drop Probability

In a TSOBS network, the burst drop probability increases with the burst length. This makes it easier for smaller bursts to pass through the network. However, we have seen that transmitting larger bursts results in better utilization of the network bandwidth from an aggregation perspective. In this section, we study the effect of the burst drop probability on the performance of the aggregation algorithm. To illustrate this effect, we analyze the performance of the algorithm when multiple concentrators transmit bursts through a TSOBS multiplexor as shown in Fig. 4.8. The concentrators send bursts on time division channels on each wavelength of the outgoing fiber. The multiplexor switches the data across timeslots when there is contention. Since each wavelength is switched independently, we study the system for one of the wavelengths. We assume that the concentrators transmit bursts on this wavelength such the bursts have exponentially distributed interarrival times. We derive the burst length distributions for different target burst lengths from the simulation experiments using heavy-tailed traffic for an aggregation period of 100 μs.

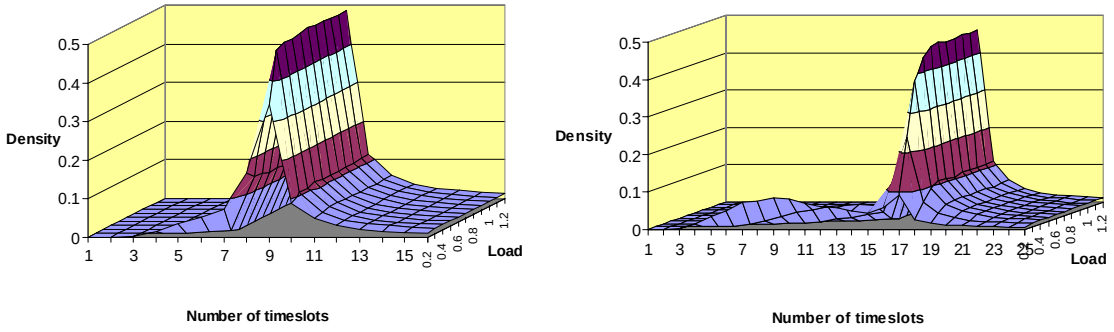

(a) Target Burst Length = 8 timeslots (b) Target Burst Length = 16 timeslots

Figure 4.9: Density functions of the burst length distributions

We refer to the load at the concentrator as the "access link load" and the term load refers to the load on the output link of the TSOBS multiplexor. The density functions of the burst length distributions for various access link loads are shown in Fig. 4.9 for a target burst length of 8 and 16 timeslots respectively.

We measure the burst drop probabilities of bursts for a TSOBS system with 128 timeslots per frame when 16 concentrators transmit through the multiplexor. To measure the performance of the aggregation process, we define a metric called *burst transmission efficiency* which is defined as the ratio of the amount of successfully transmitted data to the amount of bandwidth used to transmit it. The burst transmission efficiency is given by:

$$B_{x\text{-}eff} = (1 - P_{drop})B_{eff}$$

where P_{drop} is the burst drop probability and B_{eff} is the burst aggregation efficiency.

The burst transmission efficiency for different values of target burst lengths is shown in Fig. 4.10 for access link loads of 0.2, 0.6, and 1.0. The burst aggregation efficiency is a more dominant effect and hence, the transmission efficiency is higher for larger bursts. We can see that a target burst length of 8 to 32 timeslots results in good performance.

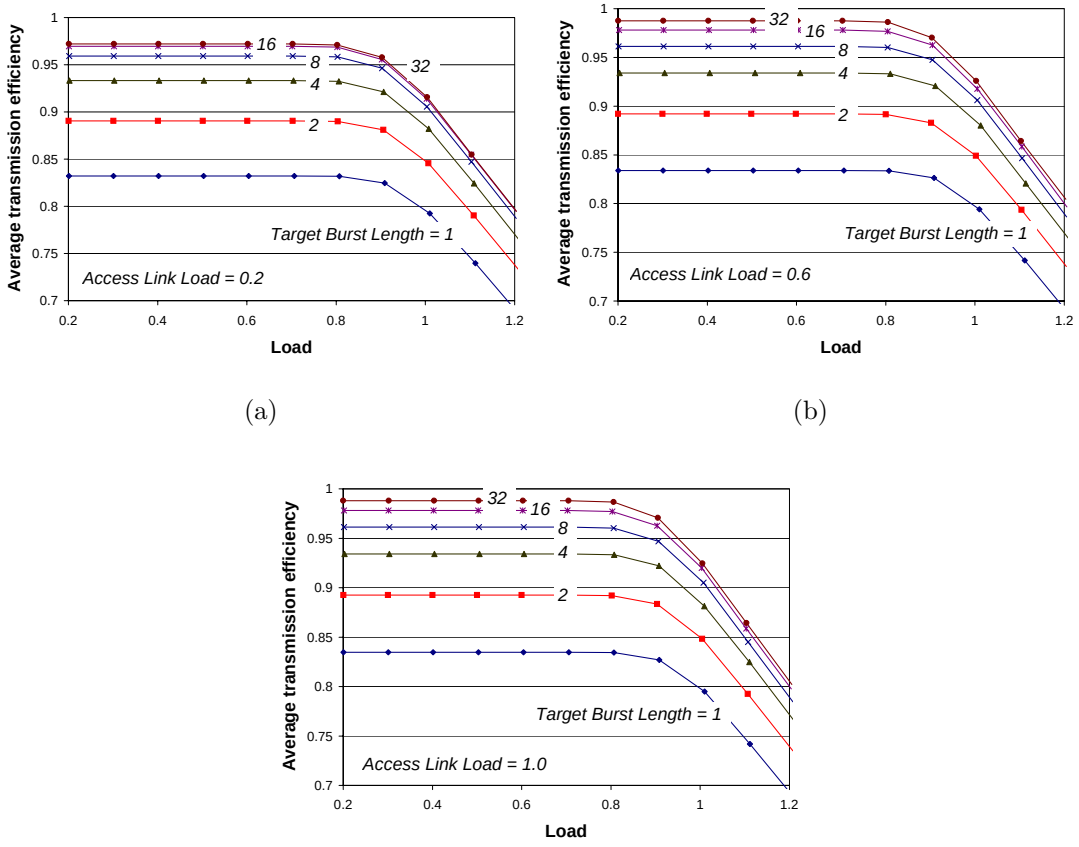

Figure 4.10: Transmission efficiency results for different target burst lengths and access link loads for a TSOBS network with $N = 128$

4.5 Conclusions

Time Sliced Optical Burst Switching (TSOBS) is a network technology in which data is transmitted in fixed size timeslots through the network. Aggregation of the data traffic from hosts that connect to the TSOBS network through concentrators results in better utilization of the network bandwidth. In this paper, we have studied this aggregation process. We presented an algorithm that can be used for aggregating data at the concentrators and presented an analysis that helps us select the parameters that determine the performance of the algorithm. Through the analysis and experiments, we have shown that a burst aggregation period of around 100 μs and a target burst length of 8 to 32 timeslots results in good performance.

4.6 Future Work

We have examined the aggregation mechanism for a broad range of typical traffic models and shown its performance from a network performance perspective. It is also important to characterize the effect of the aggregation mechanism from a single source's point of view. Sources in a TSOBS network could use a wide range of protocols (TCP, RTP, etc.) to transmit data and each protocol has different performance criteria and the aggregation mechanism can either reduce the performance of the protocol or could be beneficial. For example, in the case of TCP, it has been shown in OBS networks that the sources with small transmission rate do not perform well with aggregation and sources with larger transmission rates are positively affected by the aggregation mechanism. Additional work is necessary to study the effect of the aggregation mechanism we propose on the source's transmission characteristics.

Each aggregation queue has to deal with a large amount of traffic when the traffic going to a destination interface is large (100 Gbps, possibly more). Current memory speeds places restrictions on the data rates we can handle and typically tend to be the bottleneck in high speed routers. It is necessary to determine memory architectures that can handle very high data rates.

Chapter 5

Load Balancing in Time Sliced Optical Burst Switched Networks

In an OBS network, routers switch bursts in the wavelength domain using wavelength converting switches. When a wavelength channel of a link gets overloaded, bursts are switched to other wavelengths. Hence, the load on each wavelength is not an issue. However, in a TSOBS network, bursts are switched in the time domain and hence, bursts cannot be switched to other wavelengths during contention. If the load on a few wavelengths becomes larger than others, this leads to inefficient network usage because the traffic on the overloaded wavelengths generally have a higher burst discard probability.

In a TSOBS network (Fig. 3.1), the bursts are transmitted into the network by concentrators. Each concentrator uses the burst aggregation algorithm described in Chapter 4 to collect packets from hosts in aggregation queues and it assembles the packets into bursts. The bursts are then transmitted on a timeslot channel on one of the wavelengths of the output fiber. The network interface distributes the bursts evenly on all wavelength channels through a load balancer. This is shown in Fig. 5.1. When the burst aggregation process sends a burst, the load balancer determines a wavelength to transmit the burst and forwards the burst to the burst transmission queue corresponding to the wavelength. Laser transmitters transmit bursts from the transmission queues into the network in the TSOBS format.

Since bursts travel on different wavelength channels, they can experience variable delays in the network. Each TSOBS router can delay a burst by up to N timeslots, where N is the number of timeslots per frame in the network. Thus, two bursts leaving the concentrator at the same time and traveling on different wavelength

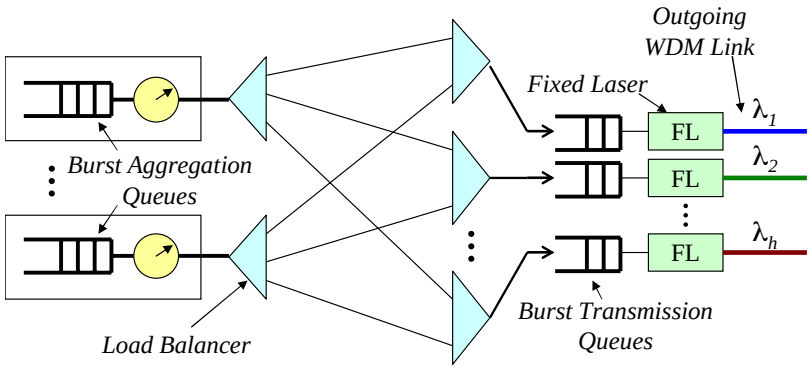

Figure 5.1: Load balancing in a network interface

channels can be off by up to NE timeslots after going through E hops in the network. At the destination interface, the bursts are stored in resequencing buffers where they are put back in sequence. The bursts are then disassembled and the packets are sent to the destination hosts.

When 100,000 hosts, each transmitting data at 100 Mbps, connect to the TSOBS network through a concentrator and 1% of them transmit to a destination interface, the net traffic originating from a concentrator to a destination interface can be as much as 100 Gbps. The bandwidth supported by one timeslot channel in a TSOBS network with 128 timeslots per frame and a transmission rate of 10 Gbps per wavelength is about 80 Mbps. Thus, within a 1 μs period, we can receive several bursts from a single aggregation queue in the concentrator.

The performance of the TSOBS network is affected by how well the load balancer distributes bursts across the wavelength channels. In this chapter, we study load balancing algorithms that result in better network utilization. The load balancing is performed on each individual aggregation queue independently. This is because the bursts in each aggregation queue have the same destination interface and can be expected to take the same path through the network, except in the event of routing changes which are not expected to occur frequently. We also assume that the load balancers of different concentrators operate independent of one another. In other words, the load balancing is performed in a completely distributed fashion. It is possible to use some form of feedback from the network to appropriately adapt the load balancers to the network conditions. The feedback messages will be delayed through the network and hence, cannot indicate the current state of the network accurately. Although network feedback could help in performing load balancing more efficiently, we do not study methods that use feedback here.

Fair load balancing on multiple channels has been studied before in the context of striping protocols in Reference [4]. It has been shown that fair load balancing can be viewed as the inverse of a certain class of fair queueing protocols. The paper also describes an algorithm to reassemble packets at the destination and put them back in sequence by using a matching fair queueing protocol at the destination. To use the fair queueing protocol to reassemble the packets, bursts from the different origin concentrators need to be stored in separate queues. This protocol has several advantages such as simplicity of implementation and requires no sequence numbers to mark packets for resequencing purposes. Since TSOBS is a new protocol, we have the flexibility of deciding the functionality that goes into the network. Thus, while it is desirable to do without sequence numbers for packets, it is not a big concern for TSOBS networks.

We now examine the effect of unevenly loaded wavelengths on the network utilization.

5.1 Effect of unevenly loaded wavelength channels on network utilization

Unevenly loaded wavelength channels result in a higher burst discard probability in the network than in a network with evenly loaded wavelength channels and hence, reduces the utilization of the network. To illustrate the effect of load imbalance on the network utilization, consider a simple TSOBS multiplexor that operates on two wavelengths and let us assume that sources transmit packets that are one timeslot long. Let the average input load on the first wavelength be ρ_1 and the average input load on the second wavelength be ρ_2. We can calculate the burst discard probabilities for each wavelength channel in the multiplexor using the M/D/1 model as shown in Fig. 3.3(a). Let the burst discard probabilities of the channels be $P(\rho_1)$ and $P(\rho_2)$ respectively. Now if we need to send a burst through the system, the burst discard probability of the system is given by $\frac{1}{2}[P(\rho_1) + P(\rho_2)]$, assuming that the burst could have been sent on either wavelength with equal probability.

On the other hand, if the wavelength channels of the multiplexor are evenly loaded, the average input load on each wavelength channel is given by $\rho = \frac{1}{2}(\rho_1 + \rho_2)$ and the burst discard probability is given by $P(\frac{1}{2}(\rho_1 + \rho_2))$.

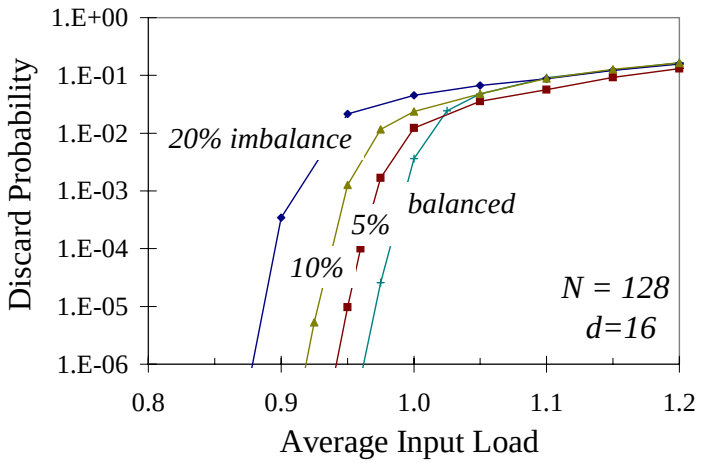

Figure 5.2: Burst discard probabilities of a TSOBS multiplexor for different values of *input load imbalance*

Define *input load imbalance* to be $(\rho_1 - \rho_2)/\rho$. This is a measure of the amount of imbalance in the input loads on each wavelength channel. The burst discard probabilities of a TSOBS multiplexor with 128 timeslots per frame ($N = 128$) and 16 concentrators connecting to it ($d = 16$) is plotted as a function of the input load in Fig. 5.2 for load imbalances of 5%, 10% and 20%. The "balanced" plot corresponds to a system when both the wavelengths are balanced and in this case, the multiplexor achieves a utilization of 96% with a burst discard probability of 10^{-6}. With a 5% imbalance, the utilization goes down to 94% and with imbalances of 10% and 20%, the utilization goes down to 92% and 88% respectively.

5.2 Causes of load imbalance in a TSOBS network

We now examine how wavelength channels become unevenly loaded in a TSOBS network. Several concentrators connect to a TSOBS network and each of them performs load balancing independently. When concentrators transmit bursts that use a particular link in the path to the destination, the load on each wavelength channel of the link is determined by the net amount of traffic sent by the concentrators on the wavelength. There are several effects that can cause load imbalances in the network.

First, when transmitting a burst, a concentrator has no information on what wavelengths the other concentrators will be using to transmit bursts. Thus, concentrators transmitting through a common link can get "synchronized" and transmit bursts using some wavelength all at the same time, causing the wavelength channel to

become overloaded. If a link has h wavelengths and if at some time, each concentrator has h bursts, the concentrators can transmit one burst on each wavelength channel and the wavelengths will be equally loaded. However, the number of bursts that each concentrator transmits need not be a multiple of h. In this case, the concentrator transmits to a subset of the wavelengths only. This can lead to overloading of the wavelengths, that are picked by more concentrators.

Second, the lengths of the bursts are variable and have a length distribution determined by the burst aggregation process as shown in Fig. 4.9. In a TSOBS network, each burst is transmitted by allocating one timeslot at the same position within a frame. In a TSOBS network that has N timeslots per frame, a burst that is x timeslots long occupies a timeslot channel in a wavelength for x frames, and the timeslot cannot be used by another burst for xF timeslots, where F is the frame duration. Thus, a long burst occupies a timeslot channel within a frame for a longer time than a short burst. Consider two wavelength channels of the link and consider the case when concentrators transmit relatively longer bursts to one wavelength channel and shorter bursts to the other. Even if the number of bursts transmitted to each wavelength channel is the same, the wavelength channel with the longer bursts is loaded for a longer period of time. Consequently, it is not sufficient to balance the number of bursts sent to each wavelength channel.

Third, all concentrators need not be equipped with transmitters that can send bursts over the entire set of wavelength channels. The number of wavelength channels a concentrator needs to support depends on the total amount of traffic sent by the hosts that are connected to the concentrator. If concentrators perform "fair" load balancing over all wavelength channels, the wavelengths supported by these concentrators will have higher load in the network.

Finally, since the cost of a TSOBS router is proportional to the number of wavelength channels, routers, that need to support a relatively lesser amount of traffic, need not implement switching over the entire range of wavelengths. Thus, the traffic from these routers can overload the wavelengths, that it supports, at a downstream router, that implements the entire set of wavelengths.

The last two are long term effects that can be dealt with over a longer period of time. In this paper, we study load balancing schemes that address the short term effects and do not study the long term ones.

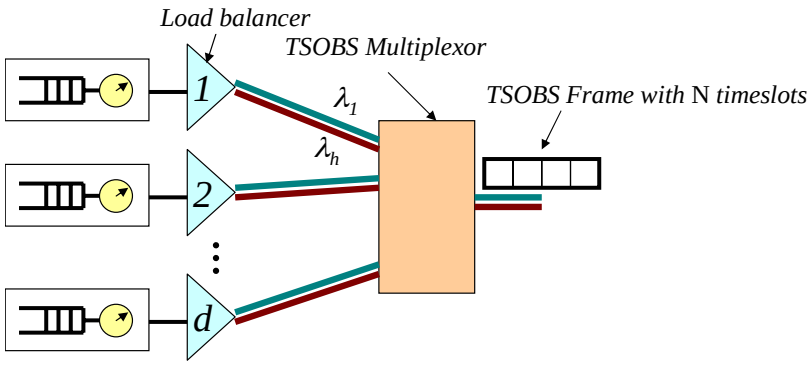

Figure 5.3: Multiplexor model for the study of load balancing algorithms

5.3 Load balancing algorithms

In this section, we study different load balancing algorithms that we can employ and evaluate their performance in a TSOBS network. Consider a link in the TSOBS network. Several concentrators, distributed across the network, send bursts through this link. This link can be modeled using a simple multiplexor as shown in Fig. 5.3. The multiplexor operates on h wavelength channels and each wavelength has N timeslots per frame. The link is used by d concentrators to send bursts and each concentrator uses a load balancer to spread the bursts across the wavelength channels. Bursts transmitted from each concentrator experience different amounts of delay through the network. However, the operation of the load balancing algorithm is unaffected by the delay. Thus, we can ignore the delay from the concentrators to the link. An algorithm that performs well and results in utilizing the link efficiently can be expected to perform well in a network setting too.

We use this model to evaluate the performance of load balancing algorithms through simulation experiments. For the purpose of the experiments, we assume that the TSOBS multiplexor operates with a timeslot duration of 1 μs. Also, we assume a Target Burst Length of 16 timeslots and a Burst Aggregation Period of 100 μs for the burst aggregation process. This gives us the burst length distributions that were determined in Chapter 4. We also assume that the load balancer receives bursts that have exponentially distributed inter-arrival times.

We saw earlier in Section 5.1 that the performance of a load balancing algorithm depends on how evenly it spreads the bursts across the wavelength channels. To evaluate how well the algorithms distribute the bursts and the load, we measure the number of bursts and the number of timeslots transmitted by the concentrators

on each wavelength channel in 500 μs intervals of time. Let $B_i(t_1, t_2)$ be the total number of bursts transmitted on wavelength i from time t_1 to t_2 and let $D_i(t_1, t_2)$ be the total number of timeslots transmitted by the concentrators on wavelength i from time t_1 to t_2.

Definition 5.3.1 *Define the* deviation ratio *of a number n_i, given a set of x numbers, $n_1, n_2, \ldots, n_x$ as the ratio of the number to the average of all the numbers in the set.*

$$DevRatio(n_i) = n_i / Avg(n_1, n_2, \ldots, n_x)$$

Define the maximum deviation ratio *of a set of x numbers as the deviation ratio of the maximum of the x numbers. Similarly, define the* minimum deviation ratio *as the deviation ratio of the minimum of the x numbers.*

The maximum and the minimum deviation ratios give us an estimate of the imbalance of a set of numbers. For a system with minimal imbalance, the maximum and the minimum deviation ratios will be close to 1. We are interested in the imbalance in the number of bursts and the number of timeslots sent to the wavelength channels of the multiplexor. The cumulative deviation ratios (maximum and minimum) of the number of bursts (and the number of timeslots) sent to the wavelength channels is the deviation ratios of the cumulative number of bursts sent until time t. This gives us an estimate of how well the load balancing algorithms distribute the bursts (or timeslots) in the long term. The cumulative deviation ratios for the number of bursts and the number of timeslots sent are given by the deviation ratios of the set of numbers, $B_i(0, t)$ and $D_i(0, t), 0 \leq i < h$ respectively.

We define the short term deviation ratios as the deviation ratios of the number of bursts and the number of timeslots sent in each 500 μs period, and is given by the deviation ratios of the set of numbers, $B_i(t, 500 + t)$ and $D_i(t, 500 + t), 0 \leq i < h$ respectively for each t (in μs). This gives us the variation in the number of bursts and timeslots sent to the multiplexor over a 500 μs period (approximately 4 frames).

We denote the maximum and minimum deviation ratios by MAX/μ and MIN/μ respectively. In the case of the short term deviation ratios for the number of timeslots, we also calculate the deviation ratio for the number of timeslots that a wavelength can handle without overflowing its capacity. Since, we assume a timeslot duration of 1 μs, the maximum number of timeslots that can be sent on any wavelength is 500. We denote this deviation ratio by $Limit/\mu$. If MAX/μ is larger than $Limit/\mu$, this results in a burst loss.

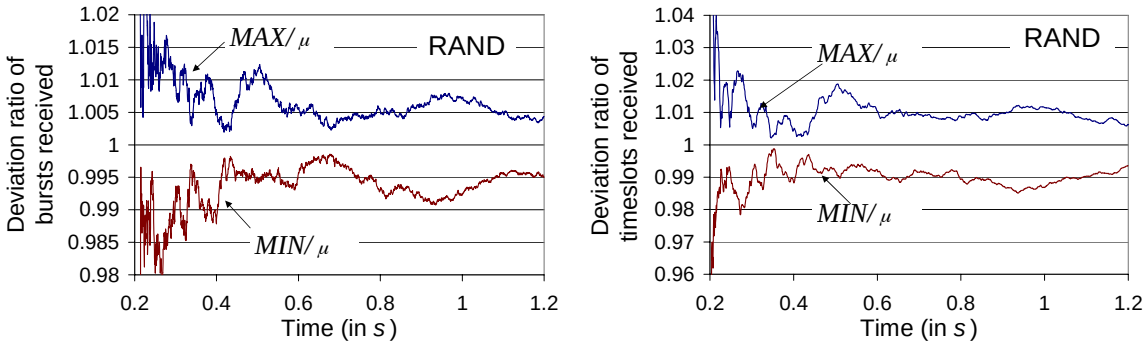

(a) Cumulative

(b) Cumulative

Figure 5.4: The deviation ratios of the number of bursts and the number of timeslots received by the multiplexor when using the RAND algorithm

We also measure the burst discard probability of the TSOBS multiplexor for the load balancing algorithms to evaluate their performance. Note that load balancing would not be an issue if each TSOBS router were equipped with wavelength converters (WCs). Wavelength converters can be used to switch the data across wavelengths and hence, during periods of overload of some wavelength, the bursts on the wavelength can be switched to a wavelength that is not as loaded. Ideally, we would like the load balancing algorithms in a network with no wavelength converters to spread the bursts across wavelengths such that the network performance is same as a network with wavelength conversion. Thus, the performance of a network with wavelength conversion is an upper bound on the performance of the load balancing algorithms. We evaluate the load balancing algorithms by comparing their performance with the performance of a network with wavelength conversion. We now present four load balancing algorithms and their performance results.

5.3.1 RAND

When a burst arrives at the load balancer from the burst aggregation process, algorithm RAND selects a wavelength channel at random and the load balancer sends the burst on this channel. The random algorithm (RAND) can be expected to distribute load evenly on a long term, but does not result in ideal load balance conditions in the short term. The advantage of using the algorithm is that it is very simple to implement and it can be done at very high speeds.

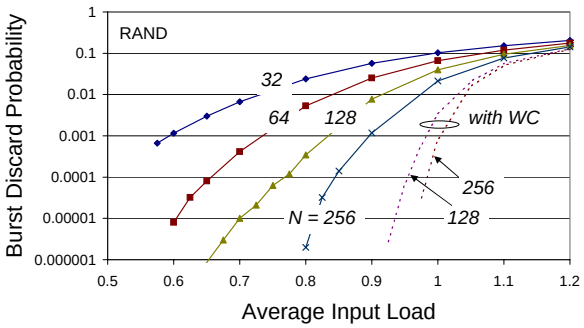

Figure 5.5: Burst discard probabilities using the RAND algorithm for various timeslots per frame (N) with $h = 8$ and $d = 16$

For determining the deviation ratios, we assume that 16 concentrators are transmitting to the multiplexor ($d = 16$), each frame carries 128 timeslots ($N = 128$), and the multiplexor operates with 4 wavelength channels ($h = 4$). Fig. 5.4(a) and Fig. 5.4(b) show the cumulative deviation ratios of the number of bursts and the number of timeslots sent for an average input load of 0.85 for a period of 1 second respectively. If the algorithm balances the load effectively, we can expect the MAX/μ and the MIN/μ curves to converge to 1. Algorithm RAND does not balance the load both in terms of the number of bursts and in terms of the number of bursts effectively and the variance in the loads of the wavelength channels is relatively large. The imbalance (given by $MAX/\mu - MIN/\mu$) in the number of bursts is within 3% and in the number of timeslots is within 4%.

For determining the burst discard probability of the load balancing algorithms in the single multiplexor model, we performed simulation experiments in which we used 16 concentrators ($d = 16$), 128 timeslots per frame ($N = 128$), and 8 wavelength channels ($h = 8$) as reference values. If we vary a parameter, we hold the others at their reference values.

Fig. 5.5 shows the burst discard probabilities of the multiplexor when the RAND algorithm is used in the load balancer for different values of N. Also shown using dashed curves are the burst discard probabilities of the system with wavelength conversion. The system using RAND achieves a utilization of about 0.68 when it operates with $N = 128$ at a burst discard probability of 10^{-6} and a utilization of 0.8 when N is 256. The optimum achievable utilization (with wavelength conversion) is approximately 0.92 and 0.96 with $N = 128$ and $N = 256$ respectively. So, the RAND algorithm achieves about 74% of the maximum achievable utilization with $N = 128$

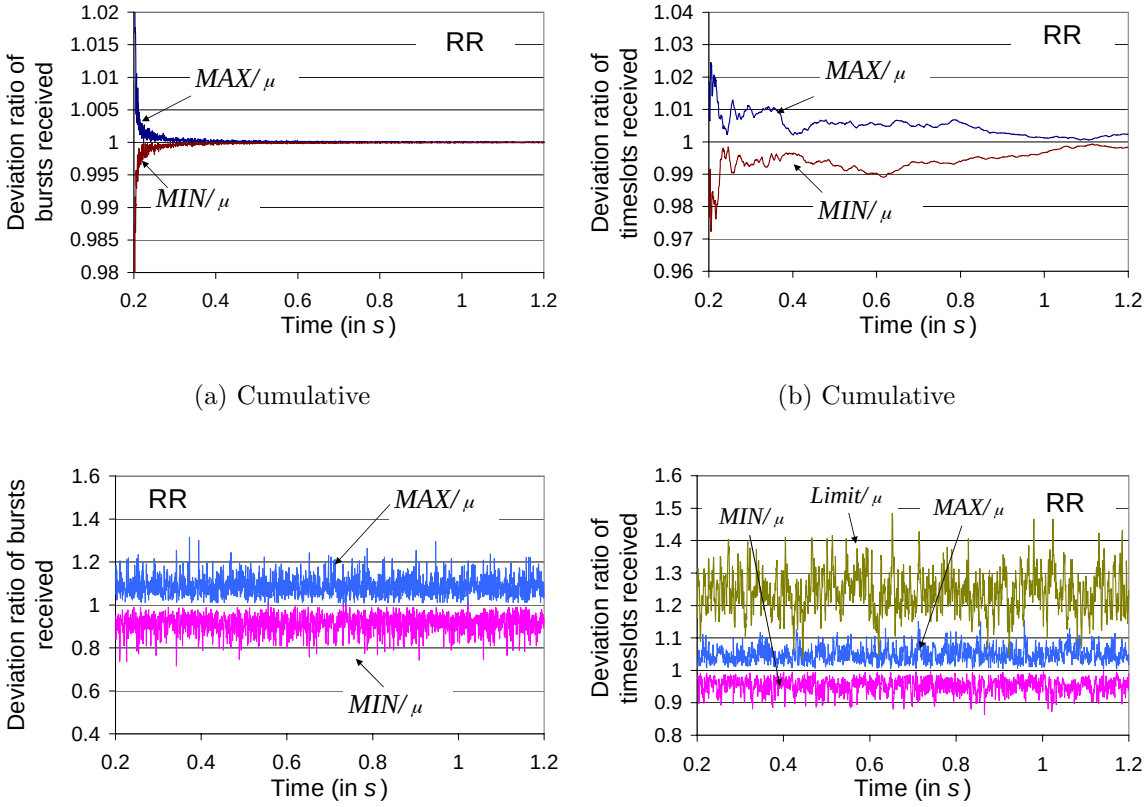

(a) Cumulative

(b) Cumulative

(c) Short Term

(d) Short Term

Figure 5.6: The deviation ratios of the number of bursts and the number of timeslots received by the multiplexor when using the RR algorithm

and about 83% with $N = 256$. Also, we observed that the performance of RAND does not improve with an increase in the number of wavelengths.

5.3.2 RR

The next algorithm we study, denoted by RR, picks a wavelength channel in a fixed round robin order to transmit the bursts that arrive from the burst aggregation process. This algorithm balances the load on the wavelength channels at a burst level and does not factor in the length of bursts when choosing the wavelength channel. This algorithm works well if we had equal length bursts. However, when the burst lengths are variable, RR has a bad worst case when the long bursts are sent on the same wavelength and the shorter bursts are sent on others.

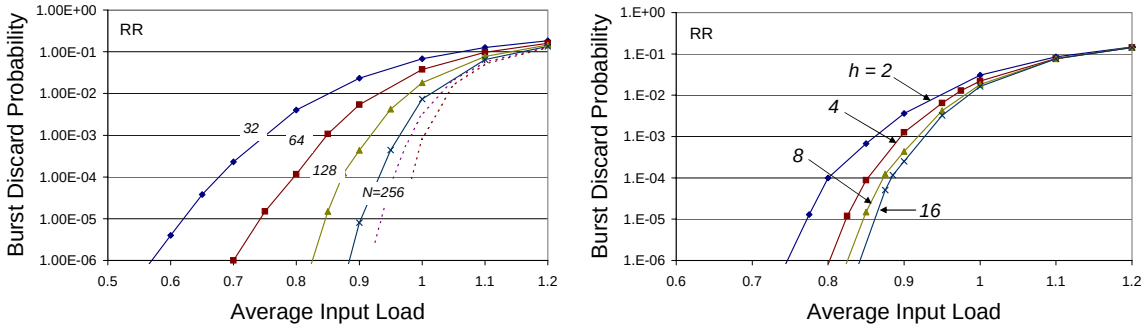

(a) $h = 8$, $d = 16$ (b) $N = 128$, $d = 16$

Figure 5.7: Results of using the RR algorithm for load balancing

Also, if a few concentrators get "synchronized" and transmit bursts on some wavelength channel, they'll transmit successive bursts on the same successive wavelength channels. Thus, they could remain synchronized for a long period of time. This problem can be alleviated by having each concentrator use a different random permutation pattern to order its burst transmissions. Even if a few concentrators send bursts using the same wavelength channel at one time, the next wavelength channel that they use is determined by the random order and hence, there is a high probability that they will not remain synchronized.

Fig. 5.6(a) and Fig. 5.6(b) show the cumulative deviation ratios for a system with $h = 4$, $d = 16$, and $N = 128$ for a system load of 0.85 over a period of 1 second. RR balances the number of bursts transmitted over the wavelength channels and we can see that the deviation ratios of the number of bursts transmitted quickly converge to 1. However, the deviation ratios of the number of timeslots transmitted do not converge to 1 quickly because RR does not balance the bursts based on their lengths.

The short term deviation ratios (over 500 μs periods) in the number of timeslots and bursts sent are shown in Fig. 5.6(c) and Fig. 5.6(d) respectively. The imbalance $(MAX/\mu - MIN/\mu)$ in the number of bursts tends to be within 40% and in the number of timeslots tends to be within 20%, in most cases.

Fig. 5.7 shows the burst discard probabilities of the system when the concentrators use the RR algorithm for load balancing. Fig. 5.7(a) shows the burst discard probabilities for different values of N. Here again, the dashed plots correspond to the case with wavelength conversion for $N = 128$ and 256 respectively. The RR algorithm

achieves a utilization of 0.82 for $N = 128$ and 0.89 for $N = 256$ and this corresponds to 90% of the achievable utilization for $N = 128$ and 93% for $N = 256$.

Fig. 5.7(b) shows the burst discard probabilities for different values of h, the number of wavelength channels. The algorithm performs better with more wavelength channels, but the performance approaches a limit as the number of channels grows beyond 8.

5.3.3 WMin

RR does not balance the bursts based on their burst lengths and this can lead to concentrators sending longer bursts to a wavelength channel, causing an imbalance in the input load. The next algorithm we study, WMin, performs load balancing based on the total volume of traffic sent on each wavelength channel. Algorithm WMin keeps track of the amount of data sent on each wavelength channel by the concentrator. When a burst arrives at the load balancer, WMin picks the wavelength that has the least amount of data sent on it.

Note that the amount of data sent on a wavelength channel i can never be larger than the amount of data sent on some other wavelength by more than the size of the burst that was last transmitted on the wavelength i. Let the amount of data transmitted on wavelength channel i be $D(i)$ and the amount of data transmitted on wavelength j be $D(j)$. Also, let the last burst transmitted on wavelength i be of size k timeslots. If $D(i) - D(j) > k$, then $D(i) - k > D(j)$. Thus, this burst should not have been sent on wavelength i because it was not the wavelength with the least amount of data sent. Thus, $D(i) - D(j) \leq k$.

Fig. 5.8(a) and Fig. 5.8(b) show the cumulative deviation ratios for a system with $h = 4$, $d = 16$, and $N = 128$ for a system load of 0.85 over a period of 1 second. WMin balances the number of timeslots sent on the wavelengths and not the number of bursts. Thus, it takes a long time for the deviation ratios of the number of bursts sent to converge to 1. However, the number of timeslots sent converge to 1 very quickly.

The short term deviation ratios in the number of timeslots and bursts sent are shown in Fig. 5.8(c) and Fig. 5.8(d) respectively. The imbalance in the number of bursts tends to be within 60% in most cases. This is more than the imbalance in the number of bursts sent by the RR algorithm and this can be expected because RR balances the number of bursts sent and WMin does not. Unexpectedly, the imbalance

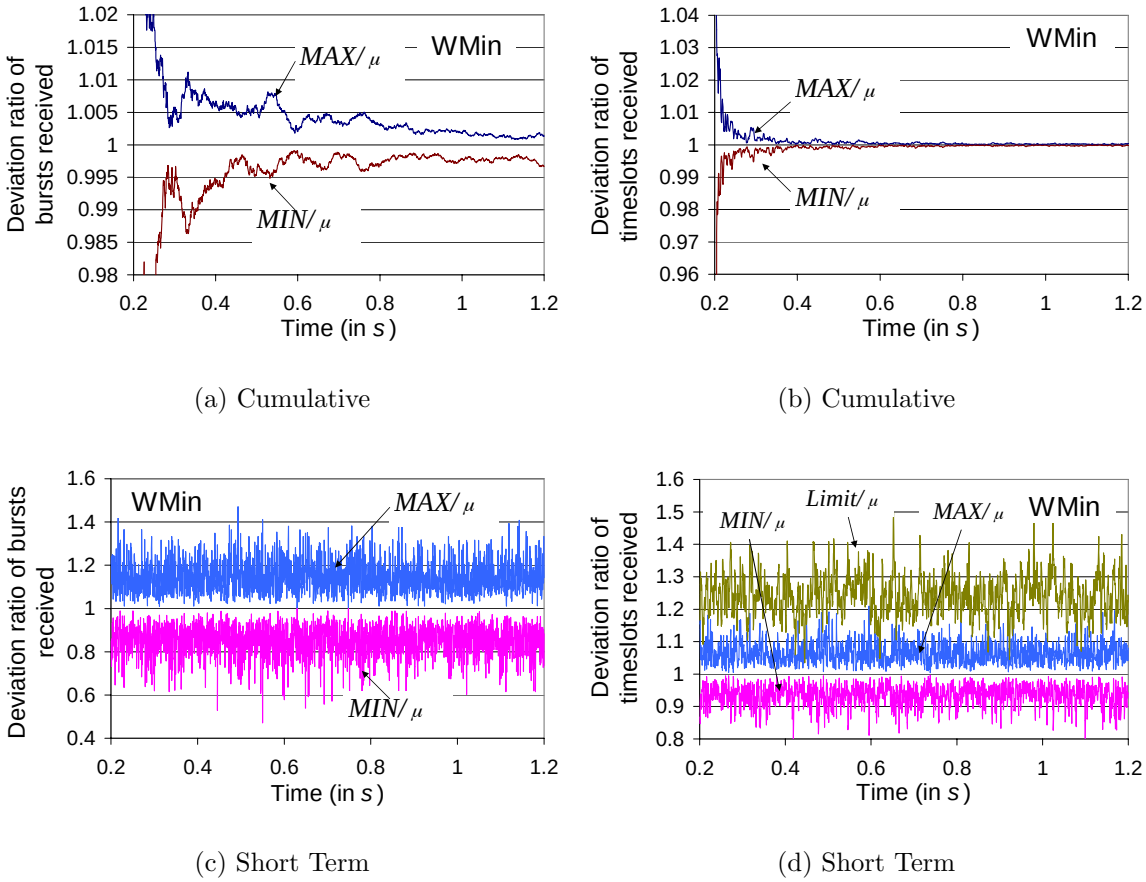

(a) Cumulative

(b) Cumulative

(c) Short Term

(d) Short Term

Figure 5.8: The deviation ratios of the number of bursts and the number of timeslots received by the multiplexor when using the WMin algorithm

in the number of timeslots is more than the imbalance when using RR and tends to be within 30%, in most cases. This is surprising because WMin balances the number of timeslots sent on the wavelengths.

The reason WMin has a larger imbalance in the number of timeslots sent than RR is because WMin can send a bunch of small bursts to some wavelength to compensate for sending a large burst on other wavelengths. To illustrate this, consider this simple example. Let us assume that a concentrator transmits bursts on two wavelengths and that it has 10 bursts to transmit at time 0, where the first burst is 10 timeslots long and the rest are 1 timeslot long. WMin sends the long burst on one wavelength and sends the remaining 9 bursts on the other wavelength. Thus, in the outgoing frame, one wavelength has 9 timeslot channels that are occupied and the other wavelength has only 1 timeslot channel that is occupied (because each burst

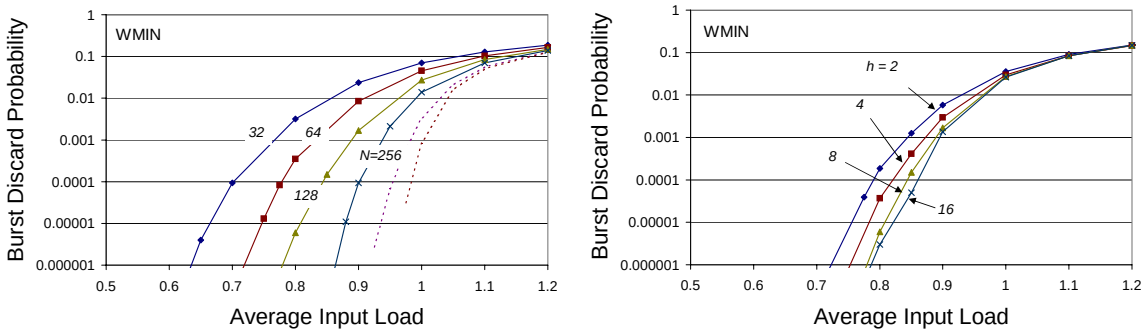

(a) $h = 8$, $d = 16$ (b) $N = 128$, $d = 16$

Figure 5.9: Results of using the WMin algorithm for load balancing

occupies only one timeslot channel in each frame). This can result in a short term overload in the number of timeslots that are sent to the multiplexor. RR, on the other hand, sends 5 bursts on each wavelength and thus, each wavelength has 5 occupied timeslot channels.

Fig. 5.9 shows the burst discard probabilities of the multiplexor when using the concentrators use the WMin algorithm for load balancing. Fig. 5.9(a) shows the burst discard probabilities for different values of N. The dashed plots correspond to the optimum performance when using wavelength conversion. The algorithm achieves a utilization of 0.78 for $N = 128$ and a utilization of 0.87 for $N = 256$ when the burst discard probability is 10^{-6}. This corresponds to 85% of the maximum achievable utilization for $N = 128$ and 90% for $N = 256$. In general, the performance of WMin is better that RR when the number of timeslots per frame is small (≤ 32). However, when N is larger, RR performs better than WMin.

Fig. 5.9(b) shows the burst discard probabilities for varying values of h, the number of wavelength channels. As with RR, the algorithm performs better with more wavelength channels. However, the performance improvements approach a limit as the number of wavelength channels grows beyond 8.

Surplus Round Robin (SRR) is an algorithm described in Reference [4] that can be used to perform load balancing. This algorithm defines a quantum of data that can be sent on each channel during a "round" in the round robin scheme. In each round, a channel can be used to transmit bursts such that the net amount of data transmitted is equal to the quantum allocated to the channel. If it exceeds its quota, the surplus is deducted from the next round's quantum. Let us denote channel i's

surplus by $S(i)$ and the quantum by $Q(i)$. For fair round robin all the quantums are the same. When sending bursts on channel i, the quantum is added to the surplus and bursts are sent until the surplus becomes negative. The main advantage of this method is that it is simple to implement. However, for it work effectively the quantum has to be at least the size of the largest burst. This is a very large value and could potentially results in a lot of small bursts being sent on a wavelength channel in one round. The number of bursts could be larger than the number that is sent by the WMin algorithm.

5.3.4 TSMin

WMin does not perform well because it balances the amount of traffic sent on each wavelength in the long term and not in the short term. This results in a large imbalance in the number of timeslot channels used in the wavelengths. Algorithm TSMin balances the number of timeslot channels that are in use at a concentrator at any given time. When a burst arrives, TSMin picks the wavelength with the least number of timeslot channels that are occupied. When there is a tie among wavelength channels, the first wavelength in some fixed order can be picked. However, all concentrators could pick the same wavelength, resulting in an imbalance. To avoid this, we select the wavelength that is closest to the wavelength, that was used to send the last burst, in some order. If the number of wavelength channels is h, and if we used wavelength i to transmit the last burst, wavelength $(i+1) \bmod h$ has the highest priority to transmit the next burst, followed by wavelength $(i+2) \bmod h$, and so on.

TSMin, clearly, does not have the problem, that WMin has, of a large imbalance in the number of timeslot channels used in the wavelengths. However, like RR, TSMin can assign longer bursts to a particular wavelength channel. To see this, consider a system at time 0 with an alternating pattern of long and short bursts. Let us assume that the length of long bursts is 10 timeslots and the length of short bursts is 2 timeslots. TSMin behaves exactly like RR for the first two frames, assigning the long bursts to one wavelength channel and the short bursts to another. However, after the first two frames, some of the short bursts exit the system, freeing the timeslot channels they were using. This creates an imbalance in the number of timeslot channels that are in use. TSMin rectifies this imbalance by assigning the next couple of bursts to the timeslot channels that were freed. RR, however, does not rectify this imbalance and continues to assign the long bursts to the overloaded

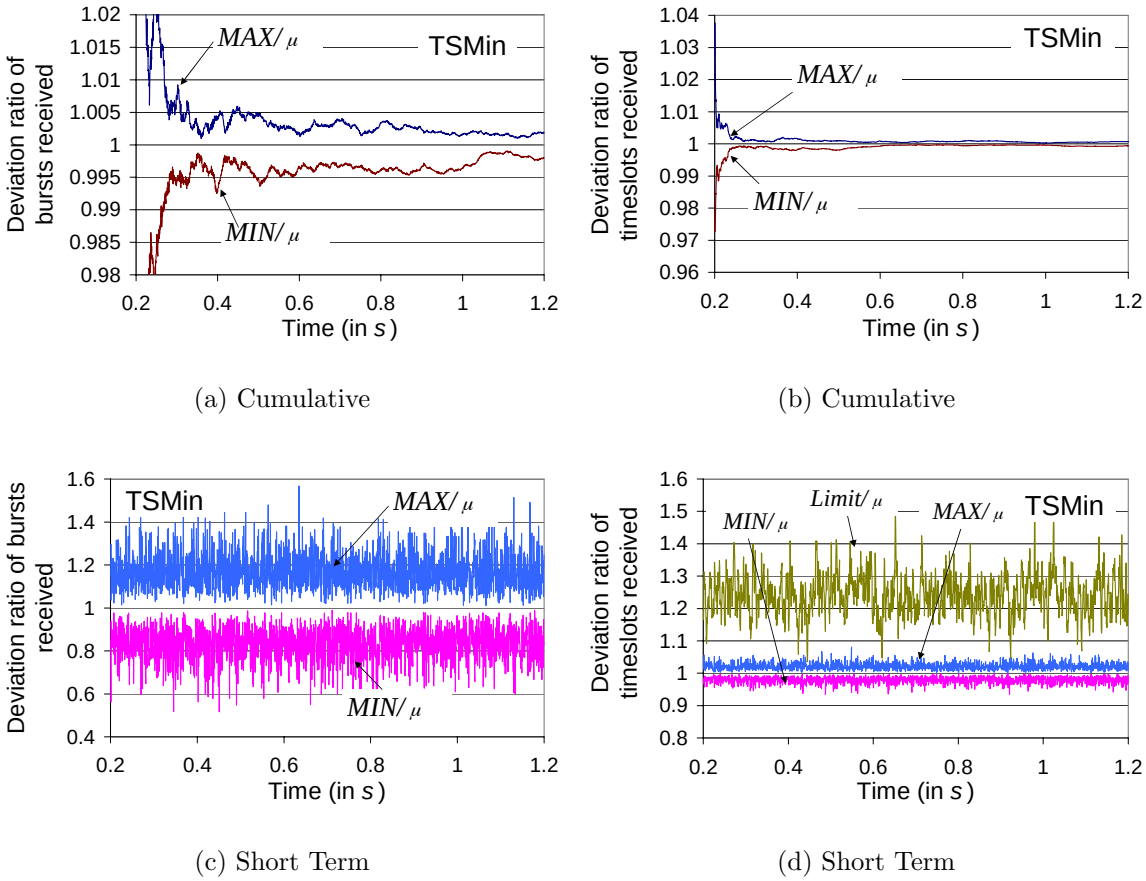

(a) Cumulative

(b) Cumulative

(c) Short Term

(d) Short Term

Figure 5.10: The deviation ratios of the number of bursts and the number of timeslots received by the multiplexor when using the TSMin algorithm

wavelength channel. Thus, while TSMin can create a short term imbalance in the load on the wavelengths by assigning longer bursts to a particular wavelength, it is better than RR because it rectifies the imbalance when it detects one. Hence, TSMin can be expected to perform better than RR too.

Fig. 5.10(a) and Fig. 5.10(b) plot the cumulative deviation ratios for the number of bursts and timeslots sent respectively, when the concentrators use TSMin to perform load balancing. The deviation ratios of the number of bursts and timeslots sent converge to 1 in the long term. However, the deviation ratios of the number of bursts do not converge as quickly as they do when using RR and the deviation ratios of the number of timeslots do not converge as quickly as they do when using WMin.

Fig. 5.10(c) and Fig. 5.10(d) show the short-term deviation ratios of the number of bursts and timeslots sent respectively. The imbalance in the number of bursts sent is almost the same as the imbalance when using WMin. However, the imbalance in

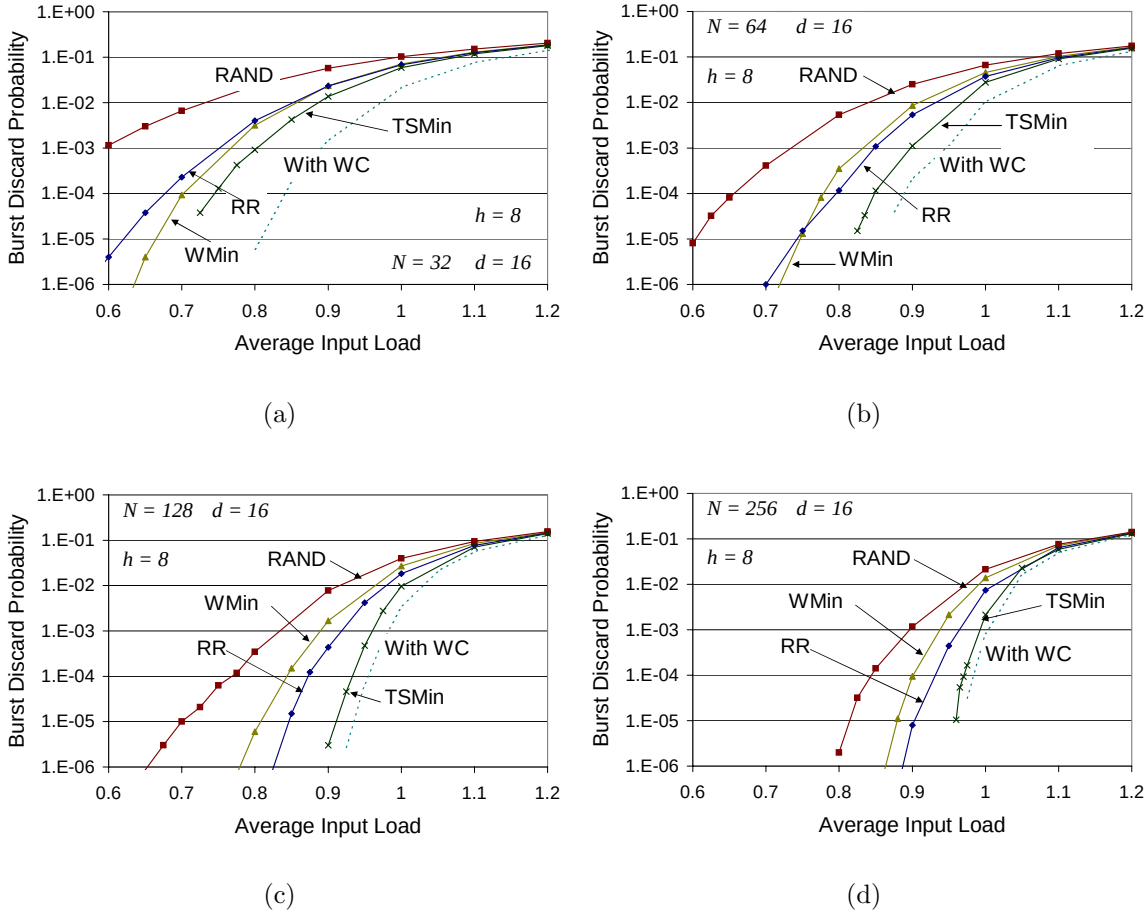

Figure 5.11: Burst discard probabilities of the system for different values of N

the number of timeslots sent is smaller than the variance when using either RR or WMin and is within 10% for most cases. This is because each concentrator balances the number of timeslots that are in use in each wavelength. The difference between $Limit/\mu$ and MAX/μ is larger than when using the other three algorithms and this implies that the probability of burst discards is relatively low.

In Fig. 5.11, we plot the burst discard probabilities of all four algorithms for varying values of N. TSMin performs the best for all values of N and the performance difference between the system using TSMin and a system with wavelength conversion becomes smaller as N grows. For $N = 128$, TSMin achieves a utilization of approximately 0.89 for a burst discard probability of 10^{-6} and this about 97% of the maximum achievable utilization. For $N = 256$, TSMin achieves a utilization of approximately 0.95 and this corresponds to 99% of the maximum achievable utilization.

Note that RR performs better than WMin when the number of timeslots per frame is large ($N = 128, 256$). However, WMin performs better when $N = 32$ and at lower loads when $N = 64$. This is because RR results in an imbalance in the long bursts that are sent to wavelength channels. When N is small, the longer bursts tend to occupy a larger fraction of the timeslot channels causing a larger burst discard probability. When N is large, the imbalance in the long bursts has a smaller effect. RAND performs the worst in all cases.

Fig. 5.12 shows the burst discard probability of a system with $N = 128$ and $d = 16$ for various values of h. The performance of TSMin is better with larger values of h and here again, the performance approaches a limit as the number of wavelength channel becomes larger.

Among the four algorithms, TSMin performs the best in all the system configurations we have studied. We have shown that it is not sufficient to balance the load in the long term and in the case of WMin, this results in a very bad short term performance, as indicated by the imbalance in the short term deviation ratios of the number of timeslots sent to the multiplexor. TSMin balances the load in the short term and this results in much better performance, even though it has a relatively larger long term imbalance in the number of timeslots sent.

5.4 Performance of load balancing algorithm in a TSOBS network

The performance of the load balancing algorithms was studied using a single TSOBS multiplexor and we expect that the algorithm that performs best can be expected to

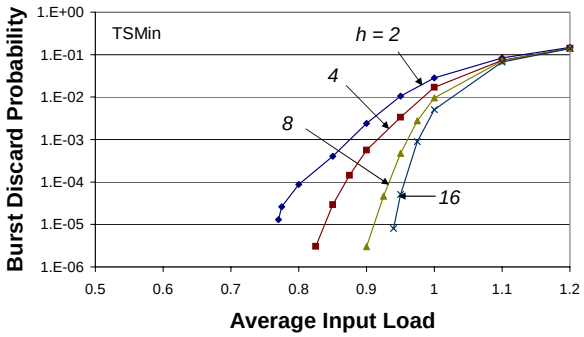

Figure 5.12: Burst discard probabilities using the TSMin algorithm for varying number of wavelength channels (h) with $N = 128$ and $d = 16$

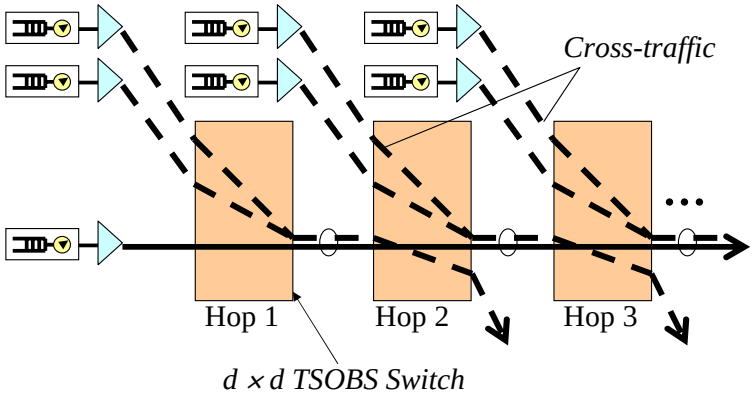

Figure 5.13: A TSOBS network model

perform the best in a network of TSOBS switches too. We can verify this claim by modeling the network as shown in Fig. 5.13. We measure the burst discard probability of the traffic originating from one concentrator that passes through D switches (or D hops). In each switch we have cross-traffic coming from $d-1$ other concentrators. This cross-traffic exits at the next switch. The average load is kept the same across all hops. The concentrators, that send the cross-traffic, perform load balancing using the same algorithm as the concentrator we measure. For very low probabilities, the burst discard probability in the network is approximately the sum of the burst discard probabilities of the individual hops.

Fig. 5.14 shows the burst discard probabilities of the TSOBS network for $D = 2, 4$, and 6 respectively for $N = 128$. In all three cases, TSMin performs the best, followed by RR and WMin respectively.

5.5 Conclusion

In Time Sliced Optical Burst Switched (TSOBS) networks, bursts are not switched across wavelengths and hence, once a burst is transmitted on some wavelength, it remains in the same wavelength channel in the network. The wavelength channel that a burst is transmitted can be chosen at the network interfaces or concentrators at the edges of the network. Since the concentrators have no knowledge of what wavelengths other concentrators are using to transmitting bursts in the network, the choice of wavelengths used by the concentrator could load certain wavelength channels more than others. An imbalance in the load of the wavelength channels directly affects

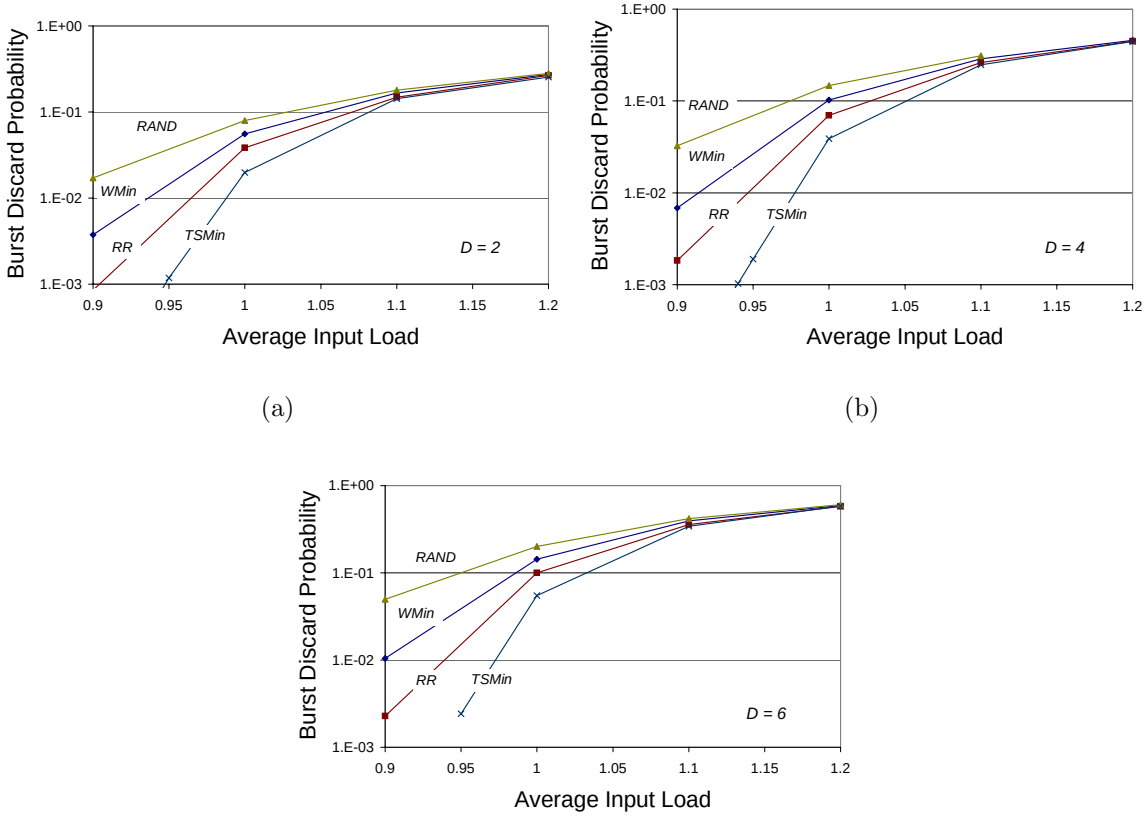

Figure 5.14: Burst discard probabilities of a TSOBS network

the utilization of the network bandwidth. In this chapter, we studied the issue of load balancing in TSOBS networks. We studied the performance of four algorithms.

RAND balances the load by choosing wavelengths at random. The imbalance in the load is fairly large and this results in a relatively high burst discard probability. RR selects wavelengths in a round robin order and balances the number of bursts sent on each wavelength. It does not, however, balance the load based on the length of the bursts. This results in a bad worst case behavior. WMin distributes bursts such that the number of timeslots sent on any wavelength channel does not exceed the number of timeslots sent on any other wavelength channel by more than the size of the largest burst. This results in very good long term balance in the amount of traffic sent on each wavelength channel. However, WMin results in a very large short term imbalance. This results in high burst discard probabilities and the performance of WMin is lesser than the performance of RR in practical TSOBS networks. We

then proposed TSMin, an algorithm that balances the load on the wavelength in a short term by balancing the number of active timeslot channels on each wavelength. This results in much better short term behavior and hence, results in much better performance in a TSOBS network.

5.6 Future Work

The load balancing algorithms examined in this chapter assumed that the concentrators operated in an isolated environment without any knowledge of the network conditions. However, the network can send feedback to the concentrators that give an estimate of the loads on each wavelength channel. This feedback could be in the form of regular messages that capture the load on each wavelength channel in the path (number of timeslot channels in use in each wavelength channel) or it could be an indicator when a burst gets dropped on a wavelength channel. These feedback signals can be used by the concentrators to modify their sending patterns and hence, improve the utilization.

Within a concentrator, the bursts need to be switched to burst transmission queues from the load balancers. When multiple load balancers transmit to the transmission queues, there is contention in the switch. We need to study the effect of this contention on determining the complexity of the switch that is necessary in the concentrator.

Due to cost factors, some concentrators need not support the entire range of wavelengths. Similarly, TSOBS routers may not implement switching for all wavelengths. The traffic from these concentrators or routers increase the load on these wavelengths. Thus, concentrators implementing the entire range of wavelengths should send lesser traffic on the wavelength channels that the "sub-equipped" concentrators or routers support to keep the load on all wavelengths balanced. We need to investigate methods that allow concentrators to adapt their load balancers to such conditions.

Chapter 6

Summary

Implementing the data path of Internet routers using optical switching techniques can be attractive because electronic switching speeds are not growing as fast as optical transmission rates. Optical switching has several other advantages such as bit rate independence, protocol transparency, and low power consumption. Unfortunately, optical switches that have been built so far have not been able to demonstrate a case for deploying optical switches commercially. Part of the reason why optical switches lack commercial appeal is that most of the systems built to date switches are complex and use expensive components. Also, it is not practical to use optical buffering because fiber delay lines are the only practical method for optical buffering and the amount of fiber required for typical buffer requirements is enormous.

Optical Burst Switching (OBS) is a network technology that combines the benefits of optical transmission in terms of its scalability and the flexibility of electronics for control processing. It gives very good statistical multiplexing performance without needing optical buffers. In this dissertation, we addressed the problem of designing optical switches for burst routers that use as fewer expensive optical components, without compromising the throughput achievable by the system.

6.1 Design of wavelength converting switches

Wavelength converting switches are essential components in optical burst routers that support wavelength conversion. We described a design for wavelength converting switches that uses tunable wavelength converters (TWCs) and passive wavelength grating routers (WGRs). Tunable wavelength converters are the only active components used in this switch and the size of the WGR needed is equal to the number of

wavelength channels, making the switch scalable to high bandwidth rates. However, the switch is not nonblocking. By formulating the routing problem as a combinatorial puzzle or game on a game board, we showed that the interconnection pattern between the input and output sections of the switch can affect the performance of the switch. We showed that WGR-based switches can achieve 89% of the throughput of routers using strictly non-blocking switches. We could increase the performance of the WGR-based switches by using additional wavelength routers or by adding buffering ports.

This design uses one tunable wavelength converter per input wavelength channel. Tunable wavelength converters use a laser or an equivalent device. This, unfortunately, makes cost of the switch high because bulk of the cost of electronic routers is contributed by the optoelectronics. However, if tunable wavelength converters become cheaper and more readily available, the WGR-based switch becomes a very appealing choice to implement the switching functionality in a router.

6.2 Time Sliced Optical Burst Switching

Optical Burst Switching systems were conceived for networks that use switches with wavelength conversion capability and they exploit the switching in the wavelength domain to provide good statistical multiplexing performance. Wavelength converters, unfortunately, are relatively expensive components. Time Sliced Optical Burst Switching (TSOBS) is a switching mechanism that switches bursts in the time domain instead of the wavelength domain. Bursts are transmitted in timeslot channels in a frame structure and fast optical switches are used to switch bursts across the network.

We studied a switch architecture that uses timeslot interchangers and a space switch to perform the time domain switching. We identified four nonblocking and a blocking design for timeslot interchangers and showed that the performance penalty incurred by using the blocking design is not much, considering the gain in terms of the cost reduction of the switch. Synchronizers play a key role in the implementation of this switch and we showed that using a guard band, that uses 10% of the timeslot bandwidth, it is possible to implement synchronizers that have a relatively low cost. Through a cost analysis, we showed that TSOBS routers are capable of becoming cost-competitive to electronic routers. Although the switches use optical crossbars,

the cost requirement on the optical crossbars is relatively low, making TSOBS a promising solution for implementing optical routers.

6.2.1 Data Aggregation in TSOBS Networks

In TSOBS networks, a timeslot is the minimum unit of data that we can transmit. Most packets of average size (for example, in the Internet) tend to have a much smaller size than a timeslot and this can lead to under-utilization of the timeslot bandwidth. A solution to this problem is to aggregate packets from sources to form bursts that have a longer duration and hence, utilize timeslots more efficiently. We described an algorithm to perform the aggregation and identified the parameters that affect the performance of the aggregation process. We then presented an analysis of the algorithm that help us determine the values of the parameters that result in good performance.

6.2.2 Load Balancing in TSOBS Networks

Since TSOBS networks switch data in the time domain, the wavelength channels of a link can get unevenly loaded. The utilization of a network with unevenly loaded wavelength channels is smaller than in a network with balanced loading. In a TSOBS network, the network interfaces at the edges of the network have the flexibility of choosing the wavelength channel a burst is sent on. We examined the problem of load balancing of the wavelength channels at the network interfaces. When the network interfaces perform load balancing without knowledge of what wavelengths other network interfaces are using, this results in load imbalance. We examined four load balancing algorithms to determine the algorithm that results in the least imbalance. We showed that algorithm WMin does not perform well, even if it balances the load in the long term. We proposed an algorithm called TSMin, that balances the load in the short term and results in the best performance.

Appendix A

Sum of geometrically distributed variables

Theorem A.0.1 *If $x_1, x_2, \ldots, x_h$ are identically and independently distributed geometric random variables with a mean $1/p$, then*

$$P(x_1 + x_2 + \ldots + x_h = j) = \binom{j-1}{h-1} p^h (1-p)^{j-h}$$

where $j \geq h$.

□

We prove the theorem using induction. For $h = 1$, the theorem is trivially true. For $h = 2$,

$$\begin{aligned} P(x_1 + x_2 = j) &= \sum_{k=1}^{j-1} P(x_1 = j-k | x_2 = k) P(x_2 = k) \\ &= \sum_{k=1}^{j-1} p(1-p)^{j-k-1} p(1-p)^{k-1} \\ &= \sum_{k=1}^{j-1} p^2 (1-p)^{j-2} \\ &= (j-1) p^2 (1-p)^{j-2} \end{aligned}$$

Assume that it is true for $h = 1, h = 2, \ldots, h = t$. Then,

$$\begin{aligned}
P(x_1 + x_2 + \ldots + x_{t+1} = j) &= \sum_{k=1}^{j-t} P(x_1 + x_2 + \ldots + x_t = j - k | x_{t+1} = k) P(x_{t+1} = k) \\
&= \sum_{k=1}^{j-t} \binom{j-k-1}{t-1} p^t (1-p)^{j-k-t} p (1-p)^{k-1} \\
&= p^{t+1} (1-p)^{j-(t+1)} \sum_{k=1}^{j-t} \binom{j-k-1}{t-1} \\
&= p^{t+1} (1-p)^{j-(t+1)} \sum_{x=t-1}^{j-2} \binom{x}{t-1}, \text{ where } x = j-k-1 \\
&= \binom{j-1}{t} p^{t+1} (1-p)^{j-(t+1)}
\end{aligned}$$

It can be easily shown by induction that $\sum_{x=t-1}^{j-2} \binom{x}{t-1} = \binom{j-1}{t}$. Hence, proved.

References

[1] The 100 × 100 project. http://100x100project.org.

[2] Samsung single mode fiber: SF-SMF. http://www.samsung.com/products/opticalfibers/e_brochure/index.htm.

[3] A. S. Acampora and I. A. Shah. Multihop lightwave networks: A comparison of store-and-forward and hot-potato routing. *IEEE/OSA Journal of Lightwave Technology*, 16:1725–1736, October 1998.

[4] H. Adiseshu, G. Parulkar, and G. Varghese. A reliable and scalable striping protocol. *Proceedings of ACM SIGCOMM*, 1996.

[5] I. Baldine, G. N. Rouskas, and H. G. Perros. Jumpstart: A just-in-time signaling architecture for WDM burst-switched networks. *IEEE Communications Magazine*, 40(2):82–89, February 2002.

[6] R. Barry. Models of blocking probability in all-optical networks with and without wavelength changers. *Proceedings of IEEE INFOCOM*, 1995.

[7] T. Battestilli and H. Perros. An introduction to optical burst switching. *IEEE Optical Communications*, August 2003.

[8] P. Bernasconi, C. Doerr, C. Dragone, M. Capuzzo, E. Laskowski, and A. Paunescu. Large N × N waveguide grating routers. *IEEE Journal of Lightwave Technology*, 18:985–991, July 2000.

[9] A. Birman. Computing approximate blocking probabilities for a class of all-optical networks. *IEEE Journal on Selected Areas in Communications*, 14(5):852–857, June 1997.

[10] D. Blumenthal, P. Prucnal, and J. Sauer. Photonic packet switches: Architectures and experimental implementation. *Proceedings of IEEE*, 82:1650–1667, November 1994.

[11] B. Bostica, M. Burzio, P. Gambini, and L. Zucchelli. Synchronization issues in optical packet switched networks. In Giancarlo Prati, editor, *Photonic Networks*. Springer Verlag, 1997.

[12] C. A. Brackett. Dense wavelength division multiplexing networks: Principles and applications. *IEEE Journal Selected Areas in Communications*, 8(6):948–964, 1990.

[13] F. Callegati, H. Cankaya, Y. Xiong, and M. Vandenhoute. Design issues of optical IP routers for internet backbone applications. *IEEE Communications Magazine*, pages 124–128, December 1999.

[14] F. Callegati, M. Casoni, C. Rafaelli, and B. Bostica. Packet optical networks for high-speed TCP-IP backbone. *IEEE Communications Magazine*, 37(1):124–129, January 1999.

[15] X. Cao, J. Li, Y. Chen, and C. Qiao. Assembling TCP/IP packets in optical burst switched networks. *Proceedings of IEEE GLOBECOM*, 2002.

[16] G. Castanon, L. Tancevski, and L. Tamil. Routing in all-optical packet switched irregular mesh networks. *Proceedings of IEEE GLOBECOM*, December 1999.

[17] G. A. Castanon and Ozan Tonguz. Analysis of hot-potato optical networks with wavelength conversion. *IEEE/OSA Journal of Lightwave Technology*, 17:525–534, April 1999.

[18] Y. Chen and J. S. Turner. WDM burst switching for petabit capacity routers. *Proceedings of MILCOM*, 1999.

[19] I. Chlamtac, V. Elek, A. Fumagalli, and C. Szabo. Scalable WDM access network architecture based on photonic slot routing. *IEEE/ACM Transactions on Networking*, 7(1), February 1999.

[20] M. E. Crovella and A. Bestavros. Self-similarity in world wide web traffic: Evidence and possible causes. *IEEE/ACM Transactions on Networking*, 5(6):835–846, December 1997.

[21] R. L. Cruz and J. T. Tsai. COD: Alternative architectures for high-speed packet switching. *IEEE/ACM Transactions on Networking*, 4:11–21, February 1996.

[22] A. Detti and M. Listanti. Impact of segments aggregation on TCP Reno flows in optical burst switching networks. *Proceedings of IEEE INFOCOM*, June 2002.

[23] Sudhir Dixit. *IP over WDM: Building the next generation optical internet*. Wiley Interscience, 2003.

[24] C. Dragone. An N×N optical multiplexor using a planar arrangement of two star couplers. *IEEE Photonic Technology Letters*, 6:812–815, September 1991.

[25] T. Durhuus, B. Mikkelsen, C. Joergensen, S. L. Danielsen, and K. E. Stubkjaer. All-optical wavelength conversion by semiconductor optical amplifiers. *IEEE Journal of Lightwave Technology*, 14:942–954, June 1996.

[26] A. Jourdan *et al.* Key building blocks for high-capacity WDM photonic transport networks. *IEEE Journal of Selected Areas in Communications*, 16(7), September 1998.

[27] A. M. Glass *et al.* Advances in fiber optics. *Bell Labs Technical Journal*, January-March 2000.

[28] B. Mikkelsen *et al.* 10 Gbps wavelength converter realised by monolithic integration of semiconductor optical amplifiers and Michelson interferometer. *Proceedings of ECOC*, 4:67–70, September 1994.

[29] C. Guillemot *et al.* Transparent optical packet switching: The European ACTS KEOPS project approach. *IEEE/OSA Journal on Lightwave Technology*, 16(12):2117–2134, August 1998.

[30] D. K. Hunter *et al.* SLOB: A switch with large optical buffers for packet switching. *IEEE/OSA Journal of Lightwave Technology*, 16:1725–1736, October 1998.

[31] D. K. Hunter *et al.* WASPNET: A wavelength switched packet network. *IEEE Communications Magazine*, pages 120–129, March 1999.

[32] E. Christian *et al.* Wavelength converter technology. *IEICE Transactions on Communications*, E82-B, February 1999.

[33] F. Dorgeuille *et al.* First array of 8 CG-SOA gates for large-scale WDM space switches. *Proceedings of European Conference on Optical Communication*, September 1998.

[34] F. Dorgeuille *et al.* 1.28 Tbps throughput 8×8 optical switch based on arrays of gain-clamped semiconductor optical amplifier gates. *Proceedings of Optical Fiber Communication conference*, March 2000.

[35] G. Bendeli *et al.* Performance assessment of a photonic ATM switch based on a wavelength controlled fiber loop buffer. *Technical Digest OFC*, pages 106–107, 1996.

[36] G. Raybon *et al.* Reconfigurable optoelectronic wavelength translation based on an integrated electroabsorption modulated laser array. *IEEE Photonic Technology Letters*, 10:215–217, 1998.

[37] I. Chlamtac *et al.* CORD: Contention resolution by delay lines. *IEEE Journal on Selected Areas in Communications*, 14(5), June 1996.

[38] M. Renaud *et al.* Network and system concepts for optical packet switching. *IEEE Communications Magazine*, April 1997.

[39] M. Schilling *et al.* 10 Gbps monolithic MQW-based wavelength converter in Michelson interferometer configuration. *Technical Digest of Optical Fiber Communication Conference*, February 1996.

[40] P. Gambini *et al.* Transparent optical packet switching: Network architecture and demonstrators in the KEOPS project. *IEEE Journal on Selected Areas in Communication*, 16:1245–1259, September 1998.

[41] S. J. B. Yoo *et al.* High-performance optical-label switching packet routers and smart edge routers for the next-generation internet. *IEEE Journal on Selected Areas in Communications*, 21(7):1041–1051, September 2003.

[42] S. L. Danielsen *et al.* Analysis of a WDM packet switch with improved performance under bursty traffic conditions due to tunable wavelength converters. *IEEE/OSA Journal of Lightwave Technology*, 16(5), May 1998.

[43] F. Forghierri, A. Bononi, and P. R. Prucnal. Analysis and comparison of hot-potato and single-buffer deflection routing in very high bit rate optical mesh networks. *IEEE Transactions on Communications*, 43(1):88–98, January 1995.

[44] J. M. Gabriagues and J. B. Jacob. OASIS: A high-speed photonic ATM switch - results and perspectives. *Proceedings of the 15th International Switching Symposium (ISS)*, pages 457–461, April 1995.

[45] M. Gagnaire and R. Sabella. Optical networks for new generation internet and data communication systems. *IEEE Computer Networks*, May 2000.

[46] P. Gambini. State of the art of photonic packet switched networks. In Giancarlo Prati, editor, *Photonic Networks*. Springer Verlag, 1997.

[47] P. Gavignet, D. Chiaroni, F. Masetti, and J. B. Jacob. Design and implementation of a fiber delay line optical buffer for multigigabit photonic switching fabrics. *European Transactions on Telecommunications*, 7(1), 1996.

[48] A. Ge, F. Callegati, and L. S. Tamil. On optical burst switching and self-similar traffic. *IEEE Communications Letters*, 4(3):98–100, March 2000.

[49] O. Gerstel, R. Ramaswami, and S. Foster. Merits of hybrid optical networking. *Proceeding of Optical Fiber Communication Conference*, pages 33–34, 2002.

[50] S. Gowda, R. K. Shenai, K. M. Sivalingam, and H. C. Cankaya. Performance evaluation of TCP over optical burst-switched (OBS) WDM networks. *Proceedings of ICC*, 2003.

[51] A. G. Greenberg and J. GOODMAN. Sharp approximate models of deflection routing in mesh networks. *IEEE Transactions on Communications*, 41(1):210–223, January 1993.

[52] J. Gripp, M. Duelk, J. Simsarian, A. Bhardwaj, P. Bernasconi, O. Laznicka, and M. Zirngibl. Optical switch fabrics for ultra-high-capacity IP routers. *IEEE/OSA Journal of Lightwave Technology*, 21(11):2839–2850, November 2003.

[53] M. Gustavsson. Technologies and application for space switching in multiwavelength networks. In Giancarlo Prati, editor, *Photonic Networks*. Springer Verlag, 1997.

[54] Z. Haas. The staggering switch: An electronically controlled optical packet switch. *IEEE/OSA Journal of Lightwave Technology*, 11(5/6), May/June 1993.

[55] H. S. Hinton. *An Introduction to Photonic Switching Fabrics*. Plenum Press, 1993.

[56] R. T. Hofmeister, C.-L. Lu, M.-C. Ho, P. Poggiolini, and L. G. Kazovsky. Distributed slot synchronization (DSS): A network-wide slot synchronization technique for packet-switched optical networks. *IEEE/OSA Journal of Lightwave Technology*, 16(12), December 1998.

[57] C.-F. Hsu, T.-L. Liu, and N.-F. Huang. Performance analysis of deflection routing in optical burst-switched networks. *Proceedings of IEEE INFOCOM*, 2002.

[58] D. K. Hunter, M. C. Chia, and I. Andonovic. Buffering in optical packet switches. *IEEE Journal of lightwave technology*, 16(12):2081–2094, December 1998.

[59] D. K. Hunter and D. G. Smith. New architectures for optical TDM switching. *IEEE/OSA Journal of Lightwave Technology*, 11(3):495–511, March 1993.

[60] M. Izal and J. Aracil. On the influence of self-similarity on optical burst switching traffic. *Proceedings of IEEE GLOBECOM*, 2002.

[61] V. Jayaraman, Z. M. Chuang, and L. A. Coldren. Theory, design, and performance of extended tuning range semiconductor lasers with sampled gratings. *IEEE Journal of Quantum Electronics*, 29:1824–1834, June 1993.

[62] M. Y. Jeon, Z. Pan, J. Cao, Y. Bansal, J. Taylor, Z. Wang, V. Akella, K. Okamoto, S. Kamei, J. Pan, and S. J. B. Yoo. Demonstration of all-optical packet switching routers with optical label swapping and 2r regeneration for scalable optical label switching network applications. *IEEE/OSA Journal of Lightwave Technology*, 21(11):2723–2733, November 2003.

[63] C. G. et al Joergensen. All-optical 40 Gbps compact integrated interferometric wavelength converters. *Technical Digest of Optical Fiber Communication Conference*, February 1997.

[64] H. F. Jordan, D. Lee, K. Y. Lee, and S. V. Ramanan. Serial array time slot interchangers and optical implementations. *IEEE Transaction on Computers*, 43(11):1309–1318, November 1994.

[65] I. Keslassy, S. T. Chuang, K. Yu, D. Miller, M. Horowitz, O. Solgaard, and N. McKeown. Scaling internet routers using optics. *Proceedings of ACM SIGCOMM*, August 2003.

[66] B. Kim, Y. Cho, J. Lee, Y. Choi, and D. Montgomery. Performance of optical burst switching techniques in multi-hop networks. *Proceedings of IEEE GLOBECOM*, 2002.

[67] W. Leland, M. Taqqu, and D. Wilson. On the self-similar nature of Ethernet traffic (extended version). *IEEE/ACM Transactions on Networking*, 2:1–15, February 1994.

[68] B. Li, X. Chu, and K. Sohraby. Routing and wavelength assignment vs wavelength converter placement in all-optical networks. *IEEE Optical Communications*, August 2003.

[69] X. Ma and G. S. Kuo. Optical switching technology comparison: Optical MEMS vs. other technologies. *IEEE Optical Communications*, November 2003.

[70] M. L. Masanovic, V. Lal, J. S. Barton, E. J. Skogen, D. J. Blumenthal, and L. A. Coldren. Monolithically integrated Mach-Zehnder interferometer wavelength converter and widely-tunable laser in InP. *IEEE/OSA Journal of Lightwave Technology*, 2003.

[71] F. Masetti. System functionalities and architectures in photonic packet switching. In Giancarlo Prati, editor, *Photonic Networks*. Springer Verlag, 1997.

[72] N. F. Maxemchuck. Comparison of deflection and store-and-forward techniques in the Manhattan street and shuffle-exchange networks. *IEEE/JLT Special Issue on Optical Networks*, 14(5):979–998, June 1996.

[73] E. Modiano. WDM-based packet networks. *IEEE Communications Magazine*, March 1999.

[74] B. Mukherjee. *Optical Communication Networks*. McGraw-Hill, 1997.

[75] T. Murphy, S. Y. Suh, B. Comissiong, A. Chen, R. Irvin, R. Grencavich, and G. Richards. A strictly non-blocking 16×16 electrooptic photonic switch module. *Proceedings of the 26th European Conference on Optical Communication*, 2000.

[76] A. Neukermans and R. Ramaswami. MEMS technology for optical networking applications. *IEEE Communications Magazine*, January 2001.

[77] A. M. Odlyzko. Internet growth: Myth and reality, use and abuse. *Journal of Computer Resource Management*, 102:23–27, Spring 2001.

[78] S. Ovadia, C. Maciocco, M. Paniccia, and R. Rajaduray. Photonic burst switching (PBS) architecture for hop and span-constrained optical networks. *IEEE Optical Communications*, November 2003.

[79] C. Qiao. Labelled optical burst switching for IP-over-WDM integration. *IEEE Communications Magazine*, 38(9):104–114, September 2000.

[80] C. Qiao and M. Yoo. Optical burst switching (OBS) - A new paradigm for an optical internet. *Journal of High Speed Networks*, (8):69–84, 1999.

[81] J. Ramamirtham and J. S. Turner. Time sliced optical burst switching. *Proceedings of IEEE INFOCOM*, April 2003.

[82] J. Ramamirtham, J. S. Turner, and J. Friedman. Design of wavelength converting switches for optical burst switching. *IEEE Journal on Selected Areas in Communications*, 21(7):1122–1132, September 2003.

[83] R. Ramaswami and K. N. Sivarajan. Optical routing and wavelength assignment in all-optical networks. *IEEE/ACM Transactions on Networking*, 3:489–500, October 1995.

[84] R. Ramaswami and K. N. Sivarajan. *Optical Networks*. Morgan Kaufman, 2002.

[85] Z. Rosberg, H. L. Vu, M. Zukerman, and J. White. Performance analyses of Optical Burst-Switching Networks. *IEEE Journal on Selected Areas in Communications*, 21(7):1187–1197, September 2003.

[86] W. W. Seo, K. Bergman, and P. R. Prucnal. Transparent optical networks with time-division multiplexing. *IEEE Journal on Selected Areas in Communications*, 14(5):1039–1051, June 1996.

[87] T. E. Stern and K. Bala. *Multiwavelength Optical Networks: A layered approach*. Addison-Wesley, 1999.

[88] A. Tam and P. J. Lin. Design and performance of a variable length optical packet switch. *Proceeding of Optical Fiber Communication Conference*, pages 219–221, 2002.

[89] L. Tamil, F. Masetti, T. McDermott, G. Castanon, A. Ge, and L. Tancevski. Optical IP routers: Design and performance issues under self-similar traffic. *Journal of High Speed Networks*, 8:59–67, August 1999.

[90] A. Tervonen. Optical enabling technologies for WDM systems. In Sudhir Dixit, editor, *IP over WDM: Building the next generation optical internet*. Wiley Interscience, 2003.

[91] J. S. Turner. Terabit burst switching. *Journal of High Speed Networks*, (8):3–16, 1999.

[92] S. Verman, H. Chaskar, and R. Ravikanth. Optical burst switching: A viable solution for terabit IP backbone. *IEEE Network*, 14(6):48–53, November/December 2000.

[93] K. G. Vlachos, I. T. Monroy, A. M. J. Koonen, C. Peucheret, and P. Jeppesen. STOLAS: Switching technologies for optical labeled signals. *IEEE Optical Communications*, November 2003.

[94] S. Watanabe, S. Takeda, G. Ishikawa, H. Ooi, J. G. Nielsen, and C. Sonne. Simultaneous wavelength conversion and optical phase conjugation of 200 Gbps (5×40 Gbps) WDM signal using a highly nonlinear fiber four-wave mixer. *Proceedings of ICOC/ECOC*, 5:1–4, September 1997.

[95] J. Y. Wei and R. McFarland. Just-In-Time signalling for WDM optical burst switching networks. *IEEE Journal of Lightwave Technology*, 18(12):2019–2037, December 2000.

[96] I. White, R. Penty, M. Webster, Y. J. Chai, A. Wonfor, and S. Shahkooh. Wavelength switching components for future photonic networks. *IEEE Communications Magazine*, 40(9):74–81, September 2002.

[97] J. White, M. Zukerman, and H. Vu. A framework for optical burst switching network design. *IEEE Communications Letters*, 6:268–270, June 2002.

[98] I. Widjaja. Performance analysis of burst admission-control protocols. *IEE Proc. Communications*, 142:7–14, February 1995.

[99] C. Xin and C. Qiao. A comparative study of OBS and OFS. *Proceeding of Optical Fiber Communication Conference*, 4:ThG71–ThG73, 2001.

[100] Y. Xiong, M. Vandenhoute, and H. Cankaya. Design and Analysis of Optical Burst-Switched Networks. *Proceedings of SPIE Conference on All Optical Networking*, 3843:12–19, September 1999.

[101] Y. Xiong, M. Vandenhoute, and H. Cankaya. Control architecture in optical burst-switched WDM networks. *IEEE Journal on Selected Areas in Communication*, 18(10):1838–1851, October 2000.

[102] L. Xu, H. Perros, and G. Rouskas. Techniques for optical packet switching and optical burst switching. *IEEE Communications Magazine*, pages 136–142, January 2001.

[103] F. Xue and S. J. B. Yoo. High-capacity multiservice optical label switching for the next generation internet. *IEEE Optical Communications*, May 2004.

[104] S. Yao, S. Dixit, and B. Mukherjee. Advances in photonic packet switching: An overview. *IEEE Communications Magazine*, pages 84–94, February 2000.

[105] S. J. B. Yoo. Wavelength conversion technologies for WDM network applications. *IEEE Journal of Lightwave Technology*, 14:955–956, June 1996.

[106] H. Zang, J. P. Jue, and B. Mukherjee. Photonic slot routing in all-optical WDM mesh networks. *Proceedings of IEEE GLOBECOM*, December 1999.

[107] H. Zang, J. P. Jue, and B. Mukherjee. A review of routing and wavelength assignment approaches for wavelength-routed optical WDM networks. *Optical Networks Magazine*, 1(1), January 2000.

[108] W. D. Zhong and R. S. Tucker. Wavelength routing-based photonic packet buffers and their applications in photonic packet switching systems. *IEEE Journal of Lightwave Technology*, 16(10):1737–1745, October 1998.

Vita

Jeyashankher Ramamirtham

Date of Birth May 20, 1978

Place of Birth Chennai, India

Degrees B.Tech. Computer Science, May 1999
D.Sc. Computer Science, August 2004

Professional Societies Institute for Electrical and Electronic Engineers

Publications

Ramamirtham J., Turner J. and Friedman J. Design of Wavelength Converting Switches for Optical Burst Switching, *IEEE Journal on Selected Areas in Communications*, September 2003.

Ramamirtham J. and Turner J. Time Sliced Optical Burst Switching, *Proceedings of IEEE INFOCOM*, April 2003.

Ramamirtham J. and Turner J. Design of Wavelength Converting Switches for Optical Burst Switching, *Proceedings of IEEE INFOCOM*, June 2002.

Keller R., Ramamirtham J., Wolf T. and Plattner B. Active Pipes: Service Composition for Programmable Networks, *Proceedings of IEEE MILCOM*, October 2001.

August 2004